Ice Ridge-WEC Collision Dynamics

Modelling the ice-structure interaction between an ice ridge and a wave energy converter

MSc Civil Engineering

Gerrit-Jan Winkels

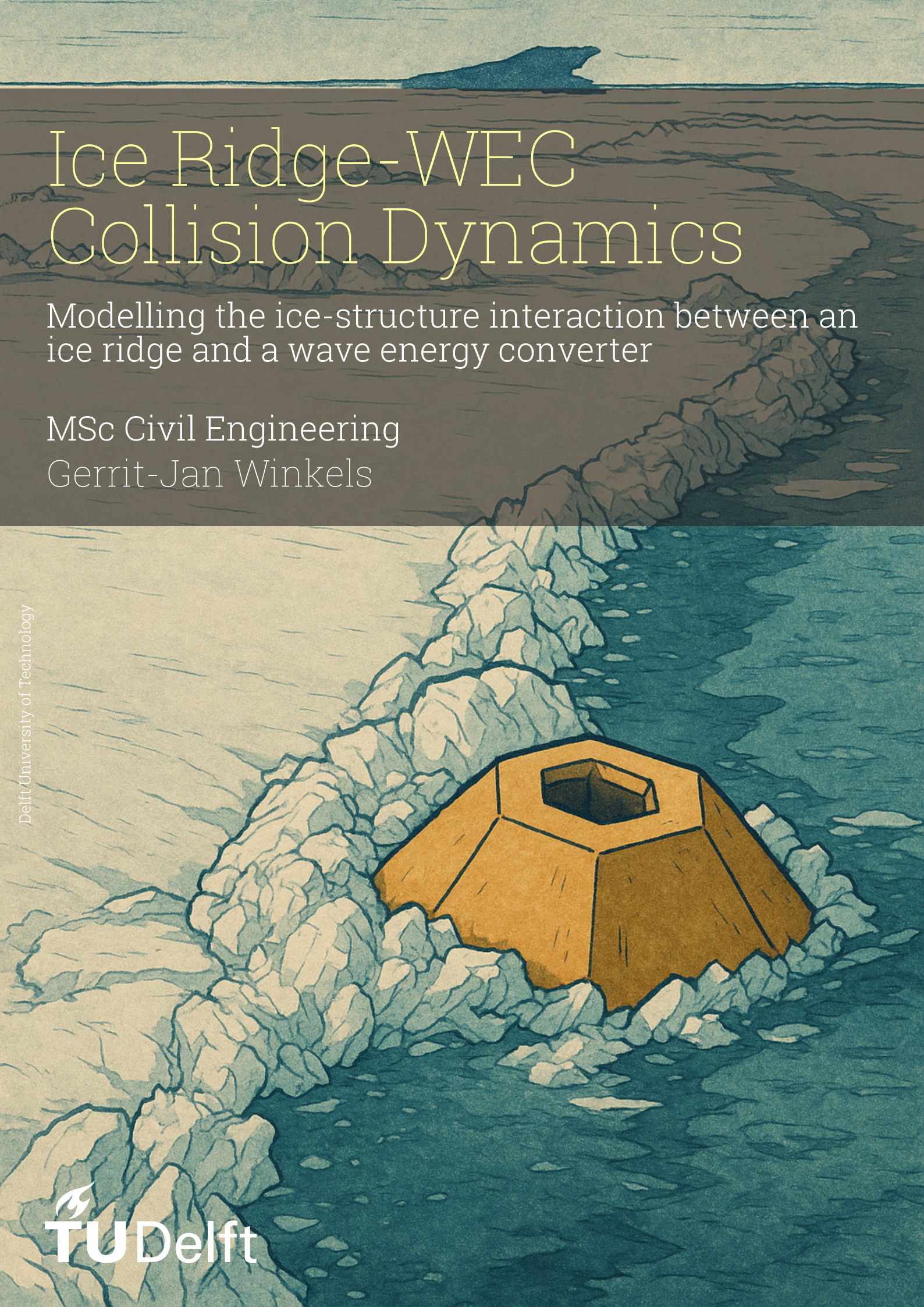

Delft University of Technology

TU Delft

Ice Ridge-WEC Collision Dynamics

Modelling the ice-structure interaction between an ice ridge and a wave energy converter

by

Gerrit-Jan Winkels

to obtain the degree of Master of Science
at the Delft University of Technology,
to be defended publicly on the 8th of July at 11:00.

Student number: 5403332
Project duration: January 20, 2025 – July 1, 2025
Thesis committee: Dr. H. (Hayo) Hendrikse, TU Delft
Dr. G. (George) Lavidas, TU Delft
Dr. A. (Alessandro) Antonini, TU Delft

Cover: AI-created image based on [1] and Figure 5.2
Style: TU Delft Report Style, with modifications by Daan Zwaneveld

An electronic version of this thesis is available at http://repository.tudelft.nl/.

TU Delft

Preface

This thesis represents the culmination of my studies at Delft University of Technology. It brings together two engineering disciplines that have always fascinated me and that formed the core of my master's program. The first is offshore renewables, which I explored through the Hydraulic & Offshore Structures track and several specializations. The second is arctic engineering, in which I earned 30 ECTS during my exchange semester at the University Centre in Svalbard. The idea for this project took shape in late 2024, and the official kick-off was on January 20, 2025. Over the past few months, I've found this work both challenging and inspiring—and it has only deepened my commitment to pursuing a career in these fields.

I owe sincere thanks to everyone who guided and supported me. First, I'm grateful to Hayo Hendrikse for sharing his expertise in arctic engineering and for serving as chairman of my thesis committee. I'd also like to thank George Lavidas for his insight into wave energy and for helping me to develop my initial topic. My appreciation goes to Alessandro Antononi for his valuable feedback during our progress meetings. Finally, I'm grateful to the university and the DelftBlue team, as without the DelftBlue supercomputer, this research would not have been possible.

To all who read these pages, I hope you find this thesis both informative and engaging.

Gerrit-Jan Winkels
Apeldoorn, July 2025

Summary

This research investigates the collision dynamics between an ice ridge and a moored point absorber-type wave energy converter (WEC). Wave energy, as a renewable energy source, presents a potential use-case for regions facing substantial energy demands that want to switch over to more renewable energy, such as the European Union and China. These regions include ice-prone marine environments, such as the Baltic Sea in Europe and the Bohai Sea in China. These seas are subject to ice actions in the winter, including the formation and drift of ice ridges. Ice ridges are substantial linear accumulations of fragmented ice created when ice sheets collide, resulting in a prominent above-water (sail) and below-water (keel) structure.

For ice-prone regions there is a wave energy potential found in the Baltic Sea in Europe, in the Bohai Sea in China and in the Sea of Okhotsk near Hokkaido, Japan. These seas are close to regions with high energy demands, have large maximum ice extents and enough wave energy power flux to be viable for a wave energy farm.

For wave energy farms to survive in ice-prone areas, they need to take into account ice ridges. Despite the critical nature of these interactions, previous studies focused on wave energy have largely overlooked the collision dynamics between moored WEC's and ice ridges. The research has so far only been focused on level-ice. Recognizing this research gap, this study developed a 3D model leveraging DualSPHysics, an SPH-based computational fluid dynamics software, tailored to resolve real-world engineering problems. This software is complemented with other software, which are MoorDyn for accurate mooring line dynamics and Project Chrono for collision dynamics.

The ice ridges within the simulations were designed based on measurements representative of typical subarctic regions, with region-specific parameters for the Baltic Sea. The ice ridge was modelled as a rigid object. The point absorber is designed as a moored buoy, as the buoy of a point absorber is the most critical part of the collision. The buoy is designed based on existing literature on ice-structure interactions. Numerous simulations were performed, each varying critical parameters such as the collision angle, the dimensions of the ice ridges, the roughness characteristics of the ice ridge surface and different maximum tension forces in the mooring lines.

The simulation findings revealed several insights into the interaction between an ice ridge and a moored point absorber. In simulations where the tension limit of the mooring lines was set to 5 MN it was demonstrated that mooring line failures predominantly occurred due to entanglement within the rough surface of ice ridge keels rather than from direct impact forces alone. As long as ice crushing was neglected. Conversely, smooth-surfaced ridges allowed mooring lines to withstand tensions up to approximately 2.2 MN. Furthermore, reducing ice ridge dimensions to 75% and 50% significantly decreased maximum fairlead tensions (from the maximum of 5 to around 3 MN) and horizontal contact forces (from 10 MN down to approximately 6 MN and 4 MN, respectively). Thus, both the surface roughness and dimensions of ice ridges are crucial factors for the interaction with the moored point absorber.

The structural integrity of the keel proved to be the most determining factor for influencing the dynamics of the collisions. A next research step is a better understanding of how much pressure an ice ridge keel can handle, where the uncertainty mainly lies within the effective contact area. The simulations were the failure was set to happen when ice crushing would occur quickly lead to failure, before the keel was reached. In the other simulations where ice crushing was neglected, horizontal contact forces were measured that were sufficient for leading to ice crushing and sequentially the point absorber getting stuck within the ice ridge.

The research provides an improvement upon understanding on a how a moored point absorber interacts with rigid ice ridges of different sizes and what the key influencing areas of the collisions are. The research also provides a working SPH-model with a simplified rigid ice ridge, suitable for initial testing of ice ridge collisions with moored point absorbers.

Contents

Nomenclature

Abbreviations

Abbreviation	Definition
WEC	Wave Energy Converter
PA	Point Absorber
EU	European Union
GW	Gigawatt (unit of power)
WMO	World Meteorological Organization
SEEZ	Swedish Exclusive Economic Zone
CFD	Computational Fluid Dynamics
DEM	Discrete Element Method
SPH	Smoothed-Particle Hydrodynamics
PDE	Partial Differential Equation
DBC	Dynamic Boundary Condition
mDBC	Modified Dynamic Boundary Condition
OPT	Ocean Power Technologies
PB3	PowerBuoy 3
OWC	Oscillating Water Columns
WESA	Wave Energy for a Sustainable Archipelago
MN	Meganewton (Unit of force)
CL	Consolidated Layer
FY	First-year (related to ice ridges)
FPU	Floating Production Unit
UTS	Ultimate Tensile Strength
CCP	Cone Complementary Problem
DVI	Discrete Variational Integrator
HSST	Hexagonal Slope Shaped Torus
NSC	Non-Smooth Contact
SMC	Smooth Contact
CUDA	Compute Unified Device Architecture
CAD	Computer-Aided Design

Symbols

The symbols are organized into four sections: the first two cover notation specific to this thesis (Latin and Greek), and the last two introduce general symbols and those used in the DualSPHysics formulation (Latin and Greek).

Symbol	Definition	Unit
$F_{impact,ice}$	Impact force of the ice ridge	[N]
$F_{impact,PA}$	Impact force of the point absorber	[N]
$F_{buoyancy,ice}$	Buoyancy force of the ice ridge	[N]
$F_{buoyancy,PA}$	Buoyancy force of the point absorber	[N]
$F_{drag,ice}$	Drag force of the ice ridge	[N]
$F_{drag,PA}$	Drag force of the point absorber	[N]
$F_{tension}$	Tension force	[N]
$F_{current}$	Current force	[N]

Symbol	Definition	Unit
$F_{g,ice}$	Gravitational force of the ice ridge	[N]
$F_{g,PA}$	Gravitational force of the point absorber	[N]
F_{wind}	Wind force	[N]
F_{wave}	Wave force	[N]
$F_{drag,mooring}$	Drag force of the mooring line	[N]
F_r	Horizontal action force caused by FY ice ridges	[N]
F_{cl}	Horizontal action force caused by CL of ice ridge	[N]
F_k	Horizontal action force caused by keel of ice ridge	[N]
p_G	Ice pressure (related to CL action)	[Pa]
p_{ice}	Ice pressure (general)	[Pa]
$p_{ice,max}$	Compressive ice strength (maximum ice pressure)	[Pa]
H_s	Sail height of the ice ridge	[m]
H_k	Keel depth of the ice ridge	[m]
H_{cl}	Consolidated layer thickness	[m]
h_1	Reference thickness of 1 meter	[m]
w_s	Sail width of the ice ridge	[m]
w_k	Keel width of the ice ridge	[m]
w_{st}	Structure width	[m]
w_{kb}	Keel base width of the ice ridge	[m]
w_{ccl}	Contact area width of CL of the ice ridge	[m]
D	Straight-line span of the mooring lines	[m]
S	Slack of the mooring lines	[m]
A_N	Nominal contact area (related to the ice ridge)	[m²]
A	Cross-sectional area (related to mooring line)	[m²]
$A_{contact}$	Contact area (related to the ice block)	[m²]
m	Empirical coefficient related to ice pressure	[-]
n	Empirical coefficient dependant on H_{cl}	[-]
f_{AR}	Empirical term	[-]
C_R	Ice strength coefficient	[Pa]
$c_{app,keel}$	Apparent keel cohesion	[Pa]
e_k	Keel porosity	[-]
W_b	Buoy weight	[kg]
α_k	Keel angle of the ice ridge	[°]
ϕ	Angle of internal friction	[°]
θ	Angle of slack mooring lines	[°]
μ_ϕ	Passive pressure coefficient	[-]
γ_e	Effective buoyancy	[Pa]
σ_{allow}	Maximum tension (related to steel)	[N]
t	Time	[s]
r	Position	[m]
v	Velocity	[m/s]
m	Mass	[kg]
p	Pressure	[Pa]
c	Speed of sound	[m/s]
g	Gravitational acceleration	[m/s²]
y_{ab}	Artificial viscosity	[m²/s]
W_{ab}	Kernel function	[-]
l	Unstretched length	[m]
d	Line diameter	[m]
E	Elasticity modulus	[Pa]
C_{int}	Internal damping coefficient	[Pa*s]
C_{dn}	Transverse drag coefficient	[-]
C_{dt}	Tangential drag coefficient	[-]
C_{an}	Transverse added mass coefficient	[-]

Symbol	Definition	Unit
C_{at}	Tangential added mass coefficient	[-]
B_i	Vertical seabed contact forces	[N]
$\mathbf{I}_m$	Identity matrix	[-]
$\mathbf{m}_{node,i}$	Node mass matrix	[-]
$\mathbf{W}_{sub,i}$	Submerged weight	[kg]
ρ	Density	[kg/m³]
ρ_0	Reference density	[kg/m³]
γ	Polytropic constant	[-]

1

Introduction

This chapter provides an overview of the research context, research problem and the research gaps found in the literature review. As well as the objectives, scope and research questions. At the end of this chapter the thesis outline is provided, which can be used to navigate to the chapter of interest.

1.1. Preliminary research

1.1.1. Research context

One of the ways to harvest renewable energy is by using a wave energy converter, shortened as WEC. Currently there are several different concepts for WEC's. They have already been deployed in several regions of the world and there are also plans for future development. For example, the European Union aims to have installed at least 1 GW of ocean energy by 2030 and 40 GW by 2050 [2]. The EU includes various countries with ice-prone waters, as they surround the Baltic Sea. The wave energy potential of this region, overlapping with the ice extent divided by the severity of the winter can be seen in Figure 1.1.

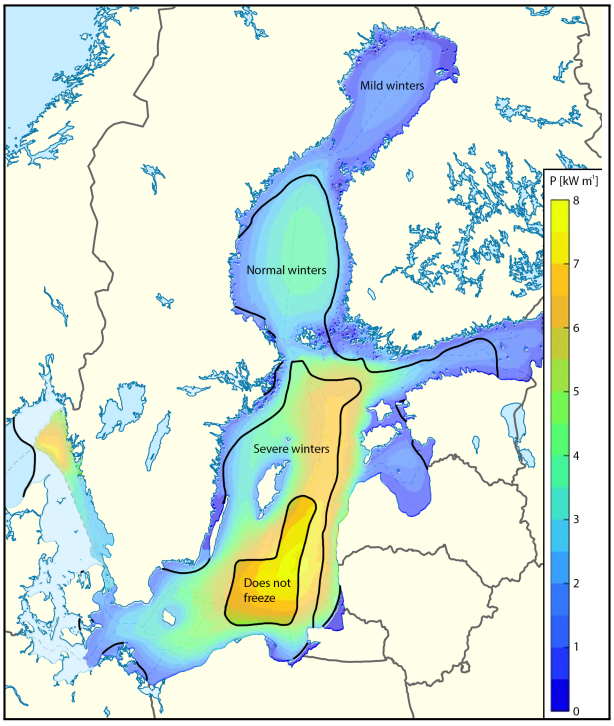

Figure 1.1: Map of the Baltic Sea with the sea ice extent [3] and the annual wave energy power [4] visualized.

Another example is China which introduced an ”Energy Law” which partly aims to facilitate large-scale development and utilization of ocean energy [5]. China is bordered by ice-prone waters, such as the Bohai Sea. The ice extent of the Bohai Sea overlapping with the wave energy potential is shown in Figure 1.2.

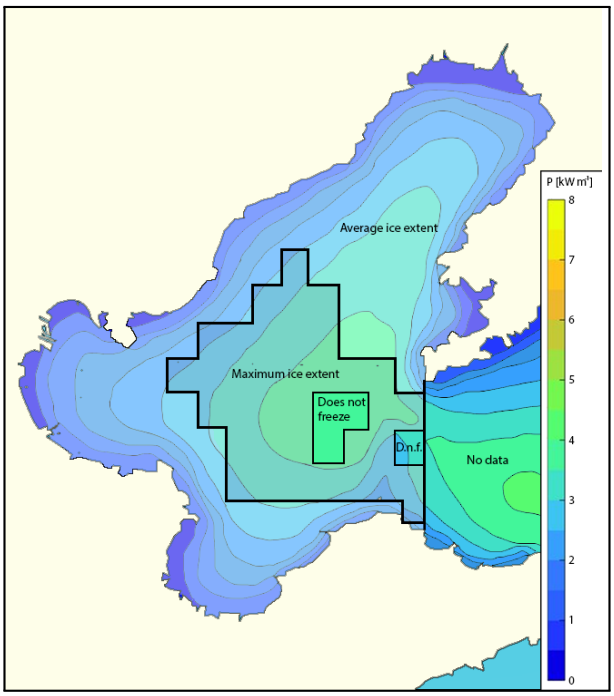

Figure 1.2: Map of the Baltic Sea with ice extent [6] and the wave energy power flux [7] visualized, D.n.f. is shortened for ”Does not freeze”.

Figure 1.1 and Figure 1.2 show that for the development of wave energy resources in these regions, the presence of ice needs to be considered.

1.1.2. Research problem

Wave energy converters show potential for deployment in ice-prone seas [8], increasing their geographical applicability. There have been studies on the impact of level ice on WEC’s [9], however this is not the only ice-related type of interaction that can occur. Besides level ice, there are ice ridges which yield higher forces and could potentially be the determining force for the design of WEC’s in areas where ice ridges are present. However, so far the collision dynamics, or more specifically the ice-structure interaction forces and behaviour after and during contact, between an ice ridge and a WEC has not been studied. The lack of research on the effects of ice ridges on WEC’s represents a crucial gap of knowledge for the applicability of WEC’s in ice-prone regions.

1.1.3. Literature review

To better understand the state-of-art of the problem, a literature review was conducted during the research proposal-phase of the thesis [10]. For this review the databases of ScienceDirect, ResearchGate, Google Scholar and the TU Delft repository were used to look for relevant research on the interaction of wave energy converters with sea ice as well as the interaction between ice ridges and floating and moored structures.

From the literature review conducted in the research proposal, it becomes clear that the effects of level ice on wave energy converters or floating buoys have already been studied and tested during full-scale measurements [9], as well as the effects of ice ridges on heavier moored constructions, such as offshore constructions and ships. Simulations on the dynamic interaction between moored ships and first-year ice ridges [11], as well as model tests on moored conical floaters in first-year sea ice ridges [12] have also been performed.

The topics that have not been addressed yet in the literature are the effects of ice ridges on wave energy converters, or lighter moored structures in general. Structures which are potentially submerged due to ice ridges. The long-term performance and survivability of WEC's in ice-prone seas has also not been assessed in the current literature. There are also no full-scale tests known in the literature on the interaction between lighter moored structures or WEC's and first-year ice ridges.

1.2. Objectives and scope

1.2.1. Research objective

The objective of this thesis is to model the effect of ice ridges on point-absorber type WEC's, with particular emphasis on the dynamic behaviour of the point absorber and the tension forces in its mooring lines. As the literature review underlines, there is a research gap on the knowledge of this interaction. The research objectives are listed below.

List of research objectives

- To identify and quantify the primary forces acting during the interaction between a moored point absorber-type WEC and an ice ridge, including hydrodynamic, ice-induced, and structural response forces.
- To develop a 3D model that simulates the interaction between a moored point absorber-type WEC and an average-sized ice ridge for a better understanding of what happens during a collision.
- To determine the critical size thresholds of ice ridges at which a moored point absorber-type WEC is likely to experience structural failure or operational disruption.
- To analyse the influence of the angle where the ice ridge and the moored point-absorber type-WEC collide, providing insight into their interaction under different impact conditions.
- To evaluate the effectiveness of various mitigation strategies designed to protect point absorber wave energy converters from damage caused by ice ridge interactions in cold climate marine environments.

1.2.2. Research scope

This research aims to investigate the interactions at play between a moored point absorber-type wave energy converter and ice ridges in cold climate environments. The limitations of the scope are as follows:

- The ice ridges are based on ice ridges that have been formed in first-year sea ice with dimensions that are typical for the subarctic seas.
- The point absorber is modelled without taking into account the internal mechanics of this WEC, this translates to a point absorber that is modelled as a moored buoy.
- The ice ridge itself is modelled as a single object, which means that the entire ice ridge has the same properties and the blocks in the keel are modelled as a rough surfaced trapezium.
- Certain forces that exist due to ice actions or ice processes are not taken into account, this includes ridge-building, rubble-building, ride-down/up of ice, buffering of surrounding ice or direct ice actions on the mooring lines. See Chapter 3.2 for an explanation on these actions.

This approach aims to provide an improvement of the understanding of how a point absorber may perform and survive in ice-prone waters. Although the study is not focused on a specific region, the dimensions and parameters of the ice ridges are derived from typical subarctic conditions, focusing on the Baltic Sea for region-dependent parameters, as this region is among the most promising ice-prone areas for wave energy harvesting and provides extensive data on ice ridge characteristics. The scope of the research is limited to point absorber-type wave energy converters, excluding other types of WEC's from consideration.

1.3. Research question

The objective of the research is to model a collision between a point absorber-type wave energy converter and an ice ridge. The main research question of the thesis is as follows:

What are the collision dynamics between an ice ridge and a moored point absorber-type wave energy converter?

The collision dynamics in this case encompass the ice–structure interaction forces, the resulting mooring line tensions, and the point-absorber's behaviour after impact. To answer the main research question, the following sub-research questions are formed:

1. What are the primary mechanisms and consequences of an interaction between ice ridges and moored point absorber-type wave energy converters?
2. What are the threshold dimensions and characteristics of an ice ridge for a collision between an ice ridge and point absorber to be critical?
3. How does the angle of collision between the ice ridge and the point absorber affect the collision dynamics?
4. How does the roughness of the surface of the ice ridge affect the collision dynamics between the ice ridge and the point absorber?
5. What are potential design modifications or operational strategies for wave energy converters to enhance their resilience against ice ridge impacts?

From these sub-research questions, question 1, 2, 3 and 4 are critical for answering the main research question. Questions 5 is used to expand on the results of the first 4 questions.

1.4. Thesis outline

The thesis outline per chapter is as follows:

Chapter 1 - Introduction: An overview of the research context, research problem and the research gaps found in the literature review. As well as the objectives, scope and research questions.

Chapter 2 - Research context: This chapter provides the background information essential to the thesis. It covers details about various ice features, particularly focusing on ice ridges. Additionally, it highlights the geographical distribution of ice ridges, identifying the specific seas and regions where they are prevalent, along with the wave energy potential in these ice-prone areas. The chapter also discusses different types of wave energy converters and reviews the existing literature on WEC-research conducted in regions affected by ice.

Chapter 3 - Ice Ridge-WEC Interaction Forces: This chapter presents an overview of all ice ridge-WEC interaction forces, it includes section about ice-related forces and geometrical properties of ice ridges. It also covers hydrodynamic forces, detailing the formulation that will be used in the model. And lastly sections about mooring forces and other additional influencing forces.

Chapter 4 - Point Absorber: This chapter provides an overview of the point absorber-type wave energy converter, covering various types of point absorbers, structural aspects such as hull integrity, different mooring line configurations and maximum mooring line tensions.

Chapter 5 - Methodology: In this chapter all used software tools are provided. As well as all properties, parameters and settings for the standard configuration of the simulation.

Chapter 6 - Results: This chapter provides the results of the performed simulations. This includes an overview of the observed modelling faults and associated limitations as well as the expected loads.

Chapter 7 - Evaluation: This chapter evaluates the results from Chapter 6. This includes a validation of the expected loads from Chapter 6.2.

Chapter 8 - Mitigation Strategies: This chapter addresses potential mitigation strategies to reduce the risks and impacts of collisions between moored floating point absorbers and ice ridges. Strategies considered include both structural adaptations and operational procedures.

Chapter 9 - Conclusions & Recommendations: This chapter repeats the research problem, objectives and questions, while giving concluding remarks on them. Key findings are provided. At the end of the chapter recommendations for further improvements are given.

2

Research Context

This chapter provides the background information essential to the thesis. It covers details about various ice features, particularly focusing on ice ridges. Additionally, it highlights the geographical distribution of ice ridges, identifying the specific seas and regions where they are prevalent, along with the wave energy potential in these ice-prone areas. The chapter also discusses different types of wave energy converters and reviews the existing literature on WEC-research conducted in regions affected by ice.

2.1. Ice features

The ice features that can potentially play a role in ice-prone regions can be roughly divided into level ice, rafted ice, broken ice (floe ice), ice ridges and icebergs [13]. From these features level ice is a flat, continuous sheet of sea ice with relatively uniform thickness, which can be found in relatively calm waters, it seen as the flat parts in Figure 2.1 (a). Rafted ice occurs when ice sheets slide over each other, which often happens due to wind or currents and it results in overlapping layers of ice, which can be seen in from Figure 2.1 (b). Broken ice refers to sea ice that has fractured into smaller pieces due to wind, waves or other forces, as shown in Figure 2.1 (c). Ice ridges are linear accumulations of broken ice formed when ice sheets collide and pile up, which creates an above-water and below-water structure (keel and sail respectively) which can be seen in Figure 2.1 (a) from above and more detailed in Figure 2.2. Ice ridges can reach significant thicknesses. Icebergs are massive pieces of ice which have broken away from glaciers, as shown in Figure 2.1 (d).

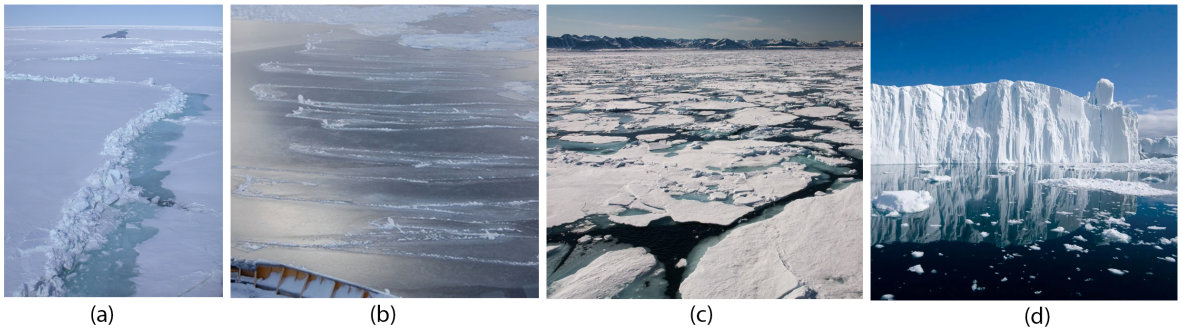

Figure 2.1: Ice features: (a) ice ridges surrounded by level ice [1], (b) rafted ice [14], (c) broken ice [15], (d) iceberg [16].

Among these ice features, the specific feature that dictates structural design forces depends on the location. If all features were present simultaneously, icebergs would invariably impose the largest forces on a structure due to their massive size. However, icebergs are typically only found in higher latitudes, such as the Arctic or Antarctica. These regions are generally not suited for wave energy harvesting, as they have low energy demand and present extremely harsh environmental conditions

for WEC operation. The second largest ice feature are ice ridges. They are more relevant for WEC-applications, as they occur in seas surrounded by areas with significant energy demand, such as the Baltic Sea in Europe or the Bohai Sea in China. A closer view of an ice ridge is shown in Figure 2.2.

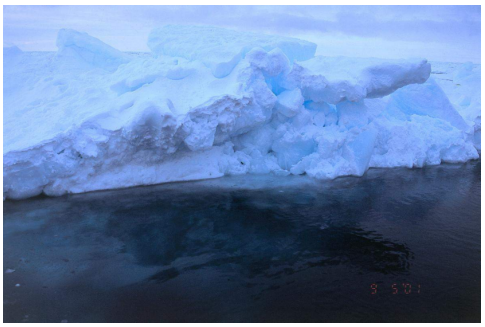

Figure 2.2: Closed-up view of first-year ice ridge [17].

2.1.1. Occurrence of ice ridges

Ice ridges can form in any area where sea ice is present, which typically includes the northern regions of Canada and the U.S. state of Alaska, Russia, surrounding Greenland, and Antarctica. Beyond these areas, ice ridges can also occur in Europe, particularly in the Baltic Sea. In Asia, they can appear in the Bohai Sea near China and in the Sea of Okhotsk near the Japanese island Hokkaido. Ice ridges can also form in the Sea of Japan, though this is generally limited to the northern part, specifically the Tatar Strait region, which only borders Russia [18]. The minimum and maximum sea ice extent of the Northern Hemisphere is visualized in Figure 2.3.

Figure 2.3: Azimuthal projection of the northern hemisphere showing historical (1982-2025) sea ice extent, data from [19].

2.2. Wave energy potential in ice-prone regions

A WEC can be used for different purposes and could even be suitable for a purpose in a remote location in the high Arctic, such as powering research stations, communication systems or other offshore platforms. But looking at the current use of WEC's, the primary focus of WEC technology development remains energy generation. Remote arctic regions typically have low energy demands, limiting the feasibility and economic justification for large-scale wave energy projects in these areas. More practical ice-prone regions for wave energy harvesting include densely populated areas such as the Baltic Sea and the Bohai Sea. Additionally, the island of Hokkaido presents an intriguing case: despite its relatively lower population density, the region is experiencing a significant rise in electricity demand driven by the growth of data centres and semiconductor manufacturing facilities [20]. Considering Japan's commitment to achieving net-zero emissions by 2050 [21], there is a compelling rationale for establishing wave energy infrastructure near Hokkaido. This sums up to at least 3 regions which can be interesting for wave energy harvesting that can simultaneously experience ice ridges. To determine if there is any wave energy potential in these regions it is required to look at the actual resource assessment of these regions. In this section the resource assessment of the Baltic Sea, the Bohai Sea and the Okhotsk Sea is assessed.

2.2.1. Potential in the Baltic Sea

In Figure 2.4 the sea ice extent with the corresponding wave energy potential is shown. The sea extent is described using the categories mild, normal and severe winters, where the severity of the winter, measured by the total ice extent, determines the type of winter. In "mild" winters the ice extent includes the northern part of the Gulf of Bothnia and the Gulf of Riga, the eastern part of the Gulf of Finland and some parts of the inner bays. In "normal" winters this is extended to all areas of the Bothnia, Finnish and Riga Gulfs as well as most coastal and Baltic waters. In "severe" winters the ice extent is the entire Baltic Sea, with an exception of the central part south of Gotland Island [3].

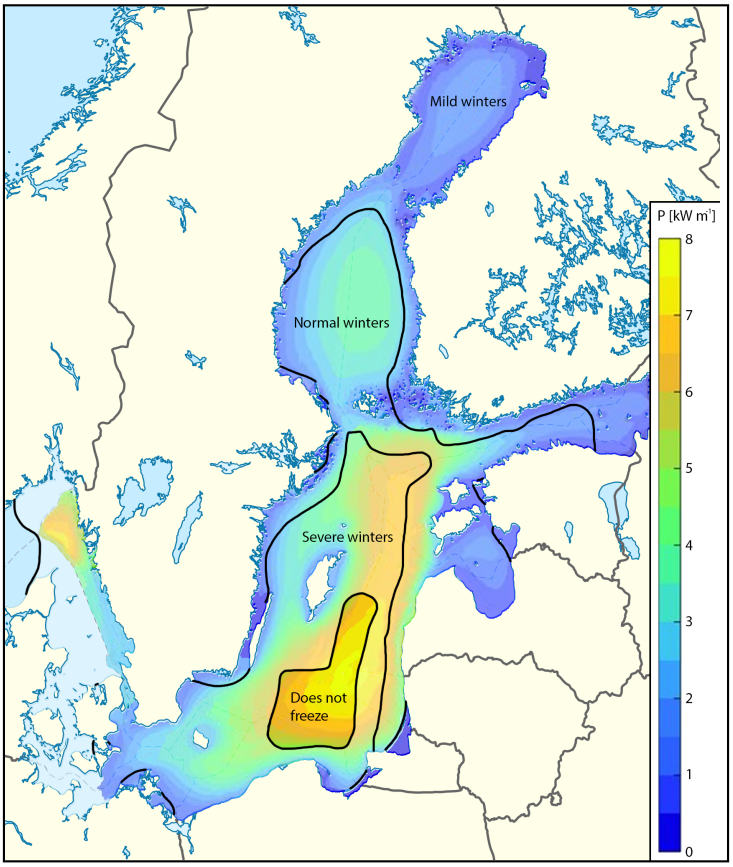

Figure 2.4: Map of the Baltic Sea with the sea ice extent [3] and the annual wave energy power [4] visualized.

Figure 2.4 also shows the wave energy potential in the Baltic Sea, which has been assessed previously [22], including more extensive studies focusing on the Swedish Exclusive Economic Zone (SEEZ) [4] and the Lithuanian Coast [23]. The studies collectively highlight that there is a moderate but viable wave energy potential, even though the seas are not as rich in wave energy as the North Sea. Especially the Eastern part of the Baltic Sea has potential, due to a predominant westerly wind direction. The study about the Lithuanian coast does show that the wave energy potential diminishes closer to the coast. As can be seen in Figure 2.4, the wave energy potential is lower in regions where the ice extent only appears in mild winters, but on the borders of the normal winters and in severe winters the wave energy power is higher and more viable for wave energy farms.

2.2.2. Potential in the Bohai Sea

An assessment of the wave energy potential in the Bohai Sea has also been performed [7], as well as a study that also includes the effects of sea ice on the wave energy flux distribution [24] and a study that shows the ice extent in the Bohai Sea [6]. The studies conclude that the Bohai Sea has a ”moderate wave energy potential” with an annual average of up to 3.5 kW/m. The offshore areas have higher wave energy potentials than the nearshore areas in the Bohai Seas. The wave resources itself can be heavily influenced by sea ice. The second study found that in the Liaodong Bay (northern bay of Bohai Sea), the wave energy flux can reduced by up to 80% due to sea ice. For the Bohai Bay (western bay) this can be up to 50%. Another finding is that even in the ice-free areas the wave energy flux is reduced due to an decrease in effective wind fetch because of sea ice in other regions. Combining the fact that nearshore areas have lower wave energy potential and are heavily influenced by sea ice concentration means that the Bohai Sea has the most potential in the centre of the region.

In Figure 2.5 the wave energy power flux combined with historical average ice extent and maximum ice extent. The same legend as Figure 2.4 is used. Note that the ice extent is based on grid-blocks from [6] with average ice thicknesses, where a non-zero value is included as a block with ice.

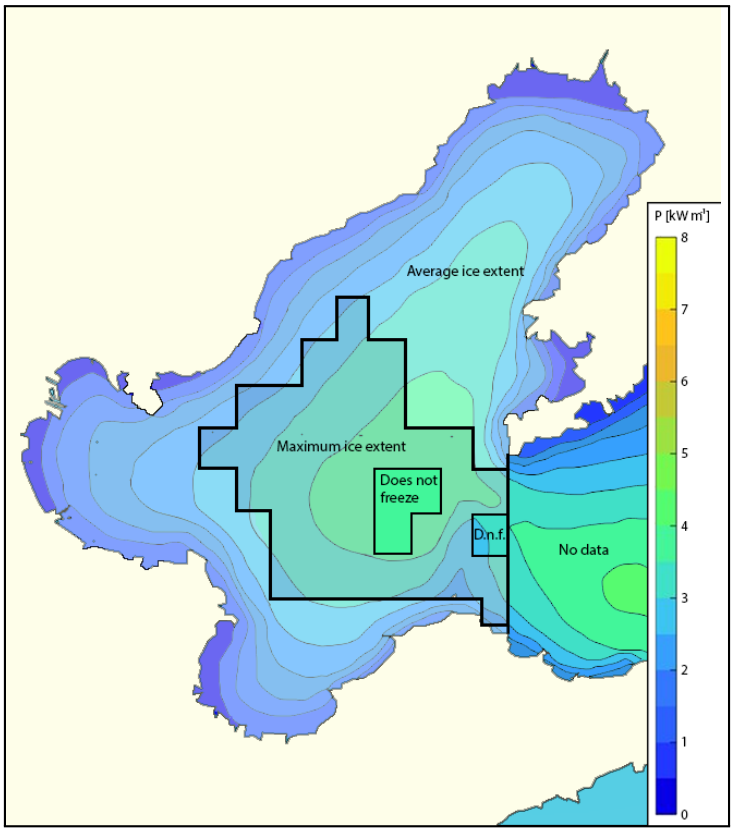

Figure 2.5: Map of the Baltic Sea with ice extent [6] and the wave energy power flux [7] visualized, D.n.f. is shortened for ”Does not freeze”.

2.2.3. Potential in the Sea of Okhotsk

For Japan, a wave resource assessment was also performed [25]. This study finds that for the Sea of Okhotsk northern of Hokkaido the wave power density ranges from 3 kW m^{-1} up to 9 kW m^{-1}, increasing by going further away from the coast. However due to an expected decrease of the sea ice extent in this region, more powerful waves are anticipated in the future [26]. This trend of increasing ocean waves will strengthen the use-case of wave energy farms.

With regards to the sea ice extent in this region, in the Okhotsk Sea the sea ice coverage in the period 2000-2020 ranged from 34.1% in extremely mild winters to 92.4% in extremely severe winters [27].

2.2.4. Concluding remarks about wave energy potential

For a wave energy farm to be considered viable, one study [28] states that it needs to have wave energy levels of at least 10 kW/m, this is identified as the minimum needed for commercial-scale wave energy projects. However a lower number does not necessarily mean that it is not possible, a point absorber can be suitable for any amount of resource as long as their size provides a reasonable performance match with metocean conditions [29]. In combination with the fact that due to technology improvements the efficiency of point absorbers is increasing [30], this means that there is already a potential for wave energy power harvesting in the Baltic, Bohai and Okhotsk sea, which can even grow in the future. Despite the relatively low values for wave energy power.

2.3. Wave energy converter types

Wave energy converters can be divided into different categories, the most common devices are point absorbers, attenuators, overtopping devices, terminators and oscillating water columns (OWC). Within these categories a wide variety of concepts has been developed, in Figure 2.6 an overview of different examples of the categories is provided. (a) represents the point absorber, where only the part above sea is visible. This concept is the PB3 Powerbuoy from Ocean Power Technologies (OPT) [31]. In (b) the Pelamis WEC is visible [32], a surface attenuator that generates electricity from the motion of surface waves. In (c) the overtopping device called Wave Dragon is shown [33], where water flows into the reservoir via a ramp, and the water drains back through a hydro-electric turbine, which generates energy. In (d) an SPAR-type OWC is visible [34], an OWC uses the vertical wave column displacements to push the airflow in the column through air turbine in order to generate electricity.

Figure 2.6: WEC concepts: (a) PB3 Powerbuoy [31], (b) Pelamis [32], (c) Wave Dragon [33], (d) SPAR-type OWC [34].

[35] provides a more extensive overview of all different concepts for wave energy converters. With regards to research done for wave energy converters and their vulnerability to sea ice, [36] stated that most WEC's are vulnerable to sea ice, except when they can be sheltered at the bottom of the sea. Another research project was WESA [37], in this project a floating buoy was designed, which can act as a point absorber but also needs to survive ice action in the winter season. This was a 6 x 5 m hexagonal slope shaped torus (HSST) buoy made out of steel, the shape of the buoy is visible in Figure 2.7. It was tested for resistance against drifting ice fields with a thickness of up to 15 cm.

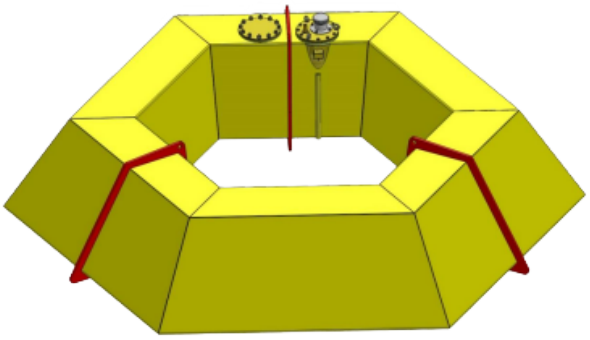

Figure 2.7: The HSST buoy adapted for ice, used in project WESA [37].

A thorough study on choosing the WEC that performs the best against ice ridges is not within the scope of this project. The study done by [38] suggests that smaller or medium-scale WEC is a better fit for lower energy seas, such as the Baltic Sea. The point absorber is a relatively small WEC and as a buoy for the point absorber which has improved resistance against ice has already been designed, the study will continue to focus on the point absorber WEC.

3

Ice Ridge-WEC Interaction Forces

This chapter presents an overview of all ice ridge-WEC interaction forces, it includes a section about ice-related forces and geometrical properties of ice ridges. It also covers hydrodynamic forces, detailing the formulation that will be used in the model. And lastly sections about mooring forces and other additional influencing forces.

3.1. Schematic overview of forces

A schematic overview of all the environmental and structural forces involved between an ice ridge and a moored point absorber is visualized in Figure 3.1. This figure excludes any time-dependent dynamic forces as radiation and damping or any forces directly related to the working of the point absorber.

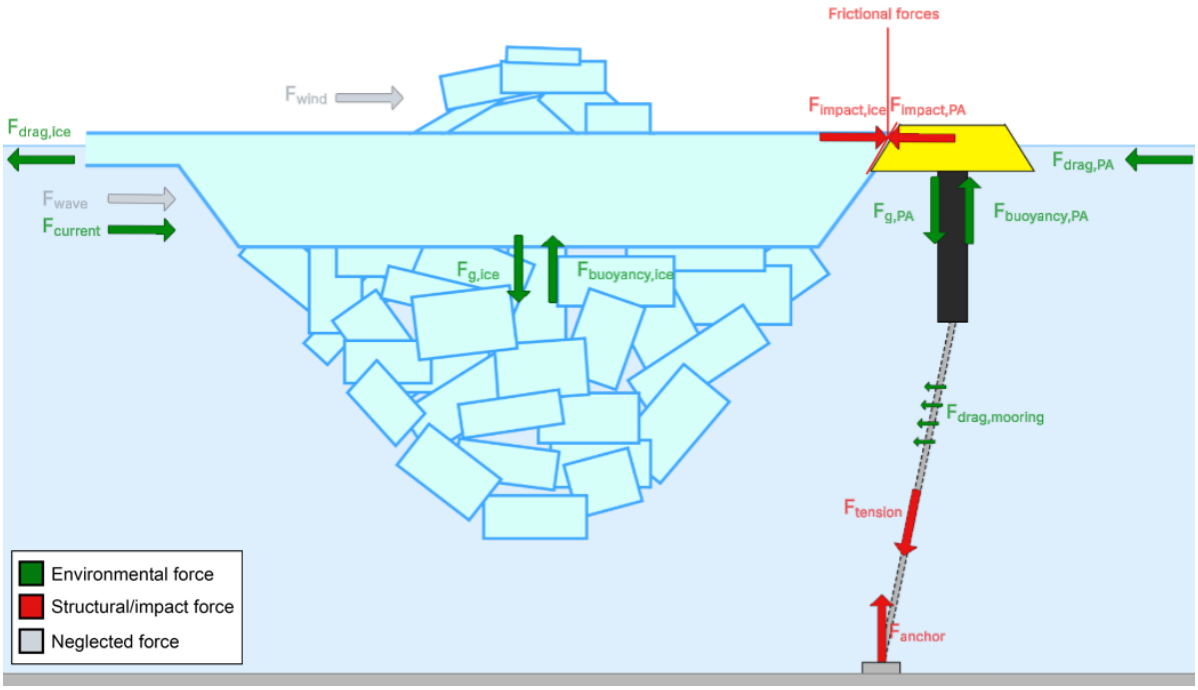

Figure 3.1: Involved forces between a collision of an ice ridge with a moored point absorber.

3.1.1. Forces considered in the model

The forces that are involved in the model are the following which are shown in Figure 3.1 are as follows:

- **Global ice actions**, as described in Chapter 3.2.3. This includes the impact force of the ice ridge

$F_{impact,ice}$ and the reaction force from the point absorber $F_{impact,PA}$.

- **Hydrodynamic forces**, this includes the buoyancy forces from the ice ridge $F_{buoyancy,ice}$ and the point absorber $F_{buoyancy,PA}$ acting from the centre of mass. The drag forces $F_{drag,ice}$, $F_{drag,PA}$ from the water. These forces are accounted for in the modelling software.
- **Mooring forces**, as described in Chapter 3.4. This includes the the tension along the mooring line $F_{tension}$, the tension in the anchor F_{anchor} and the drag on the mooring line $F_{drag,mooring}$
- **Environmental forces**: The current force $F_{current}$ set by the model to simulate the current of the sea and thereby moving the ice ridge.
- **Gravitational forces**: The gravitational forces of the ice ridge $F_{g,ice}$ and the point absorber $F_{g,PA}$, acting from the centre of mass, which are accounted for in the modelling software.
- **Frictional forces**: The friction between the ice ridge and the moored point absorber are considered in the model.

Within the model there are also forces that are not visualized in Figure 3.1 but are taken into account.

- **Internal mooring line forces**: The damping and added-mass-related forces are taken into account within MoorDyn.
- **Hydrostatic pressure**: The hydrostatic pressure (see Chapter 3.5.3) within the model is taken into account within DualSPHysics.

3.1.2. Limitations

Forces that exist but are not accounted for in the model are as follows:

- Wind forces F_{wind} and wave forces F_{wave} are not considered in the model.
- Forces within the system of the point absorber. This includes time-dependent forces, such as damping and radiation.
- Certain ice actions are not included, this includes ridge-building processes (Chapter 3.2.4 and other ice action considerations which are named in Chapter 3.2.6

3.2. Ice-related forces or Ice-ridge forces

This section first discusses the geometry of ice ridges and afterwards the global ice actions and other ice action considerations.

3.2.1. Geometry of ice ridges

Ice ridges, also known as pressure ridges, are expected to be the leading force in ice-prone climates suitable for wave energy farms. The exact definition of an ice ridge can be defined as ”a line or wall of broken ice forced up by pressure” [39]. Ice ridges can be divided into first-year ice ridges, second-year ice ridges and multi-year ice ridges, where first-year ice ridges are formed during a single winter season and haven’t survived a summer melt. Second-year or multi-year ice ridges have survived at least one summer melt season and have different properties than first-year ice ridges.

Ice ridges are made up of three divisible parts, the sail, the consolidated layer and the rubble. Another division that is often used is dividing it by the keel and the sail, where in that case the sail is still the part above the water line and the keel is the submerged part of the consolidated layer and the rubble.

- The sail: The part of the ridge that is above the water line, it is composed of piled up blocks of ice, which are frozen together due to contact between them.
- The consolidated layer: The part that forms the core of the ice ridge, located primarily below the waterline due to the buoyancy of ice. This layer consists of ice blocks that have been compressed and forced underwater during ridge formation, creating interstitial cavities that fill with seawater. Over time, as the temperature drops, the water within these voids freezes, progressively bonding the ice blocks together and solidifying the structure. While the majority of the consolidated layer is submerged, a portion may extend above the waterline, as the buoyant forces of ice cause the ridge to rise slightly above the surface.

- The rubble: The part that is underneath the consolidated layer is called the rubble. It is composed of loose ice blocks that are partially refrozen with water trapped in their interstices.

The typical composition of a first-year ice ridge is shown in Figure 3.2. The shape of the ridge has a wide variability, but are often modelled by either triangles or trapeziums. The ridges are characterized by their widths, thicknesses and angles.

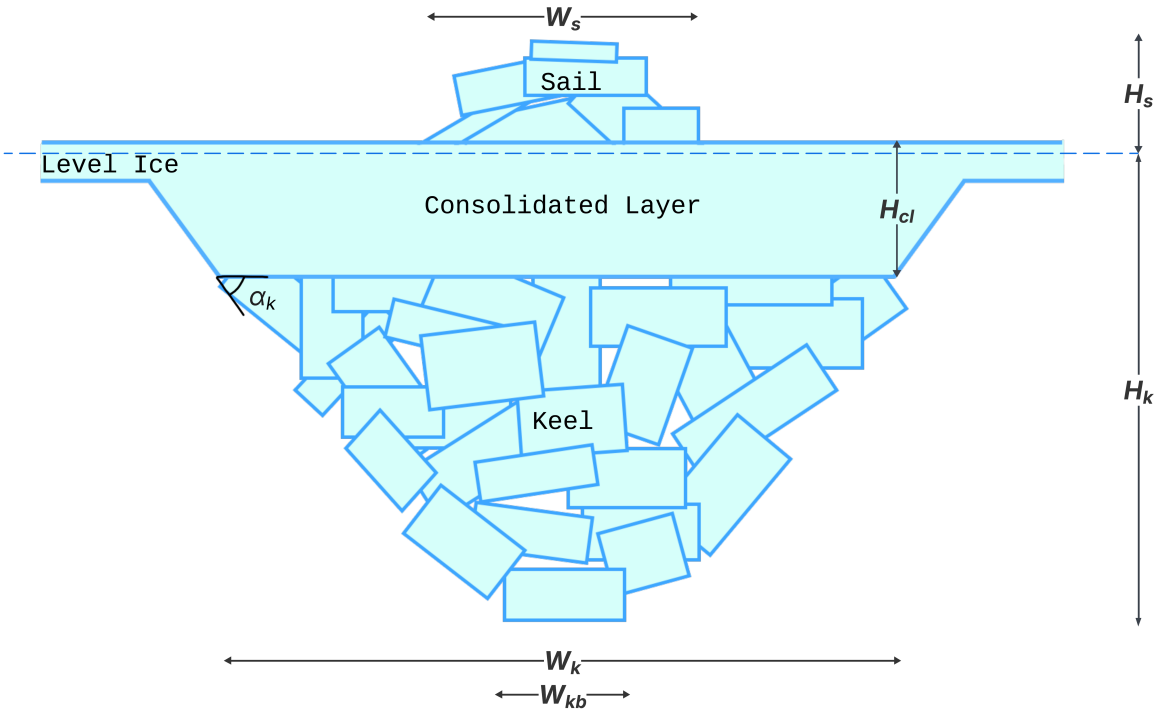

Figure 3.2: Typical model of a first-year ice ridge, indicated with sail, level ice, consolidated layer, keel and their geometrical properties.

In Figure 3.2, the geometrical properties are as follows

- H_s is the sail height, which stretches from the top of the sail to the waterline;
- H_k is the keel depth, which stretches from the waterline to the bottom of the keel;
- H_{cl} is the thickness of the consolidated layer;
- w_s is the width of sail;
- w_k is the width of the keel;
- w_{kb} is the width of the keel base, which usually varies between 0 to $5H_s$;
- α_k is the keel angle.

3.2.2. Typical geometrical ratios

In Figure 3.2 the geometrical properties of the ice ridge are provided. In this section the typical values of these properties for ice ridges are presented.

To use ice ridges for the calculations of design loads the ridge dimensions, macro-porosity, mechanical and physical properties are required, preferably in the form of mean statistical values. For ice ridges it is difficult to collect this data due to the harsh fieldwork conditions in cold regions. There are several databases created for a standardization of these properties, including [40].

[41] expanded on this topic and performed a comprehensive analysis of the morphology of first-year sea ice ridges for arctic regions (Bering and Chuckhi Seas, Beaufort Sea, Svalbard Waters, Barents Sea and Russian Arctic Ocean) and subarctic regions (East Coast Canada, Baltic Sea, Sea of Azov,

Caspian Sea and Offshore Sakhalin). From this analysis Table 3.1 is provided with key dimensions for arctic and subarctic ice ridges.

Table 3.1: Mean statistical values for ridge geometries in arctic and subarctic regions [41]

	Arctic ridges	Subarctic ridges	All ridges
Maximum sail height (m)	2.1	1.6	2.0
Average sail height (m)	0.8	0.6	0.7
Sail width (m)	12.8	9.8	12.1
Maximum keel depth (m)	8.2	7.8	8.0
Average keel depth (m)	4.8	4.2	4.5
Keel width (m)	33.6	41.2	36

Another relevant parameter for ice ridges are the block dimensions. Looking at average thicknesses for blocks, it commonly measured between 0.2 and 0.4 m [41]. Subarctic blocks can be assumed to have a maximum thickness of around 0.6 m, where as first-year blocks from an Arctic sea can be up to 2 meters in thickness, depending on the circumstances.

To assess the consolidation of the first-year ice ridges the macro-porosity (η_{macro}) and the consolidated layer needs to be studied. The macro-porosity indicates the degree of consolidation and improves the estimation of the force an ice ridge can exert on a structure, such as a point absorber. The macro-porosity is the volume of air, water or any other non-ice material in an ice ridge, divided by the total volume. The macro-porosity varies over the ice ridge. Average macro-porosities for the ridge itself are 22.1% with a region-dependent-average range of 13% up to 30.8%, for the sail it's 17.6% with a range of 4.7% to 33% and for the keel rubble 19.9% and a range of 7% to 29.5% [41]. Note that the macro-porosities are very much region dependent due to different rafting-processes per region and usually vary widely from the average numbers.

The consolidated layer itself is crucial for the determination of the horizontal action loads. The ISO-code [13] propose a relationship for the horizontal action caused by first-year ice-ridges F_r, which is the sum of the action component due to the consolidated layer F_{cl} as well as the keel action component F_k. It neglects the action component from the sail due to the small volume in comparison to the keel in first-year ice ridges.

$$F_r = F_{cl} + F_k \tag{3.1}$$

The average thickness of the consolidated layer for all ridges and ridges in the arctic and subarctic regions is visualized in Table 3.2.

Table 3.2: Statistical values for average thickness of consolidated layer in arctic and subarctic regions [41]

		Arctic	Subarctic	All ridges
Average CL thickness	Mean	1.77	1.25	1.60
	Max	6.00	3.64	6.00
	Min	0.30	0.30	0.40

3.2.3. Global ice actions

Ice ridges are expected to be the governing loads for ice actions in regions with only first-year ice. It is difficult to determine the exact loads given by an ice ridge, an upper bound estimation of the horizontal action caused by a first-year ice ridge F_R is given in Equation 3.1. For this equation, the

action component F_{cl} can be determined using Equation 3.2 for the global actions due to ice crushing [13]. The equation is designed for vertical interaction surfaces. The HSST-buoy from Project WESA, which can be seen in Figure 2.7 is sloped instead of vertical. However, as the buoy will be pushed inwards, the surface will effectively be vertical when the interaction takes place. Therefore the global ice action will be based on horizontal surfaces.

$$F_{cl} = p_G A_N \tag{3.2}$$

where

- p_G is the ice pressure averaged over the nominal contact area associated with the global action;
- A_N is the nominal contact area, which is the contact area of ice thickness H_{cl} multiplied with the width of the contact area of the consolidated layer w_{ccl}.

The ice pressure p_G tends to be one of the most crucial parameters in the design against ice loads. It is influenced by the ice temperature, the nominal contact area, the aspect ratio of the contact area, the shape and nature of the contact area, the displacements between the structure and ice, the compliance of the structure and also the relative speed. It can vary significantly in time and it's peak values usually depend on the recording frequency. The ice pressure can be calculated using the following formula (in MPa) [13]:

$$p_G = C_R \left[(\frac{H_{cl}}{h_1})^n (\frac{w_{st}}{H_{cl}})^m + f_{AR} \right] \tag{3.3}$$

where

- w_{st} is the projected width of the structure in meters;
- H_{cl} is the ice sheet thickness in meters;
- h_1 is a reference thickness of 1 meter;
- m is an empirical coefficient, equal to -0.16;
- n is also an empirical coefficient which depends on H_{cl}, it is equal to -0.50 + $H_{cl}/5$ for $H_{cl} < 1$ m and -0.30 for $H_{cl} \geq 1$ m;
- C_R is the ice strength coefficient in MPa;
- f_{AR} is an empirical term given by $f_{AR} = e^{\frac{w_{st}}{3H_{cl}}} \sqrt{1 + 5\frac{H_{cl}}{w_{st}}}$.

The unconsolidated keel action component F_k can be estimated using a passive failure model, a previously determined formula for this is [13]:

$$F_k = \mu_\phi H_k w_{st} (\frac{H_k \mu_\phi \gamma_e}{2} + 2c_{app,keel})(1 + \frac{H_k}{6w_{st}}) \tag{3.4}$$

where

- $\mu_\phi = \tan(45° + \frac{\phi}{2})$ is the passive pressure coefficient;
- ϕ is the angle of internal friction;
- $c_{app,keel}$ is the apparent keel cohesion, where an average value over the keel volume should be used;
- w_{st} is the structure width;
- H_k is the height of the keel;
- γ_e is the effective buoyancy, which is consistent with c in units.

The effective buoyancy is given by:

$$\gamma_e = (1 - e_k)(\rho_w - \rho_i)g \tag{3.5}$$

where

- e_k is the keel porosity;
- ρ_w is the water density;
- ρ_i is the ice density.

The equations from this chapter are limited to determining initial contact forces for a moored buoy. The load calculation will change during the rotation and submersion of the buoy. This interactive process is not taken into account.

3.2.4. Actions due to ridge-building processes

Ridge-building is an ice-process that occurs when an ice ridges rests against a structure, floating ice piles up behind the ice ridge, creating an extra force. Floating point absorbers will have a limited resistance against the ice ridge due to the differences in scale, therefore the influence is not expected to be significant.

3.2.5. Ice crushing

Ice crushing occurs when the contact force exerted on the ice ridge itself exceeds the maximum pressure of the ice. This will happen at the following point:

$$p_{ice} = \frac{F}{A_{contact}} \Rightarrow F_{max} = p_{ice,max} A_{contact} \tag{3.6}$$

Where

- $A_{contact}$ is the contact area of an ice block.
- $p_{ice,max}$ is the maximum ice pressure, or the compressive ice strength.

Equation 3.6 shows the dependency on the contact area and the compressive ice strength. This is also different for the ice ridge consolidated layer and the keel, as the consolidated layer is stronger. For the consolidated layer ice crushing occurs when the force is higher than the force from Equation 3.2.

For the ice ridge keel it happens more quickly due to the smaller contact area of an ice block, which is following the typical values for block dimensions in Chapter 3.2.1, approximately 0.5 times 0.5, or a contact area of 0.25 m². The compressive ice strength of first year is dependent on various factors and it is hard to pick an exact value. Estimates in the summer are up to 4.1 MPa [42].

3.2.6. Other ice action considerations

Besides the global loads, the actions due to ridge-building and ice crushing, there are several other ice actions to be taken into consideration for the collision between an ice ridge and a moored point absorber. These considerations are as follows:

- Ride-down/up of the ice from initial point of contact and/or rubble building and intrusion of ice into the point absorber structure.
- Orientational changes of the point absorber due to contact with the ice ridge.
- Ice frozen in the point absorber or presence of ice lodging to the point absorber.
- Direct ice actions on the mooring lines.
- Friction between the ice and the hull of the structure.
- The condition of the surface coating of the hull and how it performs during an entire design life service.
- Buffering of surrounding drift ice.

- Accumulation of ice during ice crushing.

3.3. Hydrodynamic forces

The hydrodynamic forces that would play a role in the collision between a point absorber and an ice ridge are the wave forces, the added mass effect on the point absorber, the drag forces due to the motion of the point absorber and the buoyancy forces. This thesis aims to solve the problem of the collision, including the hydrodynamic forces, by using Computational Fluid Dynamics (CFD). The most common type for modelling WECs while using CFD is based on an incompressible representation of the Navier-Stokes equations. Another option is the use of compressible two-phase CFD-models which is has a better use-case when the assumption of incompressibility is no longer valid, which can be the case when air has a significant effect on the dynamics of a WEC (e.g. in storm conditions). A more recent development in WEC-modelling is the use of Smoothed-Particle Hydrodynamic Models (SPH), this uses a Lagrangian meshless method. These models represent the fluid as a mass of particles that are interacting with each other, this interaction between the particles and the boundaries is dictated by the governing hydrodynamics [43].

The underlying physical laws of CFD are describing fluid flow using a system of partial differential equations (PDEs), which are the well known Navier-Stokes equations together with the continuity equation. They are given together with internal and external boundary conditions that are necessary to define the geometry of the WEC, which is in this case the point absorber. This thesis aims to model the collision between an ice ridge and a point absorber by using SPH-software.

3.3.1. SPH formulation

For the SPH-formulation this thesis focuses on the formulation used by DualSPHysics. The SPH-method uses a technique that discretises a continuum using a set of material points or particles. If this is used for fluid dynamics, this means that the discretised Navier Stokes equations (partial differential equations that describe the motion of viscous fluid substances) are locally integrated at the location of each of those particles, in accordance with the surrounding particles and their physical properties. The governing equations in SPH are the Navier-Stokes equations in discrete SPH formalism, the system of equations is thus as follows [44]:

$$\frac{d\mathbf{r}_a}{dt} = \mathbf{v}_a \tag{3.7}$$

$$\frac{d\mathbf{v}_a}{dt} = -\sum_b m_b \left(\frac{p_b + p_a}{\rho_b \rho_a} + y_{ab} \right) + \nabla_a W_{ab} + \mathbf{g} \tag{3.8}$$

$$\frac{d\rho_a}{dt} = -\sum_b m_b (\mathbf{v}_a - \mathbf{v}_b) \nabla_a W_{ab} + 2\delta hc \sum_b (\rho_b - \rho_a) \frac{\mathbf{r}_{ab} \nabla_a W_{ab}}{\mathbf{r}_{ab}^2} \frac{m_b}{\rho_b} \tag{3.9}$$

where t is the time, r is the position, v is the velocity, p is the pressure, ρ is the density, m is the mass, c is the speed of sound, g is the gravitational acceleration and y_{ab} is the viscous term, which is the artificial viscosity. W_{ab} is the kernel function, which depends on the normalized distance between a and b.

The kernel function, for the smoothing kernel is important for the performance of the SPH model. Kernels are defined as functions of the non-dimensional distance between particles, which is given by dividing the distance between any two particles (a and b) with the smoothing length. The smoothing length controls the size of the area around particle a, which considers all neighbouring particles. In SPH-software DualSPHysics you have an option to choose between two kernel definitions, namely the cubic spline and Wendland kernel function.

The mass of each particle remains constant during a weakly-compressible SPH simulation, only the associated density fluctuates. The density changes are computed by solving the conservation of mass or continuity equation in SPH form:

$$\frac{d\rho}{dt} = \rho_a \sum_b \frac{m_b}{\rho_b} \mathbf{v}_{ab} \nabla_a W_{ab} \tag{3.10}$$

DualSPHysics treats fluid as compressible. That means that fluid pressure is calculated as a function of density, rather than a Poisson-like equation. To make the time steps still reasonable, the compressibility is adjusted in order to artificially slow the speed of sound. The system is closed by the addition of Tait's equation of state [44].

$$p = \frac{c^2 \rho_0}{\gamma} \left[\left(\frac{\rho}{\rho_0} \right)^{\gamma} - 1 \right] \tag{3.11}$$

In this equation $\gamma = 7$, which is the polytropic constant which influences the stability of simulations and ρ_0 is the reference density of the fluid.

Within DualSPHysics there is also an option to implement density diffusion terms [45] and the software makes use of a shifting algorithm to prevent instabilities [46]. In DualSPHysics 2 different explicit time integration schemes are included, namely the Verlet scheme [47] and the Symplectic Position Verlet scheme [48].

DualSPHysics offer different options for boundary conditions, the boundary is explained as a set of particles which are considered to be a separate set with regards to the fluid particles. DualSPhysics allows for solid impermeable boundaries, periodic open boundaries and methods that allow boundary particles to be moved according to fixed forcing functions. The default option for boundaries is the Dynamic Boundary Condition (DBC) [49]. In this method the boundary particles satisfy the same equations as the fluid particles, while not moving according to the forces that are applied to them. The boundary particles remain either fixed or they move according to an imposed motion function, which is relevant for floating objects. Other options for boundary conditions include periodic open boundary conditions, pre-imposed boundary motion, fluid-driven objects and a modified Dynamic Boundary Condition (mDBC), which can be used as a method to assess some of the drawbacks of the DBC, such as over-dissipation, non-physical values for density and pressure or non-physically large boundary layers.

3.3.2. Collision mechanism

DualSPHysics has the functionality to be coupled with the Discrete Element Method (DEM) and other software such as Project Chrono and MoorDyn.

For solid-solid interaction DEM can be used. In DEM you consider contact laws to account for interaction forces, which allows for the computation of rigid particle dynamics. In this way you can solve solid-solid and solid-fluid interactions. In DEM the forces are split into normal and tangential components, with restitution coefficients and friction models. DEM has strict time step restrictions due to the use of the explicit integration methods, which requires small steps for stability. DEM is more suitable for more simplified cases in comparison to Project Chrono.

The other option for solid-solid interaction is Project Chrono, which is a multi-body solver that has an open-source library with many applications such as wheeled vehicles moving on deformable terrains, but more relevantly, fluid-solid interaction phenomena [50]. DualSPHysics used the rigid body, constraints and collision detection parts of Project Chrono's library. This allows DualSPHysics users to compute interactions between bodies in a more stable manner than the DEM implementation. The flowchart of coupling between DualSPHysics and Project Chrono is shown in Figure 3.3. The validation and description of the workings of project Chrono can be found in [51].

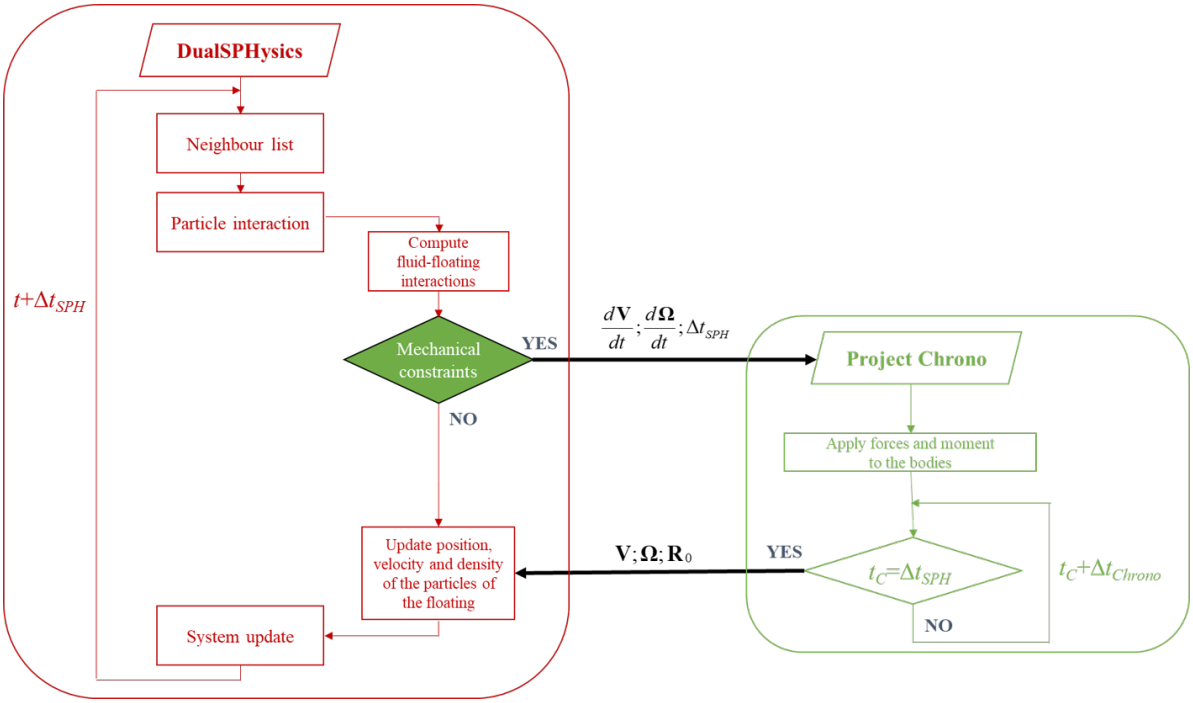

Figure 3.3: Flowchart of the coupling between DualSPHysics and Project Chrono

Within DualSPHysics project Chrono offers options for either Non Smooth Contacts (NSC) and Smooth Contacts (SMC). NSC is a rigid and complementarity-based contact model that enforces non-penetration and Coulomb friction via impulse and constraint solving. The contacts are hard and the impulses are computed instantaneously. SMC is a penalty-based contact model (as a spring-dashpot) with compliance and damping. The contacts allow for small penetrations and generate continuous forces via stiffness/damping parameters. This is suitable for soft interactions but leads to more instability within the model.

3.3.3. Mooring system

Within DualSPHysics, MoorDyn can be used. MoorDyn is a model that can be used to determine the tension forces. It is an open-source dynamic mooring line model that has been designed to be coupled with other numerical models [52]. It discretizes mooring line points as point masses (nodes i) which are connected by linear spring-damper segments to provide for elasticity in the axial direction. Using $\mathbf{r}_i$ and $\mathbf{r}_{i+1}$ to represent the absolute position vectors of adjacent nodes, you can connect the strain segment $(i+1/2)$, which is calculated as

$$e_{i+1/2} = \left(\frac{|\mathbf{r}_{i+1} + \mathbf{r}_i|}{l} - 1 \right) \tag{3.12}$$

In this equation l is the unstretched length. Next up you can calculate the tension forces that act within each segment due to material stiffness and internal damping, which are (respectively):

$$T_{i+1/2} = E\frac{\pi}{4}d^2 e_{i+1/2} \tag{3.13}$$

$$C_{i+1/2} = C_{int}\frac{\pi}{4}d^2\frac{\partial e_{i+1/2}}{\partial t} \tag{3.14}$$

Where d is the diameter of the line, E is the elasticity modulus and C_{int} is the internal damping coefficient. For chains, which exhibit minimal internal structural damping, a small amount of structural damping is incorporated into the model to critically dampen non-physical resonances that may arise at the natural frequencies of individual segments due to discretization. Bending and torsional stiffnesses

are neglected. Hydrodynamic damping and added mass are modelled using the Morison equation, applied to each node. The tangent direction at a node i is approximated as a unit vector aligned between the adjacent nodes:

$$\hat{\mathbf{q}}_I = \left(\frac{\mathbf{r}_{I+1} - \mathbf{r}_{I-1}}{|\mathbf{r}_{I+1} - \mathbf{r}_{I-1}|} \right) \tag{3.15}$$

And from the Morison equation, you have the transverse drag force $\mathbf{D}_n$ and the tangential drag force $\mathbf{D}_t$ direction, which applied to node i are then respectively:

$$\mathbf{D}_{ni} = \frac{1}{2}\rho_{,v} C_{,dn} l \cdot d \cdot \left[\left(\frac{\partial \mathbf{r}_i}{\partial t}, \mathbf{q}_i \right) \mathbf{q}_i - \frac{\partial \mathbf{r}_i}{\partial t} \left[\left(\frac{\partial \mathbf{r}_i}{\partial t}, \mathbf{q}_i \right) \mathbf{q}_i - \frac{\partial \mathbf{r}_i}{\partial t} \right] \right] \tag{3.16}$$

$$\mathbf{D}_{ii} = \frac{1}{2}\rho_w C_{di} l \cdot d \cdot \left[\left(-\frac{\partial \mathbf{r}_i}{\partial t} \cdot \mathbf{q}_i \right) \mathbf{q}_i \left[\left(-\frac{\partial \mathbf{r}_i}{\partial t} \cdot \mathbf{q}_i \right) \mathbf{q}_i \right] \right] \tag{3.17}$$

Which has the transverse C_{dn} and tangential C_{dt} drag coefficients. The forces are calculated while assuming quiescent water. In MoorDyn's calculation of hydrodynamic loads, the wave kinematics are neglected. The added mass on each node is calculated as a matrix:

$$\mathbf{a}_i = \rho_w \frac{\pi}{4} I \cdot d^2 \cdot \left[C_{an} \left(\mathbf{I}_m - \mathbf{q}_i \mathbf{q}_i^T \right) + C_{ai} \left(\mathbf{q}_i \mathbf{q}_i^T \right) \right] \tag{3.18}$$

Which has the transverse C_{an} and tangential C_{at} added mass coefficients. $\mathbf{I}_m$ represents the identity matrix. The vertical seabed contact forces B_i are modelled by using a spring-damper approach, while using a stiffness and damping coefficient with magnitude:

$$B_i = l \cdot d \left[(z_b - z_i)\, k_b - \frac{\partial z_i}{\partial t} c_b \right] \tag{3.19}$$

The model is activated when the elevation of a node, z_i, falls below the defined seabed depth, z_b. It remains active only when a node is in contact with the seabed (i.e., when $z_i \leq z_b$). The total equation of motion for each node along a mooring line, incorporating the previously mentioned terms along with the node mass (matrix $\mathbf{m}_{\text{node},i}$) and submerged weight ($\mathbf{W}_{\text{sub},i}$), is given by:

$$\left(\mathbf{m}_{\text{node},i} + \mathbf{a}_i \right) \frac{\partial^2 \mathbf{r}_i}{\partial t^2} = \mathbf{T}_{i+1/2} - \mathbf{T}_{i-1/2} + \mathbf{C}_{i+1/2} - \mathbf{C}_{i-1/2} + \mathbf{W}_{\text{sub},i} + \mathbf{B}_i + \mathbf{D}_{ni} + \mathbf{D}_{ii} \tag{3.20}$$

This is then a 3x3 matrix, solved for each node within a constant-time-step by using a second-order Runga-Kutta integrator.

MoorDyn supports the use of catenary and slack moorings, taut and semi-taut lines and can also be adjusted to account for tension leg mooring systems. The system uses a lumped-mass model with line segments that include axial stiffness, internal damping, weight/buoyancy, hydrodynamic drag and seabed contact/friction forces. MoorDyn does not have an option to just "toggle" on different configurations, but the line properties and geometry can be adjusted to obtain the desired behaviour of the mooring line.

One feature of MoorDyn is that it automatically computes the initial static equilibrium of the mooring system before the start of the simulation. This means that if a line's unstretched length exceeds the distance between the attachment points, it will sag (slack) with minimal tension and if it's shorter, the line will be stretched from the start, thus creating pretension. This option is set to kick in at 0.50 seconds as standard value.

MoorDyn has proven to be reliable & computationally efficient for common offshore energy mooring scenarios, typically in the order of twenty segments per mooring line [52]. The flowchart for two-way coupling MoorDyn with DualSPHysics is shown in Figure 3.4. Using MoorDyn itself has a negligible amount of extra computational costs in comparison to solving SPH-models.

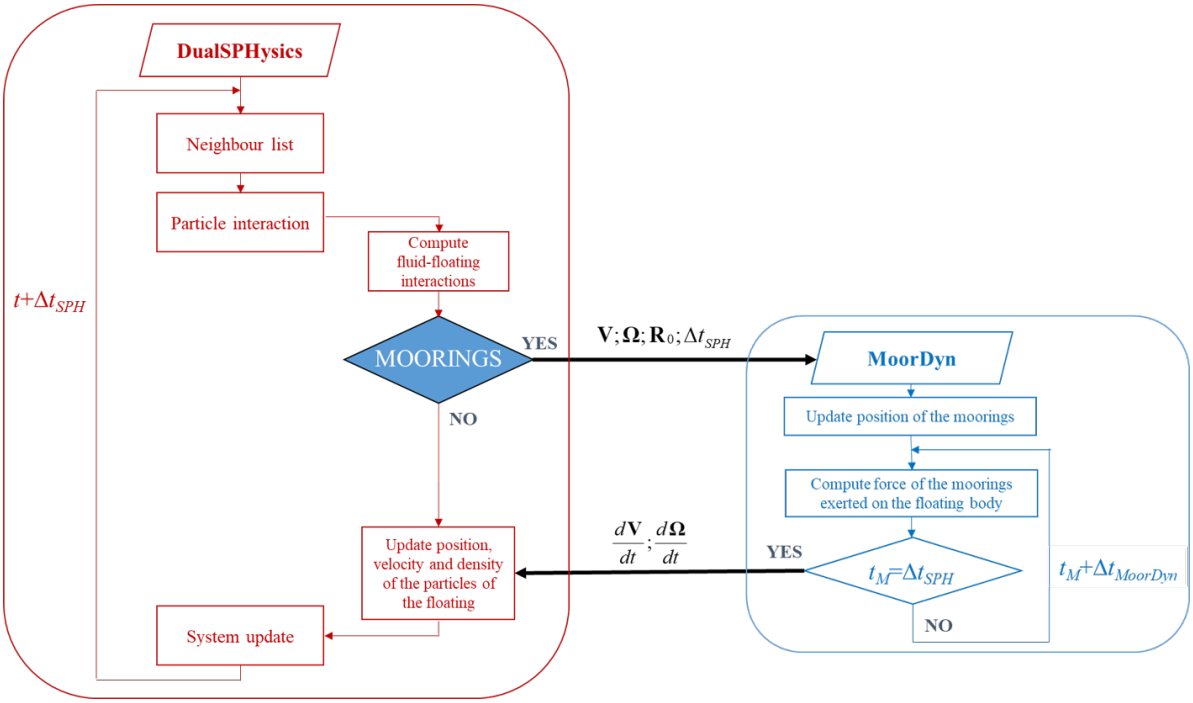

Figure 3.4: Flowchart of the coupling between DualSPHysics and MoorDyn

3.4. Mooring and anchoring forces

This section focuses on mooring and anchoring forces, the design options for the mooring lines or anchors are discussed in Chapter 4.1.

3.4.1. Mooring design

The ISO standard on Arctic Offshore Structures [13] does not provide specific guidelines for the calculation of forces on moored structures, they only provide the ice load forces discussed in Chapter 3.2.3. Regarding results from previous tests, in [12] a physical test was performed for a moored arctic floater against first-year sea ice ridges, featuring a 1:40 model of the Sevan FPU-Ice, which is a floating circular structure. The results in this test were compared to the calculated horizontal ridge forces from the ISO recommendations and showed that the ISO 19906 for the most part underestimated the measured forces, the range of discrepancy was ranging from an overestimation of 27% to an underestimation of up to 50%. The analysis of the test from [12] also showed the following findings:

1. The maximum mooring force increased with the mean cross-sectional area of the ice ridges, which is in contrast to the ISO 19906 standard which only involves the keel depth as geometric parameter in it's calculations.
2. The ISO 19906 is not able to capture any influence from the floater response, but the test showed indications that this influence does exist.

However, the Sevan FPU-Ice is not expected to act the same as a point absorber. The Sevan FPU-Ice is a stronger structure that will be able to deliver more resistance against the ice ridges. The behaviour upon impact of the ice ridge is thus expected to be different than from a point absorber.

Due to these reasons, it is unreliable to use analytical calculations provided in the ISO-guidelines. The loading forces for the mooring lines will be determined using MoorDyn, as mentioned in Chapter 3.3.1, under the paragraph of MoorDyn. The software will compute the tension force of the moorings exerted on the floating body and update the system. The formulation behind this can be found in the same paragraph.

3.4.2. Anchor design

The ISO 19906 refers to the ISO 19901-4 and ISO 19901-7 for the design of anchors, these guidelines do provide considerations when constructing in frozen soil or permafrost. This is not directly relevant for the construction of the anchors for a wave energy converter, since they can be constructed in ice-free periods and the ground underneath the sea is not subject to permafrost in the regions where wave energy farms can be expected to be built.

3.5. Additional influencing forces

Besides the forces named in the previous section, there are other forces that could play a role in modelling the collision between an ice ridge and a wave energy converter.

3.5.1. Dynamic forces

The vibrational response is a dynamic force that can play a role in the collision. The collision itself may induce vibrations in the point absorber, which then could lead to fatigue damage over time if the structure is subjected to repeated impacts. However this is beyond the scope of this thesis. Another dynamic force is resonance, but since the non-periodic nature of ice ridges it is unlikely to happen.

3.5.2. Environmental forces

Apart from the ice loads (see Chapter 3.2.3), the environmental forces on the point absorber are current, wave, and wind. Because the iceberg collision itself lasts only a few milliseconds, the impulsive contact force from the ice ridge overwhelms any wind or wave- induced loads over the same interval, so those can be safely neglected. By contrast, a steady current both pre-tensions the mooring lines (setting the floater's mean position) and sails the ice ridge into the structure, so it must be modelled. DualSPHysics accommodates this by allowing user-defined current profiles (uniform, linear or parabolic) to capture both pre-stress and advective motion.

3.5.3. Hydrostatic pressure

The collision may cause changes in hydrostatic pressure distribution around the WEC, especially if the WEC is partially submerged or if the ice ridge affects the water flow around the structure. In DualSPHysics, hydrostatic pressure is not imposed as a separate load but instead emerges naturally from the SPH formulation: each fluid particle carries density and pressure values that evolve under gravity and the chosen equation-of-state, so the solver enforces $\Delta p = \rho g$ at rest and automatically reproduces the correct buoyant forces on any submerged surface. This means that, even though we neglect hydrostatic variations during the millisecond-scale ice collision, the constant background hydrostatic pressure that sustains the WEC's flotation is inherently present in the simulation and requires no additional "buoyancy" or "hydrostatic" module.

4

Point Absorber

This chapter provides an overview of the point absorber-type wave energy converter, covering various types of point absorbers, structural aspects such as hull integrity, different mooring line configurations and maximum mooring line tensions

4.1. Point Absorbers

4.1.1. Point absorber types

Within the concept of the point absorber, or single-heaving buoys, there are different concepts. Examples of point absorbers which are in development or currently used are shown in Figure 4.1, which include the point absorbers of the Swedish company Seabased (a), which were used in the Sötenas Project in 2016 [53] and is planned to be used in projects in several countries, such as Grenada [54] and Bermuda [55]. Another Swedish company, called CorPower Ocean (b) is currently developing point absorbers that are planned to be used off the coast of West Ireland in 2029 in the Saoirse Wave Energy Project [56], and as an array of four devices in Viana do Castelo [57]. The American company OPT developed the PB3 Powerbuoy® (c) which offers a reliable solution for maritime power needs [31].

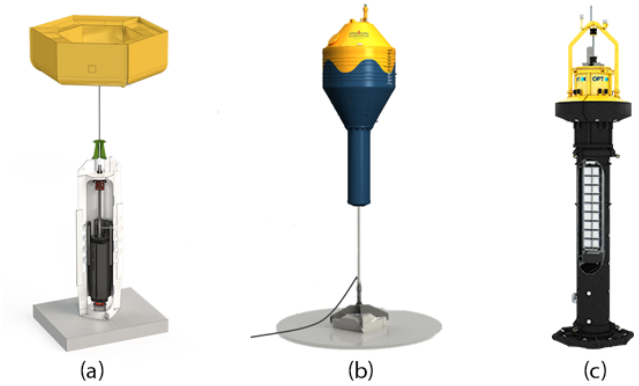

Figure 4.1: Point absorbers: (a) Seabased's WEC, (b) CorPower Ocean's WEC, (c) PTO's PB3 Powerbuoy®

Point absorbers are usually either gravity based or moored, in this thesis the scope is limited to focus on moored point absorbers. The moored point absorber can roughly be divided into 3 parts.

- The hull: The upper part of the point absorber, this part will be the first to come into contact with the ice ridge and needs to be able to handle the direct impact of the ice ridge.
- The reactor: The middle part of the point absorber, which varies per point absorber concept and consists out of several parts, such as the generator.

- Mooring system: The mooring lines underneath the WEC and the anchors, which can also be seen as the foundation of the point absorber.

4.1.2. Point absorber hull

As the hull can be exposed to large ice loads, its hull integrity is an important topic to research. For the floating buoy project within the WESA project, the buoy was made out of steel to survive the ice action, and had a hexagon shape with six sections [9]. Each section of the floating buoy had a slope shape, this shape allowed to get a vertical motion downwards under the ice pressure.

The materials used for the hull of a point absorber are usually determined on factors such as durability, buoyancy, resistance against corrosion, cost and ease of fabrication. Materials that could be used for hulls include (stainless) steel, aluminium and various forms of composite.

To survive the impact of ice ridges, the hull needs to have high impact resistance to be able to perform in low temperatures. As the buoy can be pushed down by the ice, the buoyancy management of the hull should also be taken into account. In Project WESA [37] a steel hull was used. Typically S355 steel is used in marine structures [58].

The shape of the buoy can influence it's hydrodynamic efficiency, meaning how it interacts with waves. As well as the dynamic behaviour of the WEC. It is also important for the stability and survivability of the WEC. Common used shapes are cylindrical, spherical or conical buoys.

As mentioned before in Chapter 2.3 and visualized in Figure 2.7, a HSST buoy was designed to survive ice action during the winter. The HSST buoy survived large drifting ice fields, which were made up of broken and consolidated ice with a thickness of up to 15 cm.

To withstand potential damage from ice ridge collisions, the hull must be sufficiently thick. The use of S355 steel, with its high yield strength, allows for reduced plate thickness while maintaining structural integrity. However, additional thickness is necessary to accommodate long-term corrosion and ice-induced abrasion, particularly given the point absorber's operation in saline waters. A few extra millimetres provide a practical allowance for wear and environmental degradation.

Previous studies involving point absorbers with a diameter of 6 meter recommended a minimum hull thickness of 22.5 mm to ensure structural safety under extreme wave loading conditions [59]. Although these scenarios involve significant dynamic forces, they serve as valuable benchmarks. Structural robustness can also be enhanced by incorporating internal reinforcements such as frames, bulkheads, and ribs, which reduce reliance on plate thickness alone.

By contrast, ice-breaking cones used on offshore wind turbine foundations may require hull thicknesses of up to 70 mm, as these structures are designed to actively crush ice [60]. This represents a fundamentally different loading scenario than the passive resistance expected of the point absorber.

4.1.3. Mooring line systems

The point absorber can be modelled with different types of mooring systems. An overview of the most used mooring line systems is as follows:

1. Catenary mooring: the use of heavy chains or ropes lying on the seabed, forming a natural curve. Catenary moorings are simple and robust and suitable for deep water and due to the chain weight can also reduce peak loads because of the passive damping. Downsides include the need for large horizontal space, high material and installation costs and being unsuitable for shallow or congested areas.
2. Taut Mooring: synthetic ropes (e.g. polyester) that are pre-tensioned between anchors and the device. They excel at the use of space and are ideal for arrays. They are less expensive than catenary moorings. However they don't handle large loads as well as catenary moorings.
3. Tension-leg mooring: a system with vertical tendons under high tension, anchored to the seabed.
4. Slack mooring: excess line length that allows for device movement with minimal vertical restraint. This type of mooring absorbs wave energy dynamically, which reduces peak loads and is cost effective for small devices. Downsides are collision risks in arrays due to large seabed footprint.

The difference with catenary moorings is that slack moorings have more line length which will essentially have zero initial tension, laying at the bottom.

5. Hybrid configurations: a combination of multiple mooring line systems.

As mentioned before in Chapter 3.3.1, the mooring lines will be designed using the dynamic mooring line model MoorDyn. More specific information about the underlying principles of the mooring lines within the simulation can be found in the MoorDyn paragraph in Chapter 3.3.1.

4.1.4. Mooring system failure

The mooring system failure can be determined in different ways. The straightforward is directly looking at the failure of the mooring line. However due to the nature of the model, it might be necessary to trigger failure earlier, for example when ice crushing occurs (see Chapter 3.2.5) or when the hull itself is expected to fail due to pressure on the hull.

The failure of the line can be determined by looking at the tensile capacity of a steel mooring line. The maximum tension of steel can be categorized in yielding points and ultimate tensile strength. The yielding will start at 355 to 500 MPa depending on the steel and the UTS is 500 to 900 depending on the steel.

Calculating this for a mooring line with a diameter of 0.15 m, or a radius of 0.075 m, this leads to the following values for maximum tension:

Cross-sectional area:

$$A = \pi r^2 = \pi \times (0.075)^2 = 0.0177\,\mathrm{m}^2 \tag{4.1}$$

Maximum tension for various types of steel (yielding at 355-500 MPa, UTS at 500-900 MPa):

$$\sigma_{\text{allow}} = 355\,\text{MPa} \Rightarrow F = 0.0177\,\mathrm{m}^2 \times 355 \times 10^6\,\text{Pa} \approx 6300\,\text{kN} \tag{4.2}$$

$$\sigma_{\text{allow}} = 500\,\text{MPa} \Rightarrow F = 0.0177\,\mathrm{m}^2 \times 500 \times 10^6\,\text{Pa} \approx 8850\,\text{kN} \tag{4.3}$$

$$\sigma_{\text{allow}} = 900\,\text{MPa} \Rightarrow F = 0.0177\,\mathrm{m}^2 \times 900 \times 10^6\,\text{Pa} \approx 15930\,\text{kN} \tag{4.4}$$

The failure of the hull can also be the determining failure due to plate yield or buckling of the hull. However the plate itself can be strengthened for this case and thus adjusted to survive the ice forces and therefore is not considered to be the failure point of the system.

5

Methodology

In this chapter all used software tools are provided. As well as all properties, parameters and settings for the standard configuration of the simulation and the adjustments for the other cases.

5.1. Methodology

5.1.1. Introduction

To improve understanding on the collision dynamics between an ice ridge and a moored point absorber, a 3D-model is developed using DualSPHysics and the extended functions of the program. The model serves as a simulation of the collision between the ice ridge and the moored point absorber. The goal of the model is to solve the question what will happen when an ice ridge collides with a point absorber. This will be answered by simulating the collision dynamics between the assets while using DualSPHysics.

5.1.2. Model scope

The scope of the model can be divided into the model assumptions, simplifications and limitations. The research scope has already been defined in Chapter 1.2.2. The ice ridge will be a first-year ice ridge with dimensions which are typical for a subarctic ice ridge, and with regional parameters for the Baltic Sea. The simplifications and the limitations are stated in the following subsection.

5.1.3. Simplifications and limitations

An overview of all simplifications and limitations of the model is provided here. The limitations for the forces are already stated in Chapter 3.1.1 and other limitations for the scope are provided in Chapter 1.2.2. A summary of the simplifications and limitations regarding the methodology is as follows:

- The ice ridge itself has the properties of a first-year ice ridge and dimensions typical for subarctic ice ridges with regional properties for the Baltic Sea when properties are regional-dependent.
- The ice ridge is modelled as a single rigid object, with the same physical properties over the entire ice ridge.
- The moored point absorber is simplified into a rigid moored buoy.
- The ice ridge itself is only moved by a current in this model, in a real-life situation ice ridges would be moved as part of the sea ice drift, which is driven by more aspects, which include wind, currents and internal stresses [61].
- For the properties of the seabed, the standard values provided by the modelling software (MoorDyn) are used. As the exact determination of these properties is region-dependent (even within seas) and beyond the scope of this thesis.

5.2. Implementation

5.2.1. Software and tools

The software-usage of the model can be divided into the base, the assets the visualization and the computing resources.

- **Base**: The model itself is built in DualSPHysics (version 5.2.2) [62], which is based C++ and CUDA codes. The base model will be coupled with Project Chrono [50] and MoorDyn [52]. Documentation about the programs can be found in Chapter 3.3.1. As assisting tool, the macro-plug-in DesignSPHysics (version 0.8.0) [63] in FreeCAD is used.
- **Assets**: The assets are the ice ridge and the point absorber, they are designed in Autodesk Fusion, which is a cloud-based 3D modelling tool.
- **Visualization**: The visualization of the results of the model are done in ParaView, which is an open-source visualization tool.
- **Computing resources**: For this project the TU Delft supercomputer called DelftBlue [64] is used to run the simulations at a sufficient precision.

5.3. Overview of cases

The simulation will be run for a variety of cases, which are listed below.

- Case 1: Original configuration.
- Case 1b: Original configuration with maximum tension increased to 5 MN .
- Case 2: Configuration with an adjusted angle for the ice ridge.
- Case 3: Configuration with an adjusted ice ridge size to 75% of original.
- Case 3b: Configuration with an adjusted ice ridge size to 50% of original.
- Case 3c: Configuration with an adjusted ice ridge size to 75% of original and increased maximum tension to 5MN.
- Case 3d: Configuration with an adjusted ice ridge size to 75% of original and increased maximum tension to 5MN.
- Case 4: Configuration with a smooth ice ridge.
- Case 4b: Configuration with smooth ice ridge and increased maximum tension to 5MN.

All cases are derived from the original configuration in Case 1, with targeted modifications to assess the effect of specific parameters and situations. The model parameters and inputs in Case 1 are mentioned in Chapter 5.4. All cases use the same mooring configurations as Case 1, shown in Figure 5.3. The code from Case 1 is visible in Appendix B1, the codes from the other cases are not provided as they're similar to the code from Case 1, except for the mentioned adjustments in each case.

5.4. Model parameters and inputs

In this section, the full numerical setup used to simulate the interaction between an ice ridge and a point absorber is outlined.

5.4.1. Ice ridge properties

For the simulation an ice ridge is modelled. In this chapter the geometrical and material properties of this ice ridge are provided. In Figure 5.1 the asset that simulates the ice ridge is shown. A dimensional breakdown is provided in Appendix A1.

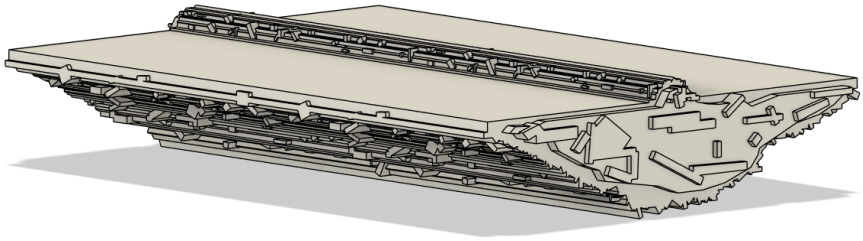

Figure 5.1: Visualization of the Fusion3D-modelled ice ridge, properties are provided in Appendix A1 and Chapter 5.4.1.

Geometrical properties

The ice ridge is modelled accordingly to the mean statistical values for subarctic ridge geometries listed in Table 3.1. To balance realism and conservatism in the model, mean maximum values for ridge geometries will be used instead of absolute maximum values. The values represent the average of the largest observed ridge dimensions in subarctic regions, providing a more representative estimate of ice ridge size while still accounting for significant loading conditions. The maximum width of the sail is decreased in the model from the mean maximum values, to better fit the other geometrical parameters. To simulate the roughness of an ice ridge, the keel is adjusted with a roughness pattern made up by various blocks of up to 0.6 m, as mentioned in Chapter 3.2.1.

For the thickness of the consolidated layer it is difficult to pick an average value, as this very much region dependent. Therefore the known values from the Baltic Sea are chosen as primary design parameters for the consolidated layer. The mean thickness of a consolidated layer of a first-year ice ridge in the Baltic Sea, or more specifically for the Bay of Bothnia region is 0.86 m [41].

The length of the ice ridge itself can be several hundreds of meters long, however to limit the computational resources required for a SPH-simulation, this is limited to 60 m.

To summarize, the properties that will be used for the model are as follows, note that due to the actual properties for keel depth and sail height are slightly different in Appendix A1 due to the added roughness of the ice ridge.

1. The maximum height of the sail is 1.60 m;
2. The maximum depth of the keel is 7.80 m;
3. The width of the sail ranges between 1.50 m up to 4.80 m;
4. The width of the keel ranges between 4.00 m up to 41.2 m;
5. The thickness of the consolidated layer is 0.86 m;
6. The block dimensions represent thicknesses of up to 0.60 m;
7. The ice ridge itself has a length of 60.00 m.

A schematic overview of the ice ridge can be found in Appendix A1. The ice ridge itself is designed in the software tool Fusion3D. The ice ridge is designed by first creating a cross section according to the dimensions mentioned above. In this cross-section the roughness of the keel is created randomly while taken into consideration that blocks are up to 0.6 m. After this the cross-section is extended to 30 m and more random blocks are carved into the side of the ice ridge for more added roughness. This ridge is then duplicated to a total width of 60 m. The total volume of the ice ridge is 14869 m³.

An adjustment for the ice ridge is done in several cases. For Case 3 and Case 3c, the ice ridge is scaled down to 75% the original size. A dimensional breakdown of the to 75% scaled down ice ridge is provided in Appendix A3. The total volume of the 75%-sized ice ridge is 6273 m³. For Case 3b and Case 3d, the ice ridge is scaled down to 50% of the original size, and doubled in length for realism purposes. A dimensional breakdown of the to 50% scaled down ice ridge is provided in Appendix A4. The total volume of the 50%-sized ice ridge is 3670 m³. For Case 4 and Case 4b a smooth ice ridge is used, which means the added roughness of the block dimensions is not applied. The dimensions of the smooth ice ridge are provided in Appendix A5.

Material properties

For the SPH-simulation the ice ridge requires to be given material properties. The relevant properties are the material density, the restitution coefficient and the kinetic friction coefficient.

- Material density: The standard value for ice of 917 kg/m³ is used as density for the ice ridge.
- Restitution coefficient: For an ice ridge, the restitution coefficient will usually vary for the unconsolidated and consolidated parts. However in this model the ice ridge is modelled as a single object thus a single value is chosen. Ice collisions can dissipate substantial amounts of energy due to processes such as deformation and micro-cracking, a lower value of 0.2 is chosen which has been used before in simulations [65].
- Kinetic Friction coefficient: The kinetic friction coefficient that is used in this simulation is 0.07, this has been used before to represent the kinetic friction between the ice and a hull [11].

5.4.2. Point absorber properties

The moored point absorber in this project will be modelled as a single object, further simplified to a moored buoy without a generator. As this buoy is the most critical component to model since it directly interacts with the ice ridge and the surrounding water. By focusing solely on a moored buoy and its interaction with the ice ridge, a solid foundation can be established for understanding the behaviour of the system. In Figure 5.2 the asset that represents the point absorber is shown. A dimensional breakdown is provided in Appendix A2.

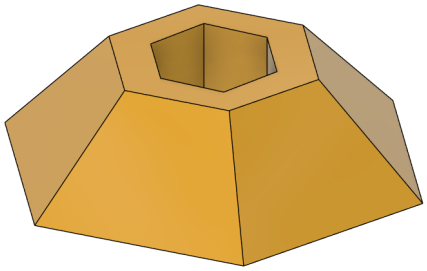

Figure 5.2: Image of the Fusion3D-modelled point absorber, properties are provided in Appendix A2 and Chapter 5.4.2

Geometrical properties

The shape of the buoy is based on the buoy used in Project WESA [37] and mentioned in Chapter 4.1. It can be seen in Figure 2.7. The dimensions of this shape are originally 6×5. As this is designed for level ice and not ice ridges, the size of the buoy will be increased. An increase in size would provide a larger surface area to distribute ice loads. The diameter will be doubled in all directions to 12×10. The original angle of the WESA-buoy is 60°. For the buoy a height of 3 meter is chosen, this allows for allows for a less steep angle than in the original WESA-buoy, which helps the by giving the point absorber more lenience for a downwards motion to go underneath the ice ridge. The sides of the buoy are angled inwards with 45-50°, depending on the side. This does also mean that diameter at the top is smaller.

The thickness of the buoy should be sufficient to withstand ice action, as mentioned in Chapter 4.1. Since the buoy is only required to survive ice actions and not to break ice, a hull thickness of 25 mm is adopted for this study. This value offers a conservative margin for wear and corrosion and aligns with thicknesses reported in similar applications. Further refinement of this thickness could be explored in future work. However, the relevance of this parameter is limited within the current scope, as it only serves to estimate the mass of the point absorber. The internal pressure distribution within the hull is beyond the scope of this thesis.

A schematic overview of the buoy and it's dimensions is visible in Appendix A2. The buoy is created using the basic functions of software tool Fusion3D.

Material properties

The relevant material properties for the point absorber are the mass-body, the restitution coefficient and the kinetic friction coefficient. For the restitution and kinetic friction coefficient the standard values provided by DualSPHysics for steel will be used, which are 0.8 and 0.35 respectively.

The mass-body is determined using the software tool Fusion3D, which calculates the total volume assuming the point absorber is made of steel. This total mass is 45220 kg. The total volume is 5761 m^3.

5.4.3. Mooring system

The mooring system is based on MoorDyn (see Chapter 3.4). Following is a list of adjusted solver options within MoorDyn and all used values and the system used for the mooring system.

Model parameters

- Mooring model time step (s): Set to 1/10th of the coupling time step used in DualSPHysics to ensure stable calculations. Set automatically on 0.0001.
- Water Depth (m): 20.0
- Free Surface (m): 0.0
- Bottom stiffness/damping constant (Pa/m): Parameter that determines the seabed's resistance to penetration. Default value of 3000000.0, it may be lower due to softer sediments that can be found in the Baltic Sea. However the influence of the bottom is beyond the scope of the thesis.
- Damping coefficient (seabed friction damping): Standard value of 200 chosen. This value can be scaled from no friction at no velocity to full friction when the velocity is large. Within the simulation a lower damping coefficient leads to higher peak tension forces.
- Ratio between static/dynamic friction: For marine purposes the static friction is assumed to be approximately 1.2 times the dynamic friction [66], however further research is needed for a better value, this is beyond the scope of this thesis.
- Convergence analysis time step (s): 1.00 (standard setting).
- Factor to scale drag coefficients: 1.00, no scaling is applied.
- Max. time for initial conditions (s): 0.50 (standard setting).

Besides the solver option, MoorDyn also needs a line configuration. In the model itself a slack mooring line set-up will be used.

- Line stiffness (N): The stiffness of the line depends on the material and construction. The line stiffness is the elasticity modulus multiplied by the cross-sectional area. For a steel line, with a typical elasticity modulus of 210 GPa and a diameter of 0.15, this is approximately 3.54×10^9 N/m.
- Line diameter (m): Mooring line diameters are based on on load-bearing capacity and hydrodynamic considerations. In this model the line diameter has been set to 150 mm. The optimal diameter for a point absorber that needs to handle the loads of ice ridges is not determined yet, for level-ice and a moored structure 125 mm is used before [67]. For offshore floating wind turbines steel chain diameters for of up to 230 mm are used [68]. A conservative estimate is made with a rope of 150 mm, which is high enough to survive tensions due to ice ridge collisions.
- Mass per unit length (kg/m): The mass per unit length depends on the material, for steel it is 138.7 kg/m and this is used in the model.
- Line internal damping (Ns): Automatically set in MoorDyn to -0.8 to give a damping ratio of 80% on each segment.
- Transverse added mass coefficient: Estimating an exact value is outside the scope of the thesis, a standard value of 1.0 for a torus is chosen [69].
- Tangential added mass coefficient: Estimating an exact value is outside the scope of the thesis, a standard value of 0.5 for a torus is chosen [69].
- Transverse drag coefficient: It is beyond the scope of the thesis to determine an exact value for the drag coefficient, the automatic value of 1.6 is chosen.

- Tangential drag coefficient: It is beyond the scope of the thesis to determine an exact value for the drag coefficient, the automatic value of 0.05 is chosen.
- Maximum tension for the lines (N): The maximum tension within the simulations is set on 0.625 MN or 5 MN depending on the case. The 0.625 MN is based on the failure mode of the ridge (see Chapter 3.2.5). Using the contact area of 0.25 m² and a slightly higher ice strength (to account for when crushing will actually occur, instead of how much the ice can handle) of 5 MPa, the strength is set on 1.25 MN. A 4-line slack setup would mean 2 lines bearing this load and thus a maximum tension of 0.625 MN. This value is used in Case 1, 2, 3, 3b and 4. The 5 MN is based on an estimate of what a single mooring line can survive, as discussed in Chapter 4.1.4. This is used in Case 1b, 3c, 3d and 4b.

Mooring line set-up

The mooring line-setup is based on a slack mooring line setup. In Figure a top-view of this setup with attachment locations and ground coordinates is shown. The line length used is 33.5 meters for the mooring lines. The mooring line set-up is visualized in Figure 5.3.

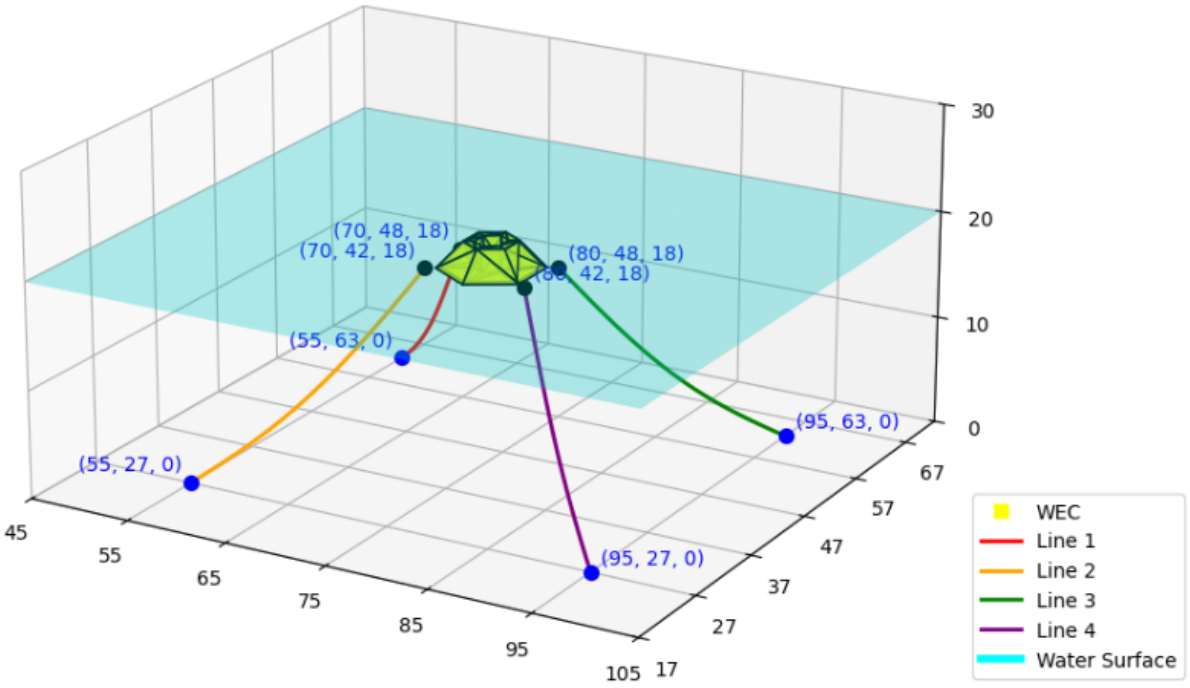

Figure 5.3: Mooring setup for the standard configuration case (note that [1] in the simulation the attachment points are actually attached underneath the WEC and not floating next to them, [2] the set-up has shorter lines in this image, but is slack within the simulations).

A top-view and a side-view of the mooring line setup mooring line set-up is visualized in Figure 5.4.

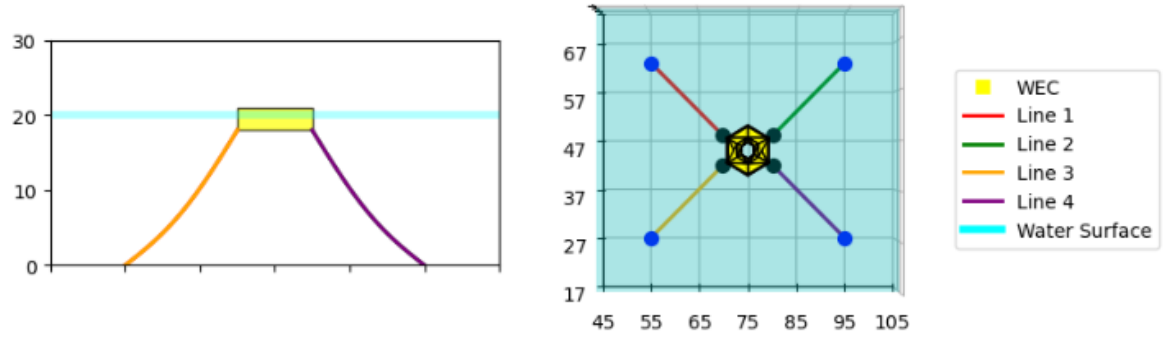

Figure 5.4: Top-view and side-view of the mooring line setup.

The coordinates are relative from the [X,Y,Z] position from the hydrodynamic model, which starts at [0,-10,0]. More information about this model can be found in the following Chapter 5.4.4.

5.4.4. Hydrodynamic model

The hydrodynamic model used is described in Chapter 3.3.1. To translate this to a realistic sea state with a current moving the ice ridge, the following criteria should at least be met in the model:

- The domain length in the wave propagation direction is at least 2-3 times the wave length, to avoid boundary effects.
- The domain width should be wide enough for the ridge to allow for free movement and interaction with waves/currents.
- The point absorber should be far enough from the boundaries to avoid interference with reflected waves or currents.
- The depth should be greater than the total depth of the ice ridge and should leave some room to prevent the ice ridge from hitting the bottom, as well as giving room for the WEC to go underneath.
- The depth should be deep enough that it does not influence the behaviour of the point absorber after the collision.
- The ice ridge should be moved by a speed that works as a compromise between realism and computational efficiency, as the run-time of the simulation will be limited by computational resources.

The criteria established in this model define a ”water-box” with dimensions of 140 × 110 × 20 m, featuring periodic boundaries in the X and Y directions to simulate wave propagation. Maximum current velocities in the Baltic Sea typically range from 0.4 to 0.8 m/s, with localized peaks reaching up to 1.4 m/s [70]. In contrast, the Bohai Sea experiences stronger currents, with values reaching up to 2.0 m/s [71]. To account for these more demanding conditions, a representative surface velocity of 2.0 m/s is selected. To simulate the currents more realistically DualSPHysics offers options for uniform, linear and parabolic velocity profiles. A parabolic vertical velocity profile is applied, with the surface velocity set at 2.0 m/s, a mid-depth velocity of 0.5 m/s, and a bottom velocity of 0.0 m/s. A top-view of the set-up is visible in Figure 5.5.

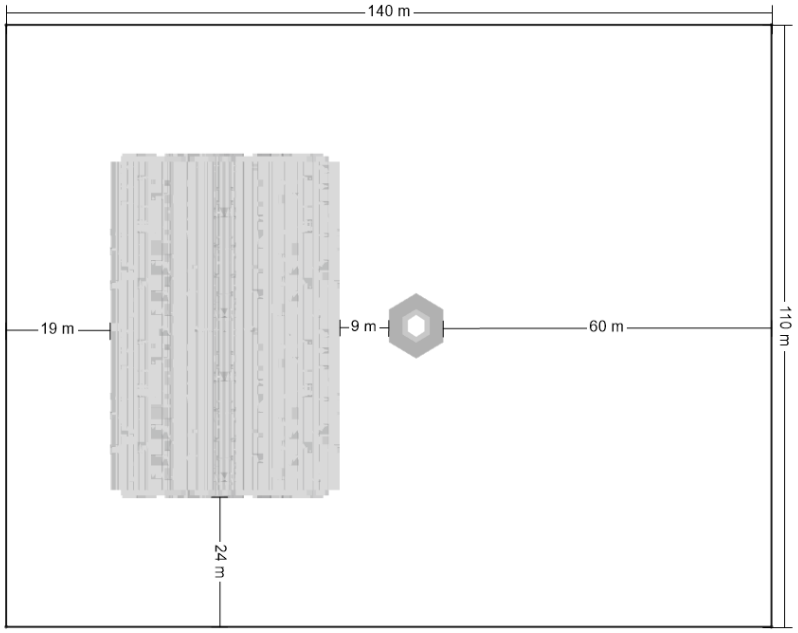

Figure 5.5: Top-view of the simulation set-up, including dimensions

It is important to note, however, that ice ridges are generally driven not by ocean currents, but by ice drift, which is primarily governed by wind and large-scale ice dynamics [61]. Ice drift velocities are typically lower and exhibit different spatial and temporal patterns than ocean currents. Nonetheless, the current-driven forcing applied in this study serves as a proxy for dynamic environmental loading and enables assessment of hydrodynamic interaction with ice features.

Case 2 involves an adjustment to the angle of the ice ridge: instead of approaching it perpendicularly, the ice ridge is rotated 10° to the right. How this translates to the set-up is shown in Figure 5.6. Note that the current direction of propagation remains unchanged.

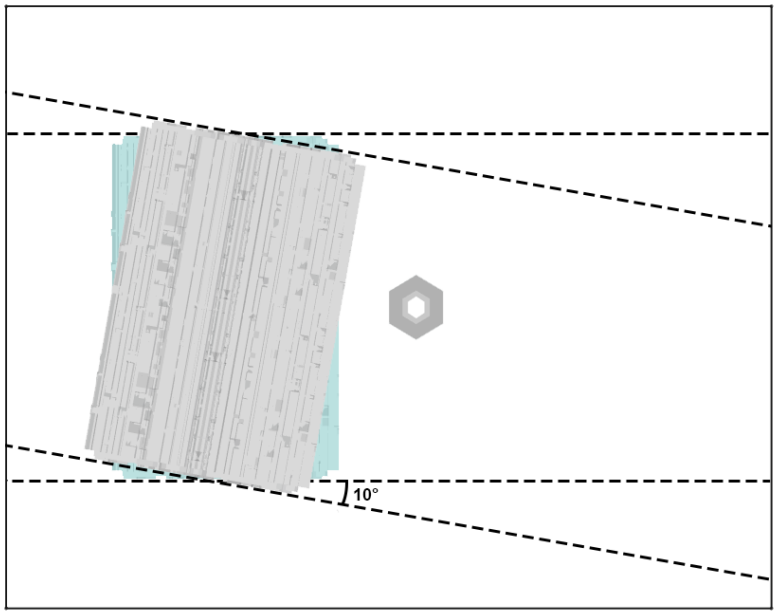

Figure 5.6: Set-up modification for the ice ridge angle adjustment, new position (gray) on top of old position (blue).

5.4.5. Collision mechanics

The collision mechanics within DualSPHysics can be managed using Project Chrono (see Chapter 3.3.2). Project Chrono has options for Non-Smooth Contacts (NSC) and Smooth Contacts (SMC). NSC handles collisions using a constraint-based approach and has as input the restitution coefficient and kinetic friction coefficient. SMC uses compliant formulations with stiffness and damping parameters. Forces are calculated based on penetration depth between bodies, which leads to smoother contact responses. SMC uses the same properties as NSC, extended with the use of the Poisson ratio and Young modulus. In this simulation the collision mechanics are set by NSC, as smooth contacts lead to instability within the results. A parameter for Project Chrono is the collision overlap, which is set by dividing the inter-particle distance by 2 ($2/dp$), which is 0.125 for the used inter-particle distance of 0.25.

5.4.6. Simulation setup

This chapter provides an overview of the simulation set-up from DualSPHysics, which includes the defined constants and the execution parameters within the set-up, as well as an explanation.

Defined constants & execution parameters

For a full overview of all constants that need to be defined and execution parameters, see [72]. In Appendix B1 all decisions are visible, the following options in the simulation are notable or different from the standard option.

- Fluid reference density: Chosen for 1025 kg/m³ based on the standard density for seawater.
- Inter-particle distance: Determines the inter-particle distance between particles in meters. A lower value leads to higher accuracy, however it increases the simulation running time exponentially. A rule-of-thumb is to have at least 10 particles in the shortest length to be realistic. In this simulation a value of 0.25 is chosen, which will be 12 particles in the shortest length (which is the 3 m height of the point absorber).
- Density diffusion term: See Chapter 3.3.1. Chosen for Fourtakes as it is better at handling large simulations and handling density changes at the surface. It is also includes the DDT value, for which 0.1 is standard.
- Solid-solid interaction: Options for SPH, DEM and Chrono. See Chapter 3.3.1 for more information, chosen for Chrono as it is the most realistic option for collisions.
- Time of simulation: Total simulation duration, adjusted based on full collision duration and extended time to look at the behaviour afterwards. Standard set to 60 seconds, but increased to 100 seconds for Case 4b. Cut short in most cases afterwards.
- Time out data: Determines how often simulation data is saved, adjusted to 0.05 to limit the amount of storage needed.
- X/Y/Z Periodicity: Enabled in all X/Y direction to simulate an ocean-like scenario.

6

Results

This chapter provides the results of the performed simulations. This includes an overview of the observed modelling faults and associated limitations as well as the expected loads.

6.1. Modelling faults and associated limitations

To properly assess the results provided in this chapter, the following model limitations should be noted:

- The maximum mooring line tension is intentionally limited to 0.625 MN in specific cases, aiming to simulate line failure when ice crushing occurs at the ice ridge keel, rather than reflecting the actual tension capacity of the mooring lines. However, in these scenarios, the mooring lines already reach the failure tension at the consolidated layer, which is significantly stronger than the keel itself, thus limiting the realism and usefulness of these simulations. Additionally, failure due to ice crushing is indirectly represented through tension in the mooring lines rather than directly through ice-structure contact forces. In the cases where mooring line tension limits are set to 5 MN, the horizontal contact force required for ice crushing is consistently reached within the ice ridge keel, yet the simulation does not reflect line failure at this point. In summary, ice crushing is likely to occur, but its representation is significantly limited by premature line failures in the 0.625 MN cases and is neglected entirely in the 5 MN cases.
- In the cases involving 75%- and 50%-sized ice ridges, the ridge lacks sufficient momentum to break through the point absorber and is instead diverted by it. This behaviour is likely due to the reduced mass of these scaled-down ridges because of the reduced length and because their motion is driven primarily by current rather than by ice drift. In real-world scenarios, however, such diversion is improbable, since the significant length and mass of ice ridges, combined with sustained ice drift forces, would likely cause the ridge to continue advancing and eventually either submerge the point absorber or lead to mooring line failure. It is therefore not possible to say that a point absorber would survive the ice ridge impacts solely because the 5 MN is not reached, as it got stuck and then diverts the ice ridge, which is extremely unlikely in a real scenario with a significantly lengthier ice ridge.
- When mooring lines fail, their visual behaviour in the animations and their numerical output both show inconsistencies. Within the animation the lines remain elongated at the failure value rather than retracting or resetting to zero. This is a fault within DualSPHysics, but it does not affect the behaviour of the point absorber or still active mooring lines. In the output for tension forces this is corrected by manually adjusting the data to zero after failure.
- After mooring line failure, the point absorber fails to resurface within the model, even though it should physically be able to do. This behaviour is unrealistic, as the point absorbers remains intact as it has no modelled failure mechanism. Therefore the post-failure behaviour of the point absorber should be interpreted with caution.
- Visually the mooring lines don't actually lay on the sea-bed floor, which would be usual for a slack

mooring set-up. In the animations they hang below it, as there is no built-in mechanism for the lines to rest flat on the seafloor.

6.2. Expected loads

For the validation of the model this section provides expected loads for the mooring line tensions in the fairleads and the horizontal interaction forces.

6.2.1. Mooring line loads

The mooring lines have a vertical and horizontal offset of 15 meters and are applied at the bottom of the point absorber (at z=18), with the water-table at z=20. The straight-line span of the mooring lines is thus as follows

$$D = \sqrt{15^2 + 15^2 + 18^2} = 27.78 \text{ m}$$

The lines are set to 33.5 m, which is approximately 1.2 times the straight-line span. The slack is $S = 33.50 - 27.78 = 5.72$ m. This means none of the lines are under taut due to the geometry.

Up to 5.72 m the slack line carries zero load, once it is fully taut it will make an angle θ with a vertical, this needs to be corrected:

$$\cos\theta = \frac{\Delta z}{D} = \frac{18}{27.78} \approx 0.648.$$

The buoy weight is $W_b = 45220$ kg $* 9.81 = 4.436 \times 10^5$ N. Split over 4 lines this leads to approximately 111 kN. Applying equilibrium in the vertical direction:

$$4\,(T_{\text{fair}})\,\cos\theta \;=\; W_b \quad\Longrightarrow\quad T_{\text{fair}} = \frac{W_b}{4\,\cos\theta} \approx \frac{4.436 \times 10^5}{4 \times 0.648} = 1.71 \times 10^5 \text{ N} = 171 \text{ kN}.$$

The expected load in the tension lines for the fairleads is thus 171 kN initially. This does not take into account the line weight per unit length, which is 45.6 kN. Based on multiplying the line weight per unit length with the gravitational constant and the total line length.

The expected load assumes all the loads are shared equally across the 4 mooring lines. However because of the current applied to move the ice ridge, the 2 lines in front of the point absorber are expected take up most of the loads. In the DualSPHysics simulation the maximum time for initial conditions to take place is set to 0.5 seconds. As the current is already applied at this point, an exact match of these results is not expected.

6.2.2. Interaction-loads

Chapter 3.2.3 provides the expected global ice actions for the horizontal action. This can not be used to verify the exact results of the simulations, as the ice ridge is modelled as a single object with only properties for material density and a restitution and kinetic friction coefficient. However this is provided to show the differences and to determine if the loads are within an order of magnitude of realistic loads.

The global ice actions are the sum of the action component due to the horizontal layer and due to the keel. The consolidated layer action is as follows:

$$F_{cl} = p_G A_N = p_G = C_R \left[(\frac{H_{cl}}{h_1})^n (\frac{w_{st}}{H_{cl}})^m + f_{AR} \right] H_{cl} w_{ccl} \tag{6.1}$$

To calculate this the following values are taken:

- The ice strength coefficient C_R is 1.8, which is taken as the provided value for ”Temperate”-regions such as the Bohai Sea and Baltic Sea [13].
- The structure width w_{st} is taken as 6 m (largest possible contact width).
- Other parameters are empirical coefficients or can be derived from the dimensions of the ice and structure width, see Chapter 3.2.3 for more information.

The total force depends on the contact area between the ice ridge and the point absorber. The thickness of the consolidated layer H_{cl} is modelled as 0.86 m. However due to the geometry of the ice ridge this can either decrease or increase. For the width of the ice w_{ccl}, it is the portion that actually touches the structure, which also varies due to geometry but is limited to the largest total width of the structure (6 m). Ranges for the total amount of force due the consolidated layer are calculated. Which are based on a horizontal layer thickness of 0.43 m up to 1 m and an ice width of 0.5 m up to 6 m. The ranges can be derived from the data provided in Table 6.1.

Table 6.1: Consolidated layer force F_{cl} (in MN) for various combinations of ice thickness h_{ice} and contact width w_{ice}.

		w_{ccl}		
		0.50	3.00	6.00
H_{cl}	0.43	1.41	2.71	4.37
	0.86	2.75	5.96	8.00
	1.00	3.53	7.77	10.09

The second aspect of the global ice action is the force due to the keel, the unconsolidated keel action component. It is estimated by using the following formula:

$$F_k = \mu_\phi h_k w_{PA}(\frac{h_k \mu_\phi \gamma_e}{2} + 2c_{app,keel})(1 + \frac{h_k}{6w_{st}}) \tag{6.2}$$

To calculate this the following values are taken:

- The angle of internal friction is 25° which is based on ISO-recommendations [13].
- The apparent keel cohesion $c_{app,keel}$ is chosen as 5.5 kPa, which is based on sea ice measurements in the Baltic Sea [73].
- The ice density is 917 kg/m³, the water density is 1025 kg/m³.
- The keel porosity is taken as 0.295. As mentioned in Chapter 3.2.1 the porosity is very region-dependent, therefore a value for the Baltic Sea is chosen [41].
- The structure width w_{st} is 6 m and the keel thickness and the height of the keel h_k is 7.8 m

Using these values and Equation 3.5 for effective buoyancy the unconsolidated keel action component F_k is 1.39 MN. The combined values of consolidated layer action and unconsolidated keel action are thus up to 11.48 MN, depending on the contact area.

6.3. Output

The output from MoorDyn and Chrono is provided in the next two sections.

6.3.1. Mooring-related forces

The mooring-related forces are obtained from the output of MoorDyn, which offers the following output:

- ”Line_X_pos”: an output with the position of each line segment per line.
- ”MoorDynPlus_force”: an output of the forces in x,y,z-direction on the anchor and fairleads, which results in the total tension.
- ”MoorDynPlus_position”: an output of the position of the anchor and the attachment points.
- ”MoorDynPlus_tension”: an output of the total tension on the anchor and fairleads per line.
- ”MoorDynPlus_velocity”: an output of the velocity of the anchor points (always zero) and the attachment points.

The forces, which lead to the the tension forces, determine when the point absorber will be detached from the mooring lines. If the maximum tension is reached the mooring lines will break within the

simulation. To limit the amount of output in this report the focus is solely on the tension forces from the fairleads, as this is the most important parameter for the simulation and decisive in when the mooring lines fail.

The results of the fairlead tensions for all the cases mentioned in Chapter 5.3 are provided in Appendix C1. The results are cut-off after the first mooring line fails due to expected ice crushing, which happens in Case 1, Case 2, Case 3, Case 3b and Case 4.

6.3.2. Interaction-related forces

The interaction-related forces are obtained from Project Chrono, which offers the following output:

- ”ChronoBody_forces”: The x,y,z-components for the total force (N), moment (Nm) on the ice ridge and point absorber and the contact force (N) and moment (Nm) between the ice ridge and point absorber.
- ”ChronoExchange_mkbound_10/20”: mk10 is the Ice Ridge and mk20 is the Point Absorber, provides with information exchanged between Chrono and DualSPHysics, such as the linear and angular acceleration applied from DualSPHysics to the object in Chrono.

To limit the amount of output in the report and only focus on the output that is studied, only the horizontal contact forces are analysed. This is most in-line with the global ice loads, which are similarly represent horizontal loads.

The time-series of horizontal contact forces for all cases described in Chapter 5.3 are presented in Appendix C2. In each simulation, the force record is truncated immediately after the first mooring line failure due to ice crushing in order to isolate the pre-failure dynamics.

In cases where the first line does not fail immediately, a two-stage filtering procedure is implemented: first, a median filter with a window length of 5 samples is used to remove isolated single-sample spikes; second, a 4th-order Butterworth low-pass filter with a cut-off frequency of 3 Hz is applied to suppress high-frequency noise while preserving physically meaningful impact transients. Note that this does lead to negative values, however they can be safely ignored. This methodology improves the realism of the response of the ice ridge-structure interaction. Both results, as well as the raw data, is visualized for the evaluation of the results.

7 Evaluation

This chapter evaluates the results from Chapter 6. This includes a validation of the expected loads from Chapter 6.2.

7.1. Model performance evaluation

This section evaluates the performance of the simulations by comparing the simulation results to the expected physical behaviour and theoretical predictions. As well as notes on the reliability and realism of the results.

7.1.1. Tension forces

As mentioned before in Chapter 6.2.1, the expected tension at the fairleads is 171 kN initially, without taking the current into affect that is expected to put most of the loads on Line 1 and Line 2. These values are expected as initial conditions. The simulation is set in a way that these initial conditions set in at 0.5 seconds. In Figure C.1 this peak can be seen after 0.5 seconds. The measured tension results at this points can be seen in Table 7.1.

Line	**Fairlead** (kN)	
	Measured	Expected
Line 1	170.22	171.14
Line 2	156.67	171.14
Line 3	111.19	171.14
Line 4	109.10	171.14

Table 7.1: DualSPHysics fairlead tensions in Case 1 at $t = 0.5$ s, compared to static predictions.

The loads are close to the expected results. The effect on the current on Line 3 and 4 is visible. The values are not exact as the current is already at play, which adjust the amount of slack in the lines, which influences the tension.

The maximum tension forces are initially based on the strength of the ice ridge keel. However in all cases with a maximum tension of 0.625 MN, the mooring lines fail at the consolidated layer, before the keel of the ice ridge is reached. At the consolidated layer a maximum tension of 12.9 MN would be more fitting before ice crushing occurs, based on the strength of the consolidated layer from Chapter 7.3.1. This means that the tension forces in Case 1, Case 2, Case 3, Case 3b and Case 4 only show that the mooring line tensions will exceed 0.625 MN before reaching the keel. As this is a very limited informative output, the evaluation will be mostly focused on the cases where the limit is set to a maximum tension of 5 MN, which is more in-line with what a mooring line can survive. But it should be noted that the system does not fail in these instances when ice crushing towards the keel of the ice ridge is expected to occur, even though the horizontal contact forces exceed values that normally lead

to ice crushing.

7.1.2. Interaction forces

Chapter 6.2.2 provides expected loads for the horizontal contact forces. In this chapter a range of 3.6 to 11.5 MN is suggested, which was dependent on the nominal contact area. With regards to Case 1, the highest peak is recorded around 3.7 MN, before the mooring system fails within the simulation. In Case 1b, where the system survives the initial impact, the forces adjusted with a Median or Butterworth filter are visibly within the 3.6 to 11.5 MN range, with a highest peak up to 10 MN. The raw data does show higher peaks of up to 25 MN. For the smooth ice ridge, the initial impact has a peak of 10 MN. This peak is higher in Case 4b, reaching 32 MN. When applying filters the median filter and the Butterworth filter, the horizontal contact forces are up to 3 MN in Case 4b.

The extreme peaks did not directly lead to failure in the mooring lines (which are set at 5 MN in this case), failure occurred later. When the point absorber is dragged along the ice ridge, which can be seen in Case 1b and Case 4b, peaks in the horizontal contact forces occur. This is largely due to both objects being defined as rigid, which means that in reality the forces are likely to be less severe. It should also be noted again that these forces thus represent a scenario that omits several real-world effects that could significantly alter the load estimates. First, both the empirical formulas and the simplified contact assumptions assume quasi-static loading; in practice, finite-speed impacts introduce strain-rate–dependent ice strength. Second, energy dissipation due to ice crushing and fracture is not captured by the empirical expressions or by the static-contact approximation, potentially leading to overestimation of peak loads. Third, the current within the simulation set is on the higher side, currents are usually lower than 2 m/s in subarctic seas and ice drift speed is also expected to be slower. And finally, as mentioned before, treating the point absorber and its mooring system as infinitely rigid neglects their compliance, which would reduce peak contact loads. But as the initial loads fall within the order of magnitude of the actual expected horizontal contact forces calculated in Chapter 6.2.2, especially when the median filter and Butterworth filter are applied, it can be used to show the reliability of the results.

7.2. Evaluation of results

This section dives into the results of the cases. In Case 1, Case 2, Case 3, Case 3b and Case 4 the mooring sensitivity strength is set to 0.625 MN, based on expected ice crushing in the keel. In all cases the mooring line system quickly fails within seconds of initial impact. This thus happens before even contacting the ice ridge keel itself, in a real scenario the unconsolidated layer is stronger and ice crushing is not expected to occur for up to 25.8 MN, according to Chapter 7.3.1. From Figure C.10, C.12, C.13 and C.14, which represent the Cases 1, 2, 3 and 3b, it can be seen that the horizontal contact forces have not surpassed this amount. In Case 4, Figure C.17, it is slightly above this boundary, which means that it might crush into the horizontal contact layer. However, for the reasons mentioned before in Chapter 7.1.2, the force is likely to be a somewhat smaller in reality, which means a value just above the maximum boundary will not necessarily lead to ice crushing. After this point the simulation is no longer useable. This shows that 0.625 MN as maximum tension is too low for even the initial impact.

For Case 1b, Case 3c, Case 3d and Case 4b the mooring sensitivity was set to 5 MN. This is more in-line with what mooring lines can be designed for. In this section the the ice ridge geometry variations and the surface characteristics are analysed.

7.2.1. Ice ridge geometry variations

The ice ridge geometry variations are tested in Case 1, Case 1b, Case 3, Case 3b, Case 3c and Case 3d. In the cases there are different sizes, namely a full-sized ice ridge, a 75%-sized ice ridge and a 50% sized ice ridge.

In Case 3c – with an increased maximum tension and a 75%-sized ice ridge – the results are compared to Case 1b. Case 1b and Case 3c are visualized next to each other in Figure 7.1. The fairlead tensions eventually reach the maximum amount of 5 MN in Case 1b. For Case 3c, this does not happen. The fairlead tensions are up to 3 MN, until eventually the fairlead tensions decrease due to the ice ridge being diverted by the point absorber, which can be seen in Animation S6. After this point the fairlead tensions decrease. In a realistic scenario the ice ridge would have more length and be driven by ice

drift, and it would be unlikely that this would happen, but in the simulation it happens due to the limited length of the ice ridge, the current being the only driving force and the ice ridge keel being rigid.

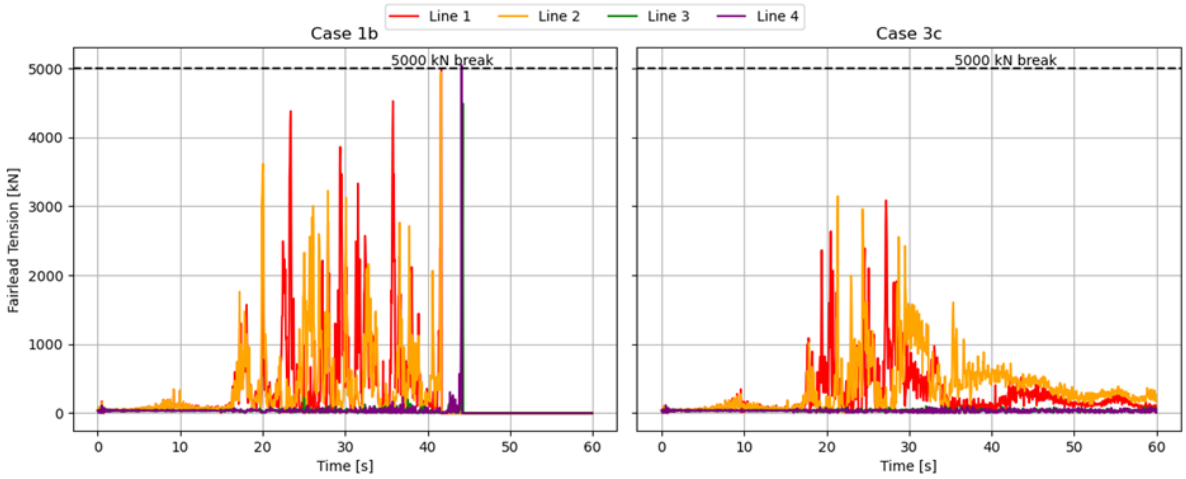

Figure 7.1: Fairlead tensions comparison between Case 1b and Case 3c.

In Case 3d – with an increased maximum tension and a 50%-sized ice ridge – the same behaviour occurs, even with similar fairlead tensions, despite the smaller size of the ice ridge. The results from Case 3d can be seen in Figure C.7 and are put next to each other in Figure 7.5.

To summarize, the simulations for Case 3c and Case 3d are inconclusive about the survivability of a moored point absorber against smaller ice ridges, it does show however that the mooring line tensions and horizontal contact forces are smaller.

Looking at the filtered results for the horizontal contact forces, Case 1b and Case 3c are shown next to each other in Figure 7.2. There is a peak in Case 1b of 10 MN. From Animation S2 it can be seen that this roughly happens at the consolidated layer part, which means it is able to survive this action in the mooring lines. However after 20 seconds, when the point absorber slides against the ice ridge, there are still several peaks up to 5 MN. With ice crushing expected to occur at 1.25 MN, the point absorber is at risk of getting stuck within the ice ridge, leading to entanglement and failure of the mooring lines due to an increase in force due to significantly higher contact areas. In Case 3c, the forces start increasing after 25 seconds. The forces reach a high of almost 6 MN, due to the point absorber being lodged within the keel, as can be seen in Animation S6.

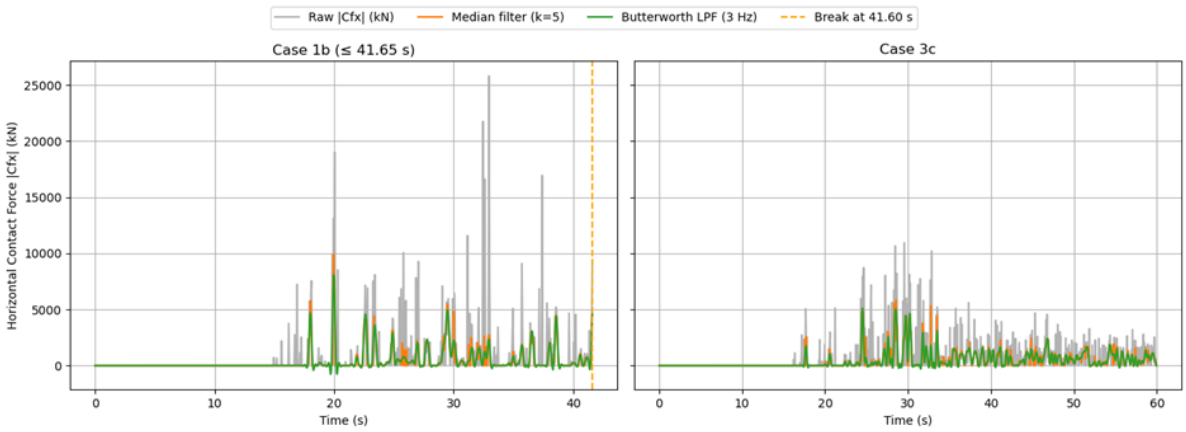

Figure 7.2: Horizontal contact forces comparison between Case 1b and Case 3c.

In Case 3d the same scenario happens, albeit with slightly lower forces up to 4 MN. This is visible

in Figure C.16 and Figure 7.6. However, in both scenarios sufficient force occurs for ice crushing to happen. But as the ice ridge keel is modelled as rigid, higher peaks in the results can be caused by relatively small bumps, which might be scraped off entirely with the point absorber being able to slide against the ridge, instead of being lodged within it.

7.2.2. Surface characteristics

The surface characteristics are adjusted to a smooth ice ridge in Case 4 and 4b. As mentioned before, in Case 4 the mooring lines failed quickly, showing that the fairlead tension forces will exceed 0.625 MN. With regards to Case 4b – where the mooring tension is increased to 5 MN – the simulation is extended to 100 seconds to show full behaviour. The comparison in fairlead tensions between Case 1b and Case 4b is shown in Figure 7.3.

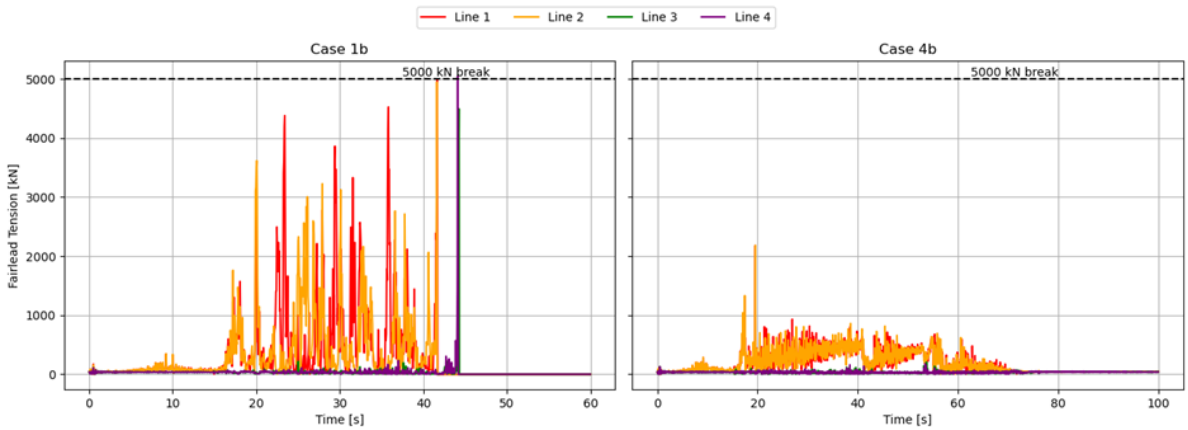

Figure 7.3: Fairlead tensions comparison between Case 1b and Case 4b.

In Animation S9 it can be seen that the point absorber survives submersion. The fairlead tensions for Case 4b have a peak of 2.2 MN in Line 1 and 2, this happens just before submersion. After this the fairlead tensions are between 0.5 and 1 MN for Line 1 and 2, and up to 0.1 MN for Line 3 and 4. From Figure 7.3 it can be seen that the fairlead tensions for a smooth ice ridge are significantly less than for a roughed-surfaced ice ridge.

The horizontal contact forces can be seen in Figure 7.4, where Case 1b is compared to Case 4b. Note that the timescales are different. The horizontal contact forces range from 0.5 MN up to 2.5 MN (with the filters are applied) when the point absorber is sliding in front of the ice ridge. Under the ice ridge the horizontal contact forces decrease to 0.1 MN and after the ice ridge the forces are up to 1 MN. Ice crushing is expected to occur at 1.25 MN, which is dependent on the nominal area. In comparison to Case 1b, Case 4b has more continuous forces with lower peaks. Which makes sense as the point absorber slides against the ice ridge without jumps that occur in the rough-surfaced ice ridge.

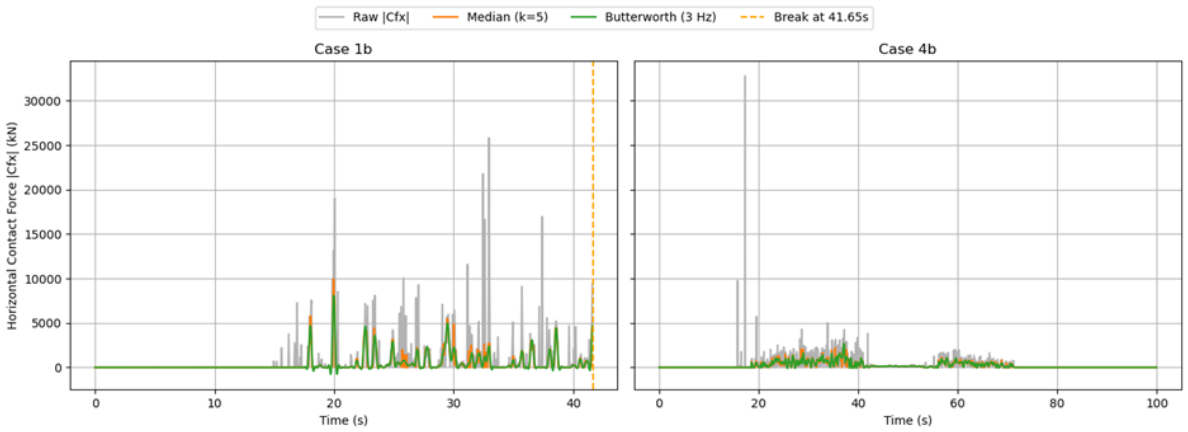

Figure 7.4: Horizontal contact forces comparison between Case 1b and Case 4b.

7.2.3. Direct comparison

In this section Case 1b, Case 3c, Case 3d and Case 4b are directly compared to each other. The direct comparison for the fairlead tensions is shown in Figure 7.5 for Line 1 and Line 2. It should be noted that the point absorber behaviour from the cases is slightly different. Case 1b fails at 41.65 seconds and Case 4b is submerged underneath the ice ridge starting from approximately 40 seconds.

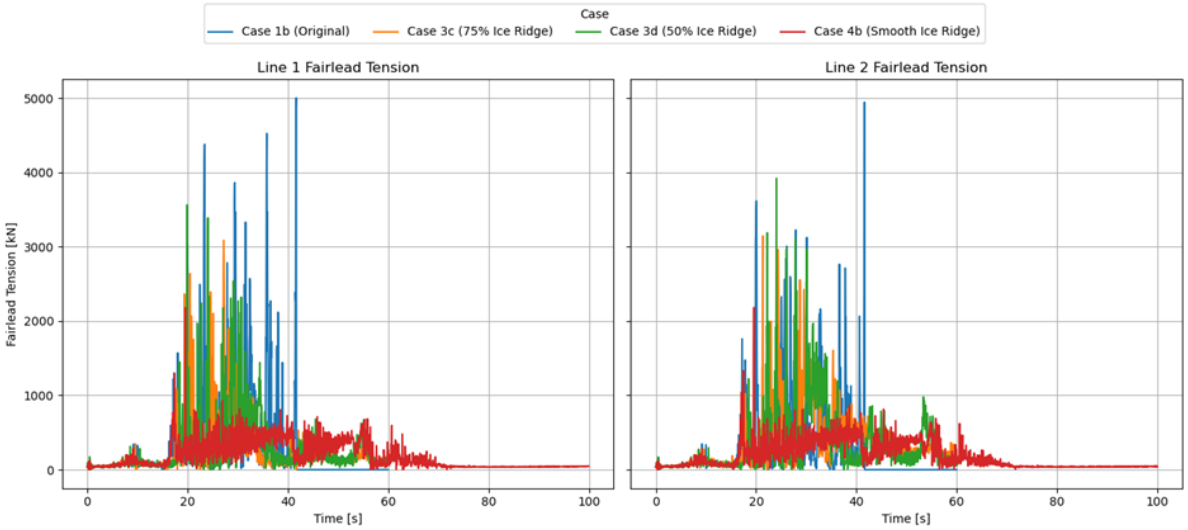

Figure 7.5: Direct comparison Line 1 and Line 2 between Case 1b, Case 3c, Case 3d and Case 4b.

From Figure 7.5 it still becomes clear how the mooring line tensions for a smooth ice ridge are significantly lower. The full-sized ice ridge leads to higher tension forces than the downscaled ice ridges. Yet, the differences between the downscaled ice ridges in Case 3c and Case 3d themselves are smaller, with Case 3d even having higher peaks than Case 3c.

The horizontal contact forces between Case 1b, Case 3c, Case 3d and Case 4b are directly compared in Figure 7.6. It should be noted again that the point absorber behaviour from the cases is slightly different. Case 1b fails at 41.65 seconds and Case 4b is submerged and underneath the ice ridge starting from approximately 40 seconds, leading to lower direct horizontal contact forces after 40 seconds.

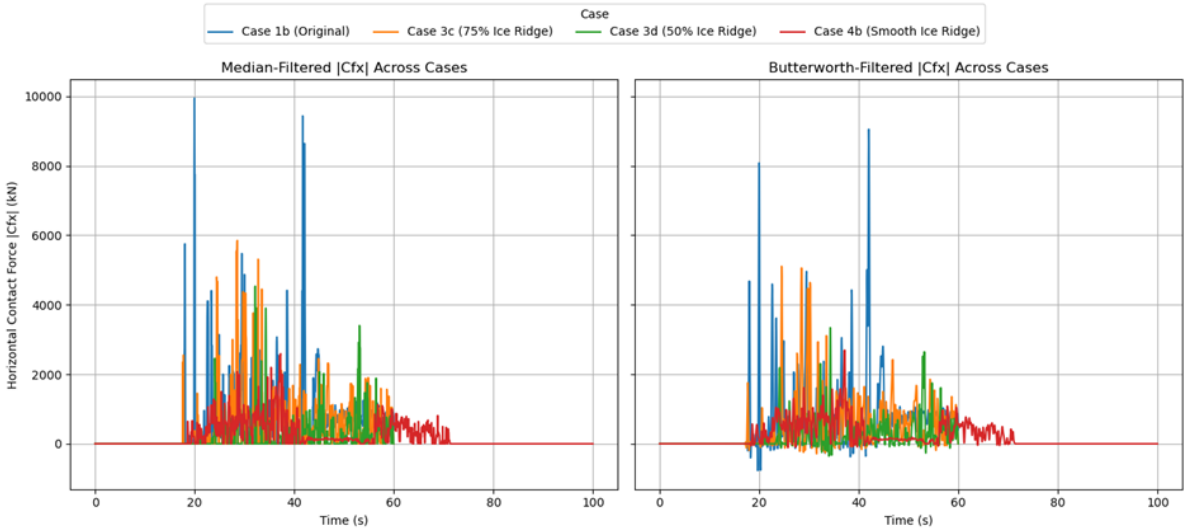

Figure 7.6: Direct comparison horizontal contact forces between Case 1b, Case 3c, Case 3d and Case 4b. The first graph is the raw data Median-Filtered and the second graph is Butterworth-Filtered.

From the data from Figure 7.6 it becomes clear that the original configuration has the largest peaks. The 75%-sized ice ridge from Case 3c is second and the 50%-sized ice ridge from Case 3d is third, as expected. The smooth ice ridge shows the lowest horizontal contact forces due to the lack of roughness.

7.3. Limitations and uncertainties

There are certain limitations and uncertainties that can influence the outcomes of the model. In Chapter 5.1.3 the simplifications of this model were summed up. This section is used to show the implications of the simplifications. In Chapter 6.1 the modelling faults are summed up. At the end of this section the location of failure of the first 2 mooring lines is discussed.

- Keel structure: The roughness of keel of the ice ridge is simulated as one rigid body. This means that the point absorber can get lodged behind a relatively small lump, which in reality might be easily scraped off due to the high forces. This can lead to higher peak tensions that wouldn't exist in a real situation. This brings a certain uncertainty to the tension loads when the ice ridge is sliding against the keel of the ice ridge.
- Seabed properties: Properties with regards to the seabed, such as the damping coefficient (seabed friction damping) can affect the outcomes of the result with regards to peak tension forces in the mooring lines. The standard value of 200 is used, however if a lower value would be more applicable (which would be the case for softer seabeds) the peak tensions would be higher and thus potentially leading to earlier failure. The bottom stiffness/damping constants are also not studied within the thesis. Standard values are used, this does mean that there is an uncertainty that you need to take into account when approaching these results. The properties of the seabed can influence the outcome of the results.
- Neglected forces: As mentioned in Chapter 5.1.3, certain forces are neglected. This includes wave & wind forces, time-dependent forces and certain ice action considerations. This is a limitation to the results of the model. Even though none of these forces is expected to cause significant differences in the outcomes, it does bring uncertainty to the model.
- Scaling of ice ridges: The ice ridges are scaled entirely to 50% and 75%. This means that the roughness pattern is also less severe for smaller ice ridges. This makes sense as smaller blocks are expected in smaller ice ridges, however this bring an uncertainty to the actual results. It is unsure how big the influence of the ice ridge itself is compared to the severity of the roughness.

7.3.1. Failure location uncertainty

In the simulations where to mooring lines break at 0.625 MN, the front 2 mooring lines break due to the momentum of the ice ridge. In the simulations with a maximum tension of 5 MN, the mooring lines survive this initial momentum (or push by the ice ridge) and the point absorber will get pushed down in the water and then fail due to being entangled in the roughness of the keel. With smooth ice ridge the mooring lines all survive, as it does not get lodged. The 0.625 MN is based on the maximum pressure on an ice block, however in the simulation this value is already reached at the part that is still considered the consolidated layer. This part is stronger and thus more likely to handle this value (as the contact area is significantly larger). In the 5 MN simulations the value that is approximately reached at the consolidated layer is around 2 MN, before the point absorber starts sliding down.

Based on a similar coefficient for compressive ice strength (5 MPa), the maximum force on the consolidated layer is as follows:

$$F_{max} = p_{ice,max} A_{contact} = 5 \times 0.86 \times 6 = 25.8 \text{ MN} \tag{7.1}$$

This is based on the thickness of the consolidated layer and the maximum width over the structure. Equation 7.1 shows that ice crushing is not expected at the consolidated layer yet, as this value – even divided over 2 – is significantly higher than 0.625 MN. The point absorber is thus expected to be submerged down without failing at the first 2 mooring lines (as happens in the simulations with max tensions at 5 MN), and then only fail later on when the point absorber reaches the keel, where the mooring line tensions or horizontal contact forces are also likely to reach 0.625 MN or 1.25 MN respectively. A better understanding of how strong the keel itself is still necessary, if the keel itself can be proven to be stronger, it is a decisive factor if the point absorber will slide against the keel or be crushed into it.

8

Mitigation strategies

This chapter addresses potential mitigation strategies to reduce the risks and impacts of collisions between moored floating point absorbers and ice ridges. Strategies considered include both structural adaptations and operational procedures.

8.1. Structural design modifications

This section explores structural design modifications for the ice ridges.

8.1.1. Hull modifications

The ice-breaking hull geometry developed in Project WESA [37] was optimized specifically for level-ice conditions. The shape of the buoy is designed to get a vertical motion pointing downward under the pressure of ice. It was designed with a slope angle of 60° to get a maximal vertical force on the HSST buoy from ice pressing on the side of the buoy. In this project this slope angle was adjusted to 40-50°, to give the point absorber more lenience to go underneath the ice ridge.

To adjust the ice-breaking hull geometry an optimization for the angle needs to be performed. From the simulations it became clear that the mooring lines can survive the impact of a smooth ice, as long as ice crushing is neglected. The largest concern is that the point absorber could be driven into the ice ridge, crushing the ice and becoming lodged. This is mostly due the relatively small contact area of ice blocks within the ice ridge keel. If the contact area of the ice can be assumed to be larger, it would mean that the ice is stronger. Making it harder for the point absorber to go crush into the ice ridge. This would open the possibility for design modifications for the hull to slide against the ridge, without being lodged into it. The total contact forces that the ice ridge needs to handle are at least 2.2 MN, assuming a smooth ice ridge.

8.1.2. Submersible or under-ice configurations

There are many design options for the buoy to be submerged. In [74] options were named such as passively moving the buoy under the ice and actively submerging the buoy underneath the ice, during an icy winter season. An active submerging system would need an option such as onboard ballast to drive the buoy below the ice before it actually makes contact. This can be done during ice season or when a large incoming ice ridges are detected.

8.2. Operational strategies

This section explores the operational strategies for wave energy farms in ice-prone seas. This is specifically suited to regions like the Baltic Sea and the Bohai Sea.

8.2.1. Ice management

Active ice management is a strategy that has been used extensively in the petroleum industry [75]. This could be an option for a wave energy farm as well. This is mostly cost-related and a study of the

feasibility of using active ice management for a wave energy farm is beyond the scope of this thesis.

8.2.2. Seasonal deployment

An operational strategy might be seasonal deployment for wave energy converters. Regions such as the Baltic Sea and Bohai Sea have ice-free seasons and wave energy converters can thus potentially be deployed only in ice-free seasons. Another option is to apply ice monitoring and retrieve the ice ridges when severe ice conditions are expected. In combination with the study done on level ice [9], which proved point absorbers able to survive ice ridges, a point absorber only would need to be retrieved in more severe situations and not the entire or every winter.

As the sea ice extent is shrinking in the arctic [76], the option for seasonal deployment might become a better alternative for certain regions than modifications to the hull itself, if the need to remove the point absorbers would only be once per a certain amount of years.

9

Conclusions & Recommendations

This chapter repeats the research problem, objectives and questions, while giving concluding remarks on them. Key findings are provided. At the end of the chapter recommendations for further improvements are given.

9.1. Research problem & Objectives

The objective of the thesis was to model the effect of ice ridges on point absorber-type WEC's with a particular emphasis on the on the dynamic behaviour of the point absorber and the tension forces in its mooring lines. The research objectives were as follows:

1. To identify and quantify the primary forces acting during the interaction between a moored point absorber-type WEC and an ice ridge, including hydrodynamic, ice-induced, and structural response forces.
2. To develop a 3D model that simulates the interaction between a moored point absorber-type WEC and an average-sized ice ridge for a better understanding of what happens during a collision.
3. To determine the critical size thresholds of ice ridges at which a moored point absorber-type WEC is likely to experience structural failure or operational disruption.
4. To analyse the influence of the angle where the ice ridge and the moored point-absorber type-WEC collide, providing insight into their interaction under different impact conditions.
5. To evaluate the effectiveness of various mitigation strategies designed to protect point absorber wave energy converters from damage caused by ice ridge interactions in cold climate marine environments.

9.1.1. Objectives guideline

This section serves as a guideline for the objectives.

- Regarding Objective 1, the forces are described in Chapter 3. The ice-induced, and structural response forces are provided in Chapter 6.
- Regarding Objective 2, the model is developed within DualSPHysics, with the code provided in Appendix B1.
- Regarding Objective 3 and 4, the critical threshold size and the influence of the angle are discussed in Chapter 7.2.1.
- Regarding Objective 5, the mitigation strategies are discussed in Chapter 8.

9.1.2. Key findings

The key findings from the objectives, which are derived from this thesis, are as follows:

- In ice-prone regions such as the Baltic Sea, Bohai Sea and the Okhotsk Sea near Japan, there is a viable wave energy potential. But as these regions experience ice during the winter, ice ridges need to be taken into account for the design of the wave energy farms.
- The numerical model is close the expected static pre-tension at the fairleads. the load distribution over the 4 lines is not even and exact, but this is due to the applied current in the model, which is not taken into consideration in calculating the pre-tensions.
- Simulated horizontal forces generally fall within the theoretical range of 3.6 to 11.5 MN. Rigid-body assumptions make the forces from the simulation on the higher side.
- A tension limit of 0.625 MN, based on ice crushing at the keel, causes immediate mooring line failure upon initial ice impact at the consolidated layer, before reaching the ice ridge keel. Ice crushing isn't realistically expected at this stage, indicating that the chosen limit of 0.625 MN provides limited useful information on interactions between ice ridges and moored point absorbers.
- With a higher tension limit of 5 MN, the front two mooring lines fail due to becoming lodged within the roughness of the ice ridge surface for a full-sized ice ridge, rather than due to direct initial impact forces. The rear two mooring lines also primarily fail due to being lodged within the ridge roughness.
- Surface roughness significantly dictates mooring line survival. Rough-surfaced ice ridges frequently cause the absorber to lodge within the surface irregularities, resulting in peak tensions that exceed the mooring line limits. Conversely, a smooth-surfaced ridge allows the mooring lines to survive impacts with tensions up to 2.2 MN, provided entanglement is avoided. This suggests that mooring lines capable of enduring at least 2.2 MN per line (and ice ridge keels capable of twice this force due to load distribution) would withstand typical ice ridge impacts under high currents.
- Reducing ice ridge dimensions to 75% and 50% decreases fairlead tensions to about 3 MN, down from the maximum 5 MN seen with full-sized ridges. Similarly, horizontal contact forces decrease significantly, from 10 MN in full-sized ridges to approximately 6 MN (75%-sized ice ridge) and 4 MN (50%-sized ice ridge). This highlights the importance of ice ridge size in determining both mooring tensions and horizontal contact forces.
- Small angular deviations ($<10^\circ$) don't significantly alter initial impact loads.
- Options for mitigation strategies include designing the hull for optimization to go underneath ice ridges, as it can survive the forces of the initial horizontal contact loads. The second option is to use ice monitoring and seasonal deployments, as the ice extent in the Arctic is shrinking and ice ridges in seas such as the Bohai Sea and Baltic Sea are becoming more rare.
- The most limiting factor in the results is the uncertainty about ice crushing during the interaction with the ice ridge keel structure. It is known at which point this is likely to happen and this point is reached in the simulations where the point absorbers survives the initial impact, however the behaviour due to ice crushing isn't measured, as ice crushing is either neglected within the simulation for the cases where the mooring line tension is set to 5 MN or not captured properly, which is the case for the other cases.

9.2. Sub-research questions

In this section the research questions are answered. The sub-research question gives an answer to the main research question, which is: What are the collision dynamics between an ice ridge and a moored point absorber-type wave energy converter?

Q1: What are the primary mechanisms and consequences of an interaction between ice ridges and moored point absorber-type wave energy converters?

The interaction between ice ridges and moored point absorber-type wave energy converters primarily involves initial impact forces and subsequent entanglement within the ice ridge structure, particularly its rough surfaced keel. The mooring lines initially experience significant tensions upon contact with the consolidated layer of the ice ridge, but these initial forces typically do not lead directly to failure. Instead, the critical mechanism is the entanglement of the buoy within the roughness of the submerged keel.

This entanglement causes sharp increases in mooring line tensions, often surpassing the designed tension limits, resulting in structural failure. This does not happen when the ice ridge is smooth, as the mooring line tensions only go up to 2.2 MN at that point. Mooring lines capable of enduring at least 2.2 MN per line and ice ridge keels capable of enduring twice this force due to load distribution would withstand typical ice ridge impacts. The horizontal contact forces show lower forces to withstand for a smooth keel structure (up to 3 MN). A rough-surfaced keel experiences forces up to 10 MN.

Q2: What are the threshold dimensions and characteristics of an ice ridge for a collision between an ice ridge and point absorber to be critical?

The threshold dimensions and characteristics for collisions between ice ridges and moored point absorbers to become critical are closely related to both the size and surface roughness of the ice ridge. Full-sized ice ridges, with typical keel depths around 8 meters, generate significantly higher horizontal contact forces (up to 10 MN) and mooring line tensions exceeding the 5 MN limit. However, even smaller ridges—scaled to 50% and 75% of the typical size—can cause critical tension loads if their surfaces are sufficiently rough. A notable finding is that smaller ice ridges lead to lower peak tensions in the mooring lines (approximately 3 MN) and horizontal contact forces (4 to 6 MN), but still potentially critical. However, the simulations for Case 3c and 3d are inconclusive about the survivability of a moored point absorber against smaller ice ridges, as the simulation was not able to capture this.

Q3: How does the angle of collision between the ice ridge and the point absorber affect the collision dynamics?

The angle of the collision, given that is below 10°, does not impact the initial impact forces.

Q4: How does the roughness of the surface of the ice ridge affect the collision dynamics between the ice ridge and the point absorber?

Surface roughness of ice ridges dramatically influences the collision dynamics with moored point absorbers. Ice ridges with rough underwater surfaces significantly increase the probability of entanglement, causing peak tensions in mooring lines that can exceed designed structural limits regardless of ridge size. Such entanglement results in abrupt tension spikes (potentially exceeding the 5 MN limit per line) and large horizontal contact forces, substantially elevating the risk of mooring line and structural failure. In contrast, simulations with smooth-surfaced ridges show markedly lower tensions (up to 2.2 MN) and reduced horizontal contact forces, enabling the point absorber to slide past the ridge without becoming lodged. So as long as the point absorber doesn't become entangled in the ice ridge, it can withstand typical ice ridge impacts – even at high currents – provided the lines can withstand at least 2.2 MN. Surface roughness, or more specifically, the circumstance of the point absorber getting lodged within the ice ridge, is identified as a critical determinant of the severity of collisions.

Q5: What are potential design modifications or operational strategies for wave energy converters to enhance their resilience against ice-ridge impacts?

Options for design modifications include adjusting the hull to survive against ice ridge and improve the willingness of the hull to be submerged by the ice ridge. The strength of the ice ridge needs to be studied, if the ice ridge has a higher effective nominal area, a larger hull area might also work to let make it easier for the hull to slide down. Another alternative is ice monitoring and seasonal deployment. Which includes removing the point absorber when ice ridges are expected, which will be increasingly less in the future.

9.3. Limitations

The following sections provide information about understudied parameters and areas of improvement.

9.3.1. Understudied parameters

The following parameters in this thesis are understudied and have had chosen default values. Improvement upon these values lead to more precise results.

- MoorDyn parameters: For certain parameters within MoorDyn standard values are used, this includes the bottom stiffness/damping constant, damping coefficient, static/dynamic friction ratio,

added mass coefficients and drag coefficients. Improvement upon these values leads to more precise results.

- Collision Mechanics: Chrono offers 2 settings for collision mechanics, SMC (Smooth Contacts) and NSC (Non-Smooth Contacts). Due to instability issues the focus in this study was on NSC, however SMC can be a promising alternative for more accurate results, as it allows for small continuous forces via stiffness/damping parameters, which makes it more suitable for soft interactions.
- DualSPHysics parameters: The effects of certain DualSPHysics options are not studied and might lead to more stable results. For these options standard values are used as there was no direct reason to deviate from them, however they might influence the results. These options include the shifting configuration, step algorithm, boundary algorithm (boundary conditions) and interaction kernel.

9.3.2. Areas of improvement

This section includes an overview of the most important areas of improvement for the simulation, for an improvement of the understanding of the feasibility for designing moored WEC's against ice ridges:

- Ice ridge keel strength: The ice ridge keel strength, which is translated to maximum tension line forces in certain cases, is based on the contact area of an ice block of only 0.25 m². In reality it could be possible that the effective contact area of the ice ridge can be assumed to be larger, which leads to a higher effective strength of the ice ridge. This would be beneficial for the point absorber, as it would be less likely to get entangled in the ice ridge and it would be easier to determine when a simulation should stop because of the likeliness of ice crushing occurring. This is also related to the limitations about keel structure mentioned in Chapter 7.3.
- Simulation of longer length of the ice ridge: In the simulations with the 75%-sized and 50%-sized ice ridges, the ice ridges themselves eventually weren't able to submerge the point absorber or fail the mooring lines. A simulation with a lengthier ice ridge would be significantly computationally more expensive, but will lead to more accurate results.
- Mooring line properties: For the model, strong mooring lines are used with a large diameter, as high loads are expected. Fine-tuning towards the ideal line diameter and related properties is an area of improvement. In reality smaller diameters might be sufficient.
- Improve of the current: The current in this simulation is set as a high maximum value which is expected in the Bohai Sea. In reality the actual ice drift might move the ice ridge slower, which can lead to lower forces. An area of improvement is adding ice drift into the model or determining a representative current for the expected ice drift.
- Deeper dive into keel angles: The research on influence of the keel angle within this thesis is limited, as only a keel angle of 10° was tested and in that case the ice ridge already failed at initial impact. No further testing was done with larger angles or with mooring line tensions of 5 MN.

9.4. Contributions to Knowledge

This research has contributed to the knowledge in the following ways:

- An overview of the ice-WEC interaction forces for ice ridges and moored point absorbers and an overview of ice-prone areas with wave energy potential with their respective ice extent.
- Advanced understanding of ice-structure interactions: Provided new insights into collision dynamics between moored point absorbers and ice ridges, specifically identifying conditions and most determining factors that lead to mooring line failure, which is the ridge roughness.
- Development of a simulation framework: Established a 3D SPH-based model for simulations in DualSPHysics, integrated with MoorDyn and Chrono for representing interactions between (simplified) ice ridges and point absorber WEC's.
- Critical ice ridge thresholds: Provided critical size and roughness thresholds of ice ridges, thus an increase of knowledge on the influence of smaller and larger ice ridges on point absorbers.

- Starting point and focus areas for improvement: Provided a starting point and focus areas for further improvement on the understanding of the collision dynamics between point absorbers and ice ridges.

9.5. Recommendations for future research

To improve the knowledge on the collision dynamics between an ice ridge and a moored point absorber, the following recommendations for future research are provided:

- Keel improvement: Improve the properties of the keel of the ice ridge, for better simulation of the behaviour when the point absorber slides against the keel of the ice ridge. This includes a better study on how strong the keel itself will act when a point absorber is sliding against it and what will be the effective nominal area and when ice crushing is likely to occur. Another recommendation is to divide the ice ridge in different parts in the simulation with different strengths, to improve the realism in the failure locations.
- Improvement of ice ridge material properties: The density of ice is used for the ice ridge, in reality the effective ice ridge density may be higher due to water inside the blocks of the keel. The use of multiple restitution coefficients and kinetic friction coefficients (different for the consolidated layer and ice ridge keel) is also an improvement for the realism.
- Improvement of the current: In the simulations the ice ridge is moved by a current of up to 2.0 m/s. This is a conservative estimate, in reality the ice ridge will be slower as the current itself is faster than ice drift. Adjustments to better represent the ice drift are recommended.
- Fine-tuning of the model: The parameters mentioned in Chapter 9.3.1 are understudied, meaning there is still room for fine-tuning. This can improve the realism of the model.
- Improvement of global ice actions: The WESA-buoy is a sloped surface. However, an equation for vertical surfaces is used for the global ice actions. This decision is made because the sloped surface will be turned inwards during the interaction and effectively be an vertical surface. This implication needs to be studied further. Another point is that the equations are limited to determining initial contact forces for a moored buoy. The load calculation will change during the rotation and submersion of the buoy, and this interactive process is not taken into account in this thesis.

There are more points mentioned in this thesis as limitations, but these points are expected to have the most influence on the outcomes.

Bibliography

[1] National Oceanic and Atmospheric Administration, Pacific Marine Environmental Laboratory. What is the difference between rubble ice and pressure ridges? https://www.pmel.noaa.gov/arctic-zone/ice-rubble-pressure.html. Image “Pressure Ridge” provided by Dr. Hajo Eicken; accessed 29 May 2025.

[2] European Union. Renewable energy targets, 2022. URL: https://shorturl.at/bNDL9.

[3] Czesław Dyrcz. Analysis of ice conditions in the baltis sea and in the puck bay. Zeszyty Naukowe Akademii Marynarki Wojennej, 210:1–1, 09 2017. doi:10.5604/01.3001.0010.6581.

[4] Erik Nilsson, Anna Rutgersson, Adam Dingwell, Jan-Victor Björkqvist, Heidi Pettersson, Lars Axell, Johan Nyberg, and Erland Strömstedt. Characterization of wave energy potential for the baltic sea with focus on the swedish exclusive economic zone. Energies, 12(5), 2019. URL: https://www.mdpi.com/1996-1073/12/5/793, doi:10.3390/en12050793.

[5] Standing Committee of the National People’s Congress of the People’s Republic of China. Zhonghua renmin gongheguo nengyuan fa (energy law of the people’s republic of china). Official website of the National Energy Administration of China, November 2024. Adopted on November 8, 2024, by the 12th Session of the 14th Standing Committee of the National People’s Congress. URL: https://www.nea.gov.cn/2024-11/09/c_1310787187.htm.

[6] Ge Li, Yan Jiao, Xue Chen, Yiding Zhao, Rui Li, Donglin Guo, Lei Ge, Qiaokun Hou, and Qingkai Wang. Investigation of the recent ice characteristics in the bohai sea in the winters of 2005–2022 using multi-source data. Water, 16(2), 2024. URL: https://www.mdpi.com/2073-4441/16/2/290, doi:10.3390/w16020290.

[7] Zhifeng Wang, Sheng Dong, Xue Li, and C. Guedes Soares. Assessments of wave energy in the bohai sea, china. Renewable Energy, 90:145–156, 2016. URL: https://www.sciencedirect.com/science/article/pii/S0960148115305644, doi:10.1016/j.renene.2015.12.060.

[8] Konstantinos Christakos, George Lavidas, Zhen Gao, and Jan-Victor Björkqvist. Long-term assessment of wave conditions and wave energy resource in the arctic ocean. Renewable Energy, 220:119678, 2024. URL: https://www.sciencedirect.com/science/article/pii/S0960148123015938, doi:10.1016/j.renene.2023.119678.

[9] A. Savin, E. Strömstedt, and M. Leijon. Full-scale measurement of reaction force caused by level ice interaction on a buoy connected to a wave energy converter. Journal of Cold Regions Engineering, 33, 2019.

[10] Gerrit-Jan Winkels. Research proposal on modeling the ice-structure interaction between wave energy converters and ice ridges, 2024. URL: https://archive.org/details/research-proposal-ice-ridge-wec-interaction.

[11] Li Zhou, Junliang Gao, and Dongqin Li. An engineering method for simulating dynamic interaction of moored ship with first-year ice ridge. Ocean Engineering, 171:417–428, 2019. URL: https://www.sciencedirect.com/science/article/pii/S0029801818321000, doi:10.1016/j.oceaneng.2018.11.027.

[12] Oddgeir Dalane, Vegard Aksnes, and Sveinung Løset. A Moored Arctic Floater in First-Year Sea Ice Ridges. Journal of Offshore Mechanics and Arctic Engineering, 137(1):011501, 02 2015. arXiv:https://asmedigitalcollection.asme.org/offshoremechanics/article-pdf/137/1/011501/6243627/omae_137_01_011501.pdf, doi:10.1115/1.4028814.

[13] ISO. Petroleum and natural gas industries - Arctic offshore structures (ISO 19906:2019). International Organization for Standardization, Vernier, Geneva, Switzerland, ISO 19906:2019(E) edition, 2019.

[14] SMHI. Sea ice, 2010. Accessed: 2025-02-27, SMHI stands for Swedish Meteorological and Hydrological Institute. URL: https://www.smhi.se/en/theme/sea-ice-1.11198.

[15] Oceanwide Expeditions. Hds06-23, reisverslag, rond spitsbergen, in het rijk van ijsbeer en ijs, 2023. Accessed: 2025-02-27. URL: https://oceanwide-expeditions.com/nl/trip-log/hds06-23-reisverslag-rond-spitsbergen-in-het-rijk-van-ijs.

[16] Encyclopædia Britannica. Arctic iceberg. https://www.britannica.com/science/iceberg/Arctic-icebergs#/media/1/281212/160285, 2023. Accessed: 2025-02-27, year is an estimation.

[17] Sveinung Løset. The ice cover and drift, 2023. Presentation at UNIS, Svalbard for the course Arctic Offshore Engineering. Year is presentation date, date taken is unknown.

[18] Sohey Nihashi, Kay I. Ohshima, and Sei-Ichi Saitoh. Sea-ice production in the northern japan sea. Deep Sea Research Part I: Oceanographic Research Papers, 127:65–76, 2017. URL: https://www.sciencedirect.com/science/article/pii/S0967063716301157, doi:10.1016/j.dsr.2017.08.003.

[19] J. C. Comiso, C. L. Parkinson, R. Gersten, A. C. Bliss, and T. Markus. Current state of sea ice cover, 2025. Last accessed: 02-07-2025. URL: https://earth.gsfc.nasa.gov/cryo/data/current-state-sea-ice-cover.

[20] Bloomberg. Hokkaido electric sees power demand surge with data center boom. https://www.bloomberg.com/news/articles/2024-11-15/hokkaido-electric-sees-power-demand-surge-with-data-center-boom, November 15 2024. Accessed: 2025-02-27.

[21] Government of Japan. Japan's commitment to achieving carbon neutrality by 2050. https://www.env.go.jp/en/air/greenhouse/strategy/net_zero.html, 2021. Accessed: 2025-02-27, also 2021 is the year when Japan announced its net-zero commitment.

[22] Urban Henfridsson, Viktoria Neimane, Kerstin Strand, Robert Kapper, Hans Bernhoff, Oskar Danielsson, Mats Leijon, Jan Sundberg, Karin Thorburn, Ellerth Ericsson, and Karl Bergman. Wave energy potential in the baltic sea and the danish part of the north sea, with reflections on the skagerrak. Renewable Energy, 32(12):2069–2084, 2007. URL: https://www.sciencedirect.com/science/article/pii/S0960148106002795, doi:10.1016/j.renene.2006.10.006.

[23] Egidijus Kasiulis, Jens Peter Kofoed, Arvydas Povilaitis, and Algirdas Radzevičius. Spatial distribution of the baltic sea near-shore wave power potential along the coast of klaipėda, lithuania. Energies, 10(12), 2017. URL: https://www.mdpi.com/1996-1073/10/12/2170, doi:10.3390/en10122170.

[24] Na Zhang, Shuai Li, Yongsheng Wu, Keh-Han Wang, Qinghe Zhang, Zai-Jin You, and Jin Wang. Effects of sea ice on wave energy flux distribution in the bohai sea. Renewable Energy, 162:2330–2343, 2020. URL: https://www.sciencedirect.com/science/article/pii/S0960148120316037, doi:10.1016/j.renene.2020.10.036.

[25] A. Webb, T. Waseda, and K. Kiyomatsu. A high-resolution, long-term wave resource assessment of japan with wave–current effects. Renewable Energy, 161:1341–1358, 2020. URL: https://www.sciencedirect.com/science/article/pii/S096014812030728X, doi:10.1016/j.renene.2020.05.030.

[26] Shinsuke Iwasaki. Increase in the wave power caused by decreasing sea ice over the sea of okhotsk in winter. Scientific Reports, 13(1):2539, Feb 2023. doi:10.1038/s41598-023-29692-9.

[27] V. Pishchal'nik, Pavel Truskov, V. Romanyuk, and I. Minervin. Interannual variability of ice volume in the sea of okhotsk during the maximum development of ice extent for 2000–2020. Cold Regions Science and Technology, 189:103326, 06 2021. doi:10.1016/j.coldregions.2021.103326.

[28] Seongho Ahn, Vincent S. Neary, and Kevin A. Haas. Global wave energy resource classification system for regional energy planning and project development. Renewable and Sustainable Energy Reviews, 162:112438, 2022. URL: https://www.sciencedirect.com/science/article/pii/S1364032122003446, doi:10.1016/j.rser.2022.112438.

[29] Nicolas Guillou, George Lavidas, and Georges Chapalain. Wave energy resource assessment for exploitation—a review. Journal of Marine Science and Engineering, 8(9), 2020. URL: https://www.mdpi.com/2077-1312/8/9/705, doi:10.3390/jmse8090705.

[30] Aleix Maria-Arenas, Aitor J. Garrido, and Izaskun Garrido. Enhancing wave energy converters: Dynamic inertia strategies for efficiency improvement. Journal of Marine Science and Engineering, 12(8), 2024. URL: https://www.mdpi.com/2077-1312/12/8/1285, doi:10.3390/jmse12081285.

[31] Anela Dokso. Opt's pb3 powerbuoy marks operational milestone, August 2020. Accessed: 2025-02-13. URL: https://www.offshore-energy.biz/opts-pb3-powerbuoy-marks-operational-milestone/.

[32] Cameron Thomson, Gareth Harrison, and John Chick. An lca of the pelamis wave energy converter. The International Journal of Life Cycle Assessment, 24(1):51–63, 2019. URL: https://www.ncbi.nlm.nih.gov/pmc/articles/PMC6383585/, doi:10.1007/s11367-018-1504-6.

[33] Jens Peter Kofoed, Peter Frigaard, Erik Friis-Madsen, and Hans Chr. Sørensen. Prototype testing of the wave energy converter wave dragon. Renewable Energy, 31(2):181–189, 2006. doi:10.1016/j.renene.2005.08.021.

[34] António F. de O. Falcão and João C. C. Henriques. Oscillating-water-column wave energy converters and air turbines: A review. In Proceedings of the 12th European Wave and Tidal Energy Conference (EWTEC), 2016. URL: https://www.researchgate.net/publication/327878820_Experimental_Tests_of_a_116th-Scale_Model_of_the_Spar-Buoy_OWC_in_a_Large_Scale_Wave_Flume_in_Regular_Waves.

[35] Alicia Terrero González, Peter Dunning, Ian Howard, Kristoffer McKee, and Marian Wiercigroch. Is wave energy untapped potential? International Journal of Mechanical Sciences, 205:106544, 2021. URL: https://www.sciencedirect.com/science/article/pii/S0020740321002794, doi:10.1016/j.ijmecsci.2021.106544.

[36] Olga Kovaleva, Maris Eelsalu, and Tarmo Soomere. Hot-spots of large wave energy resources in relatively sheltered sections of the baltic sea coast. Renewable and Sustainable Energy Reviews, 74:424–437, 2017. URL: https://www.sciencedirect.com/science/article/pii/S1364032117302496, doi:10.1016/j.rser.2017.02.033.

[37] E. Strömstedt, A. Savin, H. Heino, K. Antbrams, K. Haikonen, and T. Götschl. Project wesa (wave energy for a sustainable archipelago) - a single heaving buoy wave energy converter operating and surviving ice interaction in the baltic sea. In 10th European Wave and Tidal Conference (EWTEC), 2013. URL: https://urn.kb.se/resolve?urn=urn:nbn:se:uu:diva-212882.

[38] Spyros Foteinis. Wave energy converters in low energy seas: Current state and opportunities. Renewable and Sustainable Energy Reviews, 162:112448, 2022. URL: https://www.sciencedirect.com/science/article/pii/S1364032122003549, doi:10.1016/j.rser.2022.112448.

[39] WMO. Wmo sea ice nomenclature. (WMO No. 259, volume 1 – Terminology and Codes, Volume II – Illustrated Glossary and III – International System of Sea-Ice Symbols, 2014.

[40] Denise Sudom, Garry Timco, Bjørnar Sand, and Lennart Fransson. Analysis of first-year and old ice ridge characteristics. Proceedings of the International Conference on Port and Ocean Engineering under Arctic Conditions, POAC, 1:732–742, 01 2011.

[41] Lucie Strub-Klein and Denise Sudom. A comprehensive analysis of the morphology of first-year sea ice ridges. Cold Regions Science and Technology, 82:94–109, 2012. URL: https://www.sciencedirect.com/science/article/pii/S0165232X12001152, doi:10.1016/j.coldregions.2012.05.014.

[42] Alexandra Pliss, Knut Vilhelm Høyland, and Bernt Johan Leira. Geometry, morphology, physical properties and structure of sea ice ridges during the transition period from first-year to second-year in the summer 2023 and 2024. Journal of Marine Science and Engineering, 13(2), 2025. URL: https://www.mdpi.com/2077-1312/13/2/335, doi:10.3390/jmse13020335.

[43] C. Mingham, L. Qian, and D. Causon. Chapter 6 - computational fluid dynamics (cfd) models. In Matt Folley, editor, Numerical Modelling of Wave Energy Converters, pages 105–122. Academic Press, 2016. URL: https://www.sciencedirect.com/science/article/pii/B9780128032107000062, doi:10.1016/B978-0-12-803210-7.00006-2.

[44] José M. Domínguez, Alejandro J.C. Crespo, Matthew Hall, Corrado Altomare, Minghao Wu, Vasiliki Stratigaki, Peter Troch, Lorenzo Cappietti, and Moncho Gómez-Gesteira. Sph simulation of floating structures with moorings. Coastal Engineering, 153:103560, 2019. URL: https://www.sciencedirect.com/science/article/pii/S0378383918305581, doi:10.1016/j.coastaleng.2019.103560.

[45] Diego Molteni and Andrea Colagrossi. A simple procedure to improve the pressure evaluation in hydrodynamic context using the sph. Computer Physics Communications, 180(6):861–872, 2009. URL: https://www.sciencedirect.com/science/article/pii/S0010465508004219, doi:10.1016/j.cpc.2008.12.004.

[46] Rui Xu, Peter Stansby, and Dominique Laurence. Accuracy and stability in incompressible sph (isph) based on the projection method and a new approach. Journal of Computational Physics, 228(18):6703–6725, 2009. URL: https://www.sciencedirect.com/science/article/pii/S0021999109002885, doi:10.1016/j.jcp.2009.05.032.

[47] Loup Verlet. Computer experiments on classical fluids. i. thermodynamical properties of lennard-jones molecules. Physical Review, 159(1):98–103, 1967.

[48] Ben Leimkuhler and Charles Matthews. Efficient molecular dynamics using geodesic integration and solvent–solute splitting. Proceedings of the Royal Society A: Mathematical, Physical and Engineering Science, 472:20160138, 05 2016. doi:10.1098/rspa.2016.0138.

[49] Alejandro Crespo, Moncho Gesteira, and R.A. Dalrymple. Boundary conditions generated by dynamic particles in sph methods. CMC. Computers, Materials, and Continua, 3, 06 2007.

[50] Alessandro Tasora, Radu Serban, Hammad Mazhar, et al. Project chrono: An open-source multi-physics simulation engine, 2023. Accessed: [2025]. URL: https://projectchrono.org.

[51] Ricardo Canelas, José Domínguez, Alejandro Crespo, Moncho Gesteira, and Rui Ferreira. A smooth particle hydrodynamics discretization for the modelling of free surface flows and rigid body dynamics. International Journal for Numerical Methods in Fluids, 78, 03 2015. doi:10.1002/fld.4031.

[52] Matthew Hall and Andrew Goupee. Validation of a lumped-mass mooring line model with deepcwind semisubmersible model test data. Ocean Engineering, 104:590–603, 2015. URL: https://www.sciencedirect.com/science/article/pii/S0029801815002279, doi:10.1016/j.oceaneng.2015.05.035.

[53] Pacific Northwest National Laboratory. Sotenäs project. https://tethys.pnnl.gov/project-sites/sotenas-project, 2024. Accessed: 2025-02-13.

[54] NOW Grenada. Grenada signs landmark wave energy mou at cop29, November 2024. Accessed: 2025-02-13. URL: https://nowgrenada.com/2024/11/grenada-signs-landmark-wave-energy-mou-at-cop29/.

[55] Renewable Energy Magazine. Bermuda and seabased show how islands can transition to ocean energy, March 2024. Accessed: 2025-02-13. URL: https://www.renewableenergymagazine.com/ocean_energy/bermuda-and-seabased-show-how-islands-can-20240314.

[56] Zerina Maksumic. Corpower ocean locks €32m funding to scale wave energy commercialization, October 2024. Accessed: 2025-02-13. URL: https://www.offshore-energy.biz/corpower-ocean-locks-e32m-funding-to-scale-wave-energy-commercialization/.

[57] CorPower Ocean. Corpower c4 system assembly completed, 2023. Accessed: [18-2-2025]. URL: https://corpowerocean.com/corpower-c4-system-assembly-completed/.

[58] Athanasios Kolios, Loris Francesco Di Maio, Lin Wang, Lin Cui, and Qihu Sheng. Reliability assessment of point-absorber wave energy converters. Ocean Engineering, 163:40–50, 2018. URL: https://www.sciencedirect.com/science/article/pii/S0029801818309089, doi:10.1016/j.oceaneng.2018.05.048.

[59] Patrick Singh, Zhenmu Chen, and Young Do Choi. 15kw-class wave energy converter floater design and structural analysis. Journal of the Korean Society of Marine Engineering, 40:146–151, 02 2016. doi:10.5916/jkosme.2016.40.2.146.

[60] Guojun Wang, Dayong Zhang, Qianjin Yue, and Songsong Yu. Study on the dynamic ice load of offshore wind turbines with installed ice-breaking cones in cold regions. Energies, 15(9), 2022. URL: https://www.mdpi.com/1996-1073/15/9/3357, doi:10.3390/en15093357.

[61] Matti Leppäranta. The Drift of Sea Ice. Springer Praxis Books. Springer Berlin Heidelberg, 2 edition, 2011. Softcover ISBN: 978-3-642-26757-4 (Apr. 21, 2013); eBook ISBN: 978-3-642-04683-4 (Mar. 22, 2011). Jointly published with Praxis Publishing, UK. doi:10.1007/978-3-642-04683-4.

[62] Joaquín M. Domínguez, Georgia Fourtakas, Claudio Altomare, and .... Dualsphysics: From fluid dynamics to multiphysics problems. Computational Particle Mechanics, 9:867–895, 2022. doi:10.1007/s40571-021-00404-2.

[63] Ivan Martinez Estevez and Andres Vieira. DesignSPHysics: A smoothed particle hydrodynamics toolkit. Software package, EPHYSLAB Environmental Physics Laboratory, Universidade de Vigo; EPHYTECH Environmental Physics Technologies, 2025. © 2025 Ivan Martinez Estevez and Andres Vieira. Licensed under the DesignSPHysics end-user license.

[64] Delft High Performance Computing Centre (DHPC). DelftBlue Supercomputer (Phase 2). https://www.tudelft.nl/dhpc/ark:/44463/DelftBluePhase2, 2024.

[65] Ivan Metrikin and Sveinung Løset. Nonsmooth 3d discrete element simulation of a drillship in discontinuous ice. In Proceedings of the 22nd International Conference on Port and Ocean Engineering under Arctic Conditions (POAC'13), 2013. URL: http://www.poac.com/Papers/2013/pdf/POAC13_051.pdf.

[66] R. Taylor and P. Valent. Design Guide for Drag Embedment Anchors. Technical Report TN-1688, Naval Civil Engineering Laboratory, Port Hueneme, California, Port Hueneme, CA, January 1984. URL: https://apps.dtic.mil/sti/citations/ADB080279.

[67] Li Zhou, Biao Su, Kaj Riska, and Torgeir Moan. Numerical simulation of moored structure station keeping in level ice. Cold Regions Science and Technology, 71:54–66, 2012. URL: https://www.sciencedirect.com/science/article/pii/S0165232X11002254, doi:10.1016/j.coldregions.2011.10.008.

[68] Acteon Group. Understanding the Scale of Mooring Components for Floating Wind Projects. https://acteon.com/blog/understanding-the-scale-of-mooring-components-for-floating-wind-projects/?utm_source=chatgpt.com, 2024. [Online; accessed 02-June-2025].

[69] Touvia Miloh, G. Waisman, and Daniel Weihs. The added-mass coefficients of a torus. Journal of Engineering Mathematics, 12:1–13, 11 1978. doi:10.1007/BF00042801.

[70] Steffen Suchandt, Andreas Lehmann, and Hartmut Runge. Analysis of ocean surface currents with tandem-x ati: A case study in the baltic sea. In 2014 IEEE International Geoscience and Remote Sensing Symposium (IGARSS), page 6947341. IEEE, 2014. URL: https://www.researchgate.net/publication/264315121, doi:10.1109/IGARSS.2014.6947341.

[71] Pengcheng Ma, Hongyuan Shi, Huaiyuan Xue, Pingping Li, and Yongkang Sun. Analysis of tidal current energy potential in the major channels of the bohai strait based on delft3d. Journal of Ocean University of China, 23(4):859–870, 2024. doi:10.1007/s11802-024-5721-y.

[72] DualSPHysics Project Team. 3. sph formulation, 2023. Accessed: 2025-04-11. URL: https://github.com/DualSPHysics/DualSPHysics/wiki/3.-SPH-formulation.

[73] C2Wind. Sea ice site conditions assessment: Kriegers flak ii offshore wind farm. Technical Report 24021-04-064, C2Wind, January 2025. URL: https://c2wind.com/f/content/24021-04-064---kriegers-flak-ii---sea-ice-site-conditions-assessment.pdf.

[74] Hanna Heino. Utilisation of Wave Power in the Baltic Sea Region. Number 9/2013 in FFRC eBOOK. University of Turku, Turku School of Economics, Turku, Finland, 2019. URL: https://www.utupub.fi/handle/10024/147510.

[75] Kai-Tung Ma, Yong Luo, Thomas Kwan, and Yongyan Wu. Chapter 3 - environmental loads and vessel motions. In Kai-Tung Ma, Yong Luo, Thomas Kwan, and Yongyan Wu, editors, Mooring System Engineering for Offshore Structures, pages 41–62. Gulf Professional Publishing, 2019. URL: https://www.sciencedirect.com/science/article/pii/B978012818551300003X, doi:10.1016/B978-0-12-818551-3.00003-X.

[76] National Snow and Ice Data Center. Arctic sea ice sets a record low maximum in 2025. https://nsidc.org/sea-ice-today/analyses/arctic-sea-ice-sets-record-low-maximum-2025, March 27 2025. Accessed: June 1, 2025.

Animations

Animation S1: Case 1: Original configuration. Available at: https://www.youtube.com/watch?v=TpZKMWHENLQ

Animation S2: Case 1b: Maximum tension increased to 5 MN. Available at: https://www.youtube.com/watch?v=8mg5C8QnGAA

Animation S3: Case 2: Configuration with an adjusted angle for the ice ridge. Available at: https://www.youtube.com/watch?v=roF67e2tFVM

Animation S4: Case 3: Configuration with ice ridge size adjusted to 75%. Available at: https://www.youtube.com/watch?v=P-tIo8fEnsg

Animation S5: Case 3: Configuration with ice ridge size adjusted to 50%. Available at: https://www.youtube.com/watch?v=GrXb09PWxCo

Animation S6: Case 3: Configuration with ice ridge size adjusted to 75% and maximum tension increased to 5 MN. Available at: https://www.youtube.com/watch?v=UfiNWN46oC0

Animation S7: Case 3: Configuration with ice ridge size adjusted to 50% and maximum tension increased to 5 MN. Available at: https://www.youtube.com/watch?v=v6H7xHK51vw

Animation S8: Case 4: Configuration with smooth ice ridge. Available at: https://www.youtube.com/watch?v=ktI46HctFdk

Animation S9: Case 4b: Configuration with smooth ice ridge with 5MN max. tension. Available at: https://www.youtube.com/watch?v=9LyNyBP5dyU

A

Technical Drawings

A1. Standard-Sized Ice Ridge Drawing

1 - Front view [1:400]

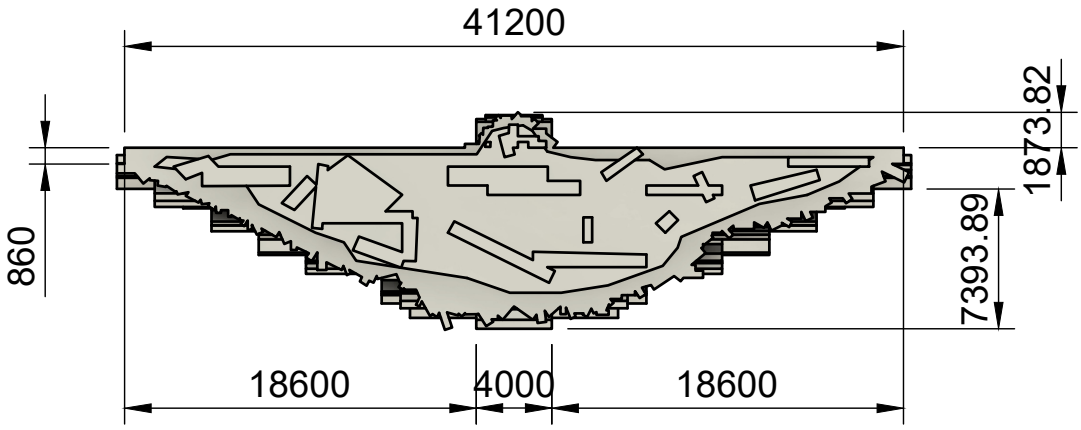

2 - Side view [1:500]

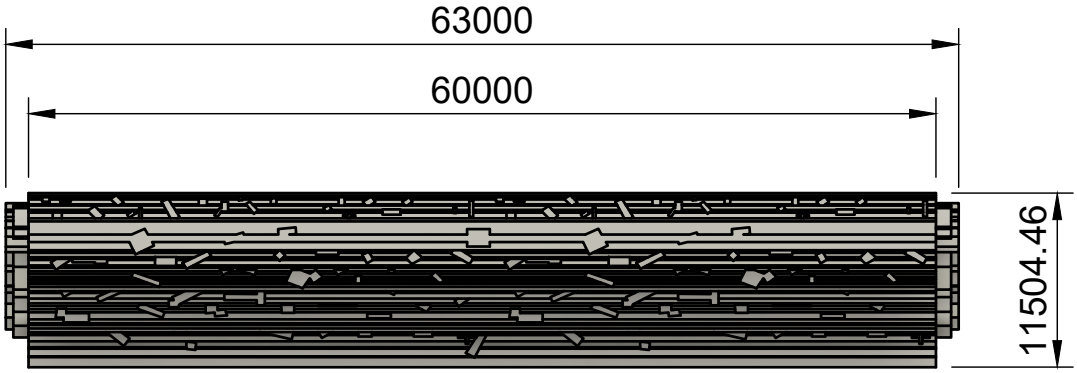

3 - 3D view [1:1000]

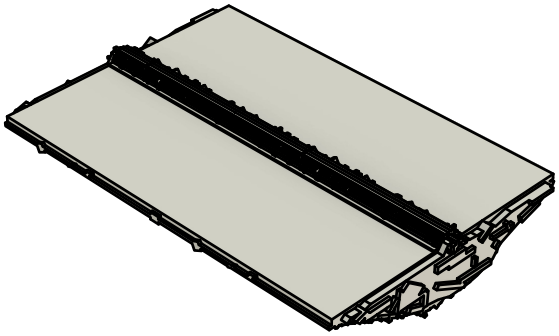

4 - Top view [1:1000]

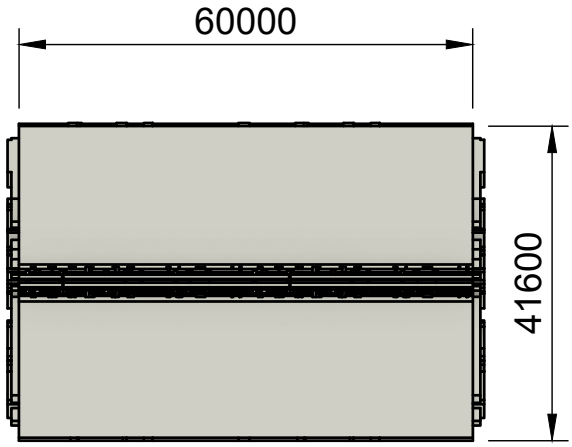

Author	Gerrit-Jan Winkels
Project	Ice Ridge-WEC Collision Dynamics Thesis
Object	Standard-Sized Ice Ridge
Units	mm

A2. Point Absorber Buoy Drawing

1 - Front view [1:100]

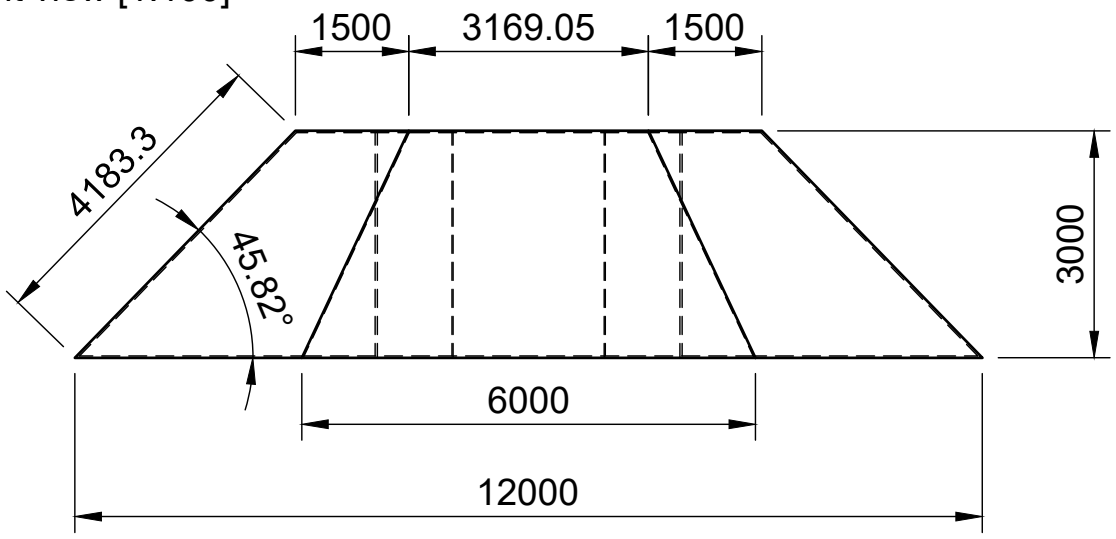

2 - Side view [1:100]

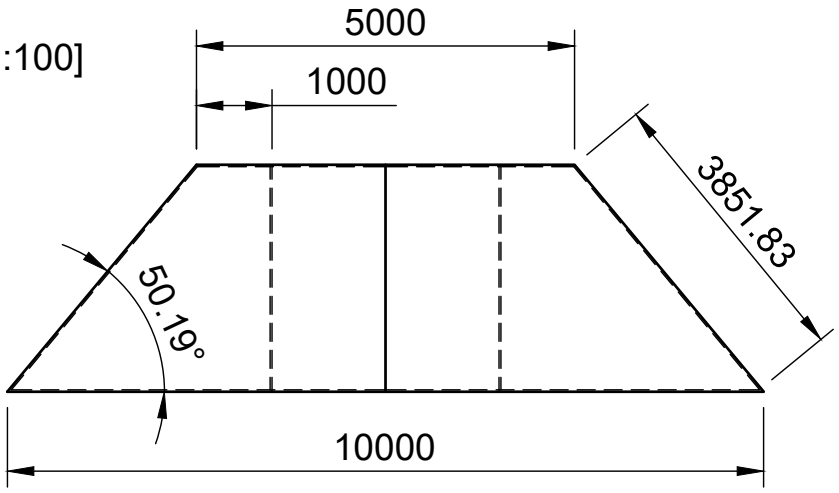

3 - 3D view [1:200]

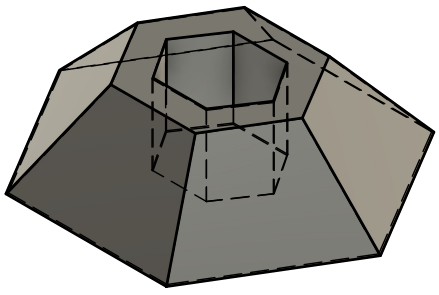

4 Top view [1:200]

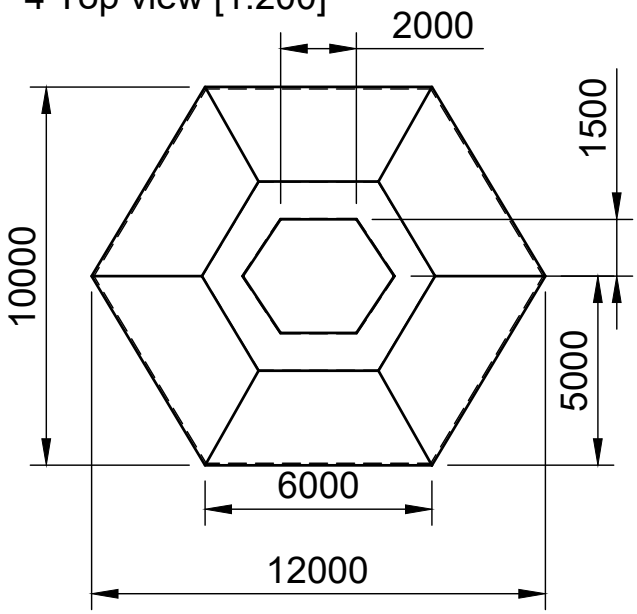

Author	Gerrit-Jan Winkels
Project	Ice Ridge-WEC Collision Dynamics Thesis
Object	Point Absorber Buoy Model
Units	mm

A3. 75%-Sized Ice Ridge Drawing

1 - Front view [1:250]

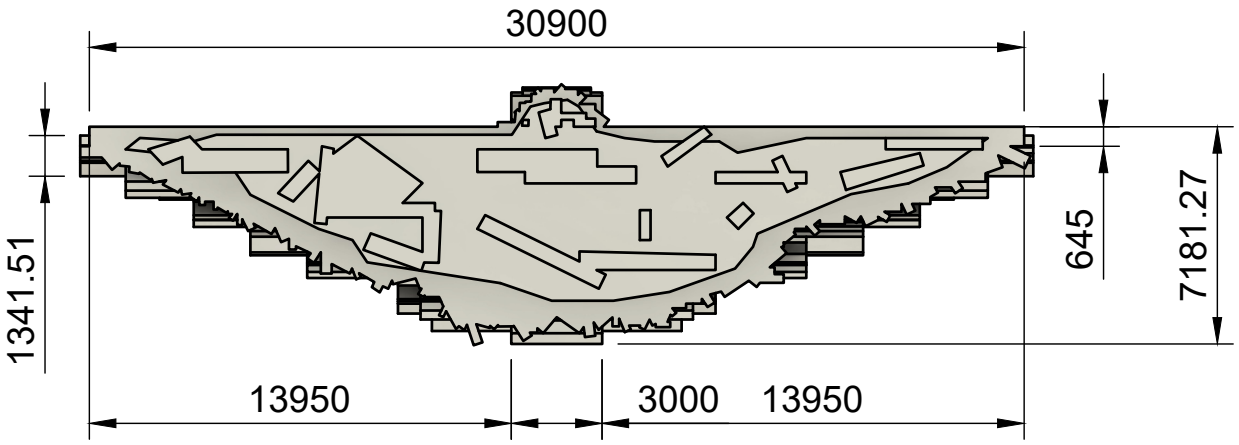

2 - Side view [1:400]

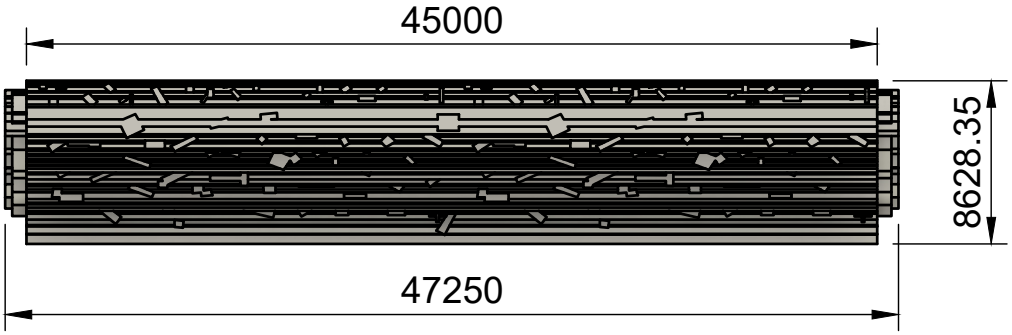

3 - 3D View [1:1000]

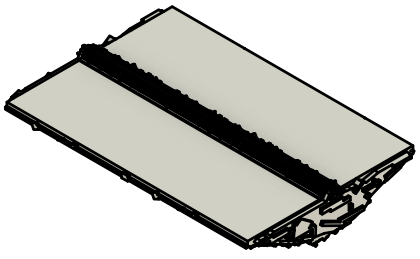

4 - Top view [1:1000]

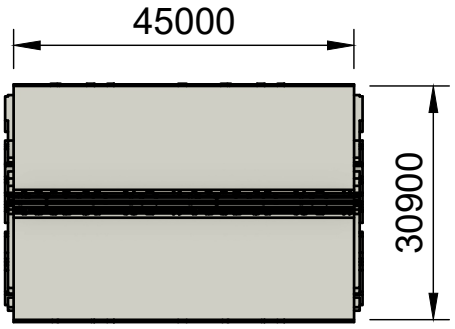

Author	Gerrit-Jan Winkels
Project	Ice Ridge-WEC Collision Dynamics Thesis
Object	75%-Sized Ice Ridge
Units	mm

A4. 50%-Sized Ice Ridge Drawing

1 - Front view [1:200]

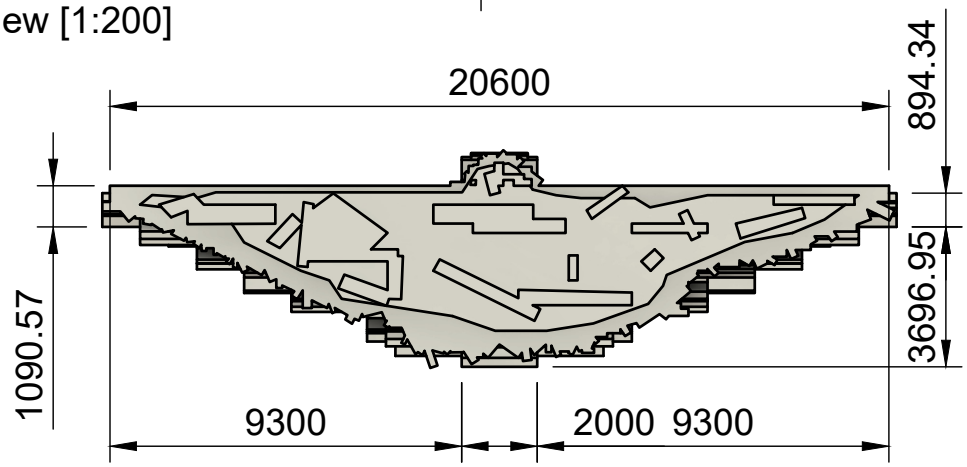

2 - Side view [1:500]

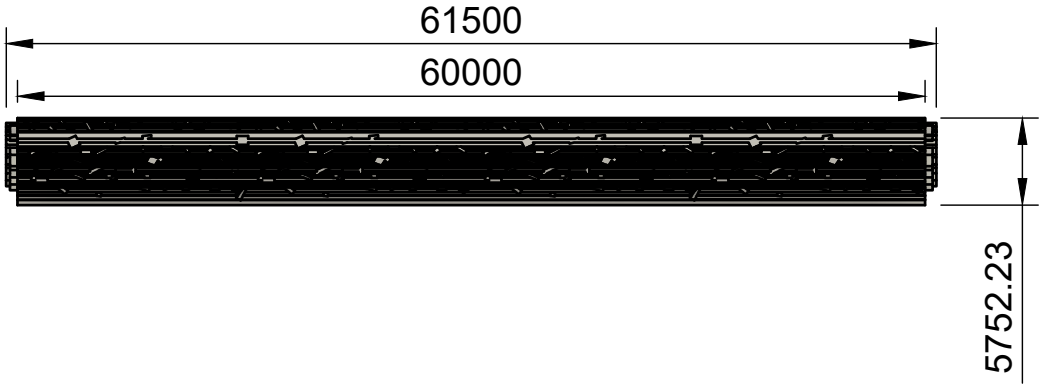

3 - 3D View [1:1000]

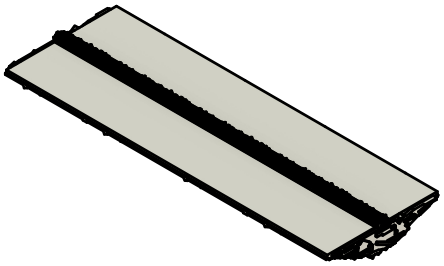

4 - Top View [1:1000]

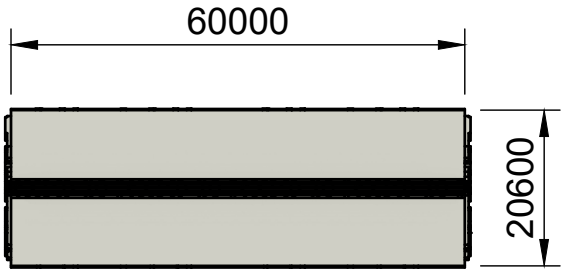

Author	Gerrit-Jan Winkels
Project	Ice Ridge-WEC Collision Dynamics Thesis
Object	50%-Sized Ice Ridge
Units	mm

A5. Smooth Standard-Sized Ice Ridge Drawing

1 - Front view [1:400]

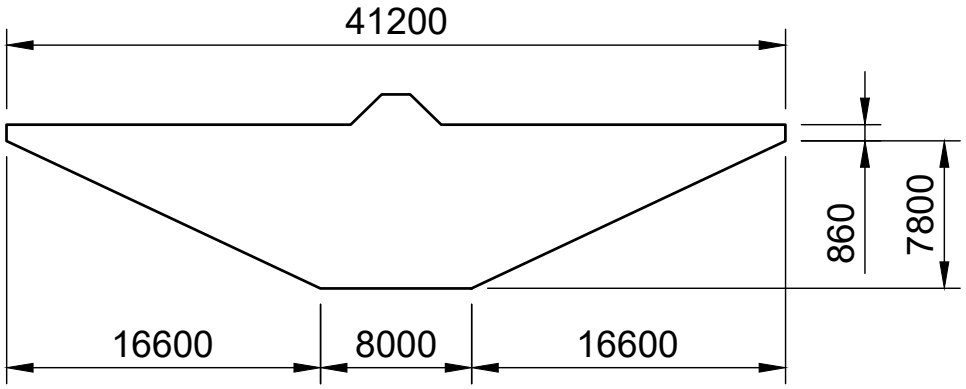

2 - Side view [1:500]

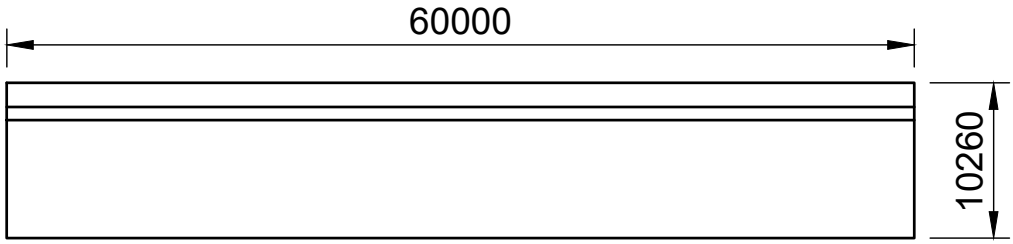

3 - 3D view [1:1000]

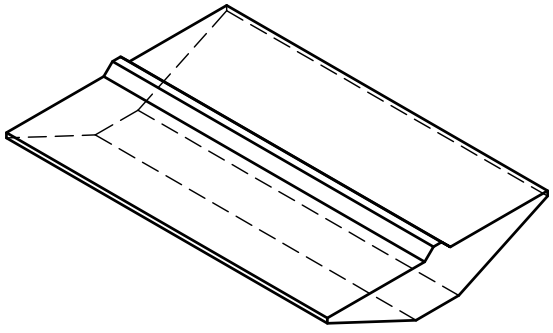

4 - Top view [1:1000]

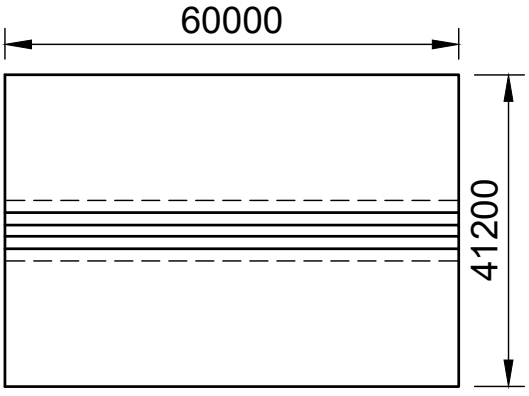

Author	Gerrit-Jan Winkels
Project	Ice Ridge-WEC Collision Dynamics Thesis
Object	Smooth Standard-Sized Ice Ridge
Units	mm

B

DualSPHysics Code

B1. Standard Configuration Definition

```
<!-- Case name: 1_Standard_Configuration -->
<?xml version="1.0" encoding="UTF-8" ?>
<case app="DesignSPHysics v0.8.0" date="26-05-2025 19:56:02">
    <casedef>
        <constantsdef>
            <gravity x="0.0" y="0.0" z="-9.81" comment="Gravitational acceleration"
                units_comment="m/s^2" />
            <rhop0 value="1025.0" comment="Reference density of the fluid" units_comment="kg/m^3
                " />
            <rhopgradient value="2" comment="Initial density gradient 1:Rhop0, 2:Water column, 3:
                Max. water height (default=2)." units_comment="-" />
            <hswl value="0.0" auto="true" comment="Maximum still water level to calculate
                speedofsound using coefsound" units_comment="metres (m)" />
            <gamma value="7.0" comment="Polytropic constant for water used in the state equation
                " />
            <speedsystem value="0.0" auto="true" comment="Maximum system speed (by default the
                dam-break propagation is used)" />
            <coefsound value="20.0" comment="Coefficient to multiply speedsystem" />
            <speedsound value="0.0" auto="true" comment="Speed of sound to use in the simulation
                (by default speedofsound=coefsound*speedsystem)" />
            <coefh value="1.2" comment="Coefficient to calculate the smoothing length (h=coefh*
                sqrt(3*dp^2) in 3D)" />
            <cflnumber value="0.2" comment="Coefficient to multiply dt" />
            <h value="0.0" auto="true" units_comment="metres (m)" />
            <b value="0.0" auto="true" units_comment="Pascal (Pa)" />
            <massbound value="0" auto="true" units_comment="kg" />
            <massfluid value="0" auto="true" units_comment="kg" />
        </constantsdef>
        <mkconfig boundcount="241" fluidcount="9">
        </mkconfig>
        <geometry>
            <definition dp="0.25" comment="Initial inter-particle distance" units_comment="
                metres (m)">
                <pointref x="0.0" y="0.0" z="0.0" />
                <pointmin x="-10.0" y="-20.0" z="-0.01" />
                <pointmax x="150.0" y="110.0" z="29.99" />
            </definition>
            <commands>
                <mainlist>
                <setshapemode>actual | dp | bound</setshapemode>
                <move x="0.0" y="-10.0" z="-0.01" />
```

```
            <setmkfluid mk="0"/>
            <fillbox x="80.0" y="60.0" z="5.01" objname="Ocean">
                <modefill>void</modefill>
                <point x="0" y="0" z="0" />
                <size x="140.0" y="110.0" z="20.0" />
            </fillbox>
            <matrixreset />
            <setmkbound mk="0"/>
            <setdrawmode mode="full"/>
            <drawbox objname="Seabed">
                <boxfill>solid</boxfill>
                                <layers vdp="" />
                <point x="0.0" y="-10.0" z="-0.01" />
                <size x="140.0" y="110.0" z="0.01" />
            </drawbox>
            <setmkbound mk="10"/>
            <drawfilestl file="external_GEO_Improved_Ice_Ridge_v3.stl" objname="Ice_Ridge"
                autofill="false" advanced="false" reverse="false" >

                <drawscale x="0.001" y="0.001" z="0.001" />
                <drawmove x="40.0" y="45.0" z="20.0" />
                <drawrotate angx="0.0" angy="0.0" angz="89.99999999999999" />
            </drawfilestl>
            <setmkbound mk="20"/>
            <drawfilestl file="external_GEO_Point_Absorber_v3.stl" objname="Point_Absorber"
                autofill="false" advanced="false" reverse="false" >

                <drawscale x="0.001" y="0.001" z="0.001" />
                <drawmove x="80.0" y="48.0" z="18.0" />
                <drawrotate angx="0.0" angy="0.0" angz="89.99999999999999" />
            </drawfilestl>
                <shapeout file="" />
            </mainlist>
        </commands>
    </geometry>
    <properties>
        <propertyfile file="materials.xml" path="materials" />
        <links>
            <link mkbound="0" property="lime-stone" />
            <link mkbound="10" property="ice-ridge" />
            <link mkbound="20" property="steel" />
        </links>
    </properties>
    <floatings>
        <floating mkbound="10" rhopbody="917.0" property="">
        </floating>
        <floating mkbound="20" property="">
            <massbody value="45220.0" />
        </floating>
    </floatings>
</casedef>
<execution>
    <special>
    <initialize>
        <fluidvelocity mkfluid="0">
            <direction x="2.0" y="0.0" z="0.0" />
            <velocity3 v="2.0" v2="0.5" v3="0.0" z="20.0" z2="10.0" z3="0.0" comment="
                Parabolic␣profile␣velocity" units_comment="m/s" />
        </fluidvelocity>
    </initialize>
        <chrono>
```

```
91              <savedata value="0.05" comment="Saves␣CSV␣with␣data␣exchange␣for␣each␣time␣
                    interval␣(0=all␣steps)" />
92              <collision activate="true">
93                  <distancedp value="0.125" comment="Allowed␣collision␣overlap␣according␣Dp␣(
                        default=0.5)" />
94                  <contactmethod value="0" comment="Contact␣method␣type.␣0:NSC␣(Non␣Smooth␣
                        Contacts),␣1:SMC␣(SMooth␣Contacts).␣(default=0)" />
95              </collision>
96              <bodyfixed id="Seabed" mkbound="0" modelfile="AutoActual" modelnormal="original"
                    />
97              <bodyfloating id="Point_Absorber" mkbound="20" modelfile="AutoActual" modelnormal
                    ="original"/>
98              <bodyfloating id="Ice_Ridge" mkbound="10" modelfile="AutoActual" modelnormal="
                    original"/>
99          </chrono>
100         <moorings>
101             <savevtk_moorings value="true" comment="Saves␣vtk␣with␣moorings␣(default=true)"
                    />
102             <savecsv_points value="true" comment="Saves␣csv␣with␣link␣points␣(default=true)"
                    />
103             <savevtk_points value="false" comment="Saves␣vtk␣with␣link␣points␣(default=false)
                    " />
104             <mooredfloatings>
105                 <floating mkbound="20" comment="Mkbound␣of␣the␣Floating␣body␣the␣mooring␣is␣
                        linked␣to" />
106             </mooredfloatings>
107             <moordynplus comment="MoorDynPlus␣configuration">
108                 <solverOptions>
109                     <waterDepth value="20.0" comment="Water␣depth" units_comment="(m)"/>
110                     <freesurface value="0.0" comment="Z␣position␣of␣the␣water␣free␣surface.(
                            default=0)" />
111                     <kBot value="3000000.0" comment="Bottom␣stiffness␣constant.␣(default=3.0e6
                            )" units_comment="Pa/m" />
112                     <cBot value="3000000.0" comment="Bottom␣damping␣constant.␣(default=3.0e5)"
                             units_comment="Pa*s/m" />
113                     <dtM value="0.0001" auto="true" comment="Desired␣mooring␣model␣time␣step.␣
                            (default=0.0001)" />
114                     <waveKin value="0" comment="Wave␣kinematics␣flag␣(␣0:␣neglect␣[the␣only␣
                            option␣currently␣supported]␣).␣(default=0)" />
115                     <writeUnits value="yes" comment="Write␣units␣line.␣value=[yes|no].␣(
                            default=yes)" />
116                     <frictionCoefficient value="0.0" comment="General␣bottom␣friction␣
                            coefficient,␣as␣a␣start.␣(default=0.0)" />
117                     <fricDamp value="200.0" comment="Damping␣coefficient␣used␣to␣model␣the␣
                            friction␣with␣speeds␣near␣zero.␣(default=200.0)" />
118                     <statDynFricScale value="1.2" comment="Ratio␣between␣static␣and␣dynamic␣
                            friction␣(mu_static/mu_dynamic).␣(default=1.0)" />
119                     <dtIC value="1.0" comment="Period␣to␣analyze␣convergence␣of␣dynamic␣
                            relaxation␣for␣initial␣conditions.␣(default=1.0)" units_comment="s" />
120                     <cdScaleIC value="1.0" comment="Factor␣to␣scale␣drag␣coefficients␣during␣
                            dynamic␣relaxation␣for␣initial␣conditions.␣(default=5)" />
121                     <threshIC value="0.01" comment="Convergence␣threshold␣for␣for␣initial␣
                            conditions.␣(default=0.001)" />
122                     <tmaxIC value="0.5" comment="Maximum␣time␣for␣initial␣conditions␣without␣
                            convergence.(default=0)" units_comment="s" />
123                 </solverOptions>
124                 <bodies>
125                     <body ref="20" comment="Fluid␣driven␣object␣to␣attach␣mooring␣lines."/>
126                 </bodies>
127                 <lines>
128                     <linedefault>
```

```
129                         <ea value="3540000000.0" comment="Line␣stiffness,␣product␣of␣
                                elasticity␣modulus␣and␣cross-sectional␣area." units_comment="N" />
130                         <diameter value="0.15" comment="Volume-equivalent␣diameter␣of␣the␣line.
                                " units_comment="m" />
131                         <massDenInAir value="138.7" comment="Mass␣per␣unit␣length␣of␣the␣line.
                                " units_comment="kg/m" />
132                         <ba value="-0.8" comment="Line␣internal␣damping␣(BA/-zeta).␣(default
                                =-0.8)" units_comment="Ns" />
133                         <can value="1.0" comment="Transverse␣added␣mass␣coefficient␣(with␣
                                respect␣to␣line␣displacement).␣(default=1.0)" />
134                         <cat value="0.5" comment="Tangential␣added␣mass␣coefficient␣(with␣
                                respect␣to␣line␣displacement).␣(default=0.0)" />
135                         <cdn value="1.6" comment="Transverse␣drag␣coefficient␣(with␣respect␣to
                                ␣frontal␣area,␣d*l).␣(default=1.6)" />
136                         <cdt value="0.05" comment="Tangential␣drag␣coefficient␣(with␣respect␣
                                to␣surface␣area,␣ *d*l).␣(default=0.05)" />
137                         <breaktension value="625000.0" comment="Maximum␣value␣of␣tension␣for␣
                                the␣lines.␣value=0␣Break␣Tension␣is␣not␣used.␣(default=0)"
                                units_comment="N" />
138                         <outputFlags value="p" comment="Node␣output␣properties.(default=-)␣[-:
                                None|p:Positions|v:Velocities|U:Wave␣Velocities|t:Tension|D:
                                Hydrodynamic␣Drag␣Force|c=Internal␣Damping|s:Strain␣of␣each␣
                                segment|d:␣rate␣of␣strain␣of␣each␣segment]" />
139                     </linedefault>
140                     <line>
141                         <vesselconnection bodyref="20" x="70.0" y="48.0" z="18.0" />
142                         <fixconnection x="55.0" y="63.0" z="0.0" />
143                         <length value="33.5" comment="(m)"/>
144                         <segments value="30" />
145                     </line>
146                     <line>
147                         <vesselconnection bodyref="20" x="70.0" y="42.0" z="18.0" />
148                         <fixconnection x="55.0" y="27.0" z="0.0" />
149                         <length value="33.5" comment="(m)"/>
150                         <segments value="30" />
151                     </line>
152                     <line>
153                         <vesselconnection bodyref="20" x="80.0" y="48.0" z="18.0" />
154                         <fixconnection x="95.0" y="63.0" z="0.0" />
155                         <length value="33.5" comment="(m)"/>
156                         <segments value="30" />
157                     </line>
158                     <line>
159                         <vesselconnection bodyref="20" x="80.0" y="42.0" z="18.0" />
160                         <fixconnection x="95.0" y="27.0" z="0.0" />
161                         <length value="33.5" comment="(m)"/>
162                         <segments value="30" />
163                     </line>
164                 </lines>
165                 <savedata comment="Saves␣CSV␣with␣the␣connection␣properties" >
166                     <tension value="true" comment="Store␣tensions.(default:␣value=false)"/>
167                     <force value="true" comment="Store␣forces.(default:␣value=false)"/>
168                     <velocity value="true" comment="Store␣velocities.(default:␣value=false)"/>
169                     <position value="true" comment="Store␣positions.(default:␣value=false)"/>
170                 </savedata>
171             </moordynplus>
172         </moorings>
173         <gauges>
174         </gauges>
175     <outputparts preselection="all" comment="Initial␣selection:␣all␣or␣none">
176             <ignore nparts="0" comment="Ignore␣filters␣every␣nparts␣output␣files␣(default=0)"
```

```
                />
177         </outputparts>
178         </special>
179         <parameters>
180             <parameter key="SavePosDouble" value="0" comment="Saves particle position using
                    double precision (default=0)" />
181             <parameter key="Boundary" value="1" comment="Boundary method 1:DBC, 2:mDBC (default
                    =1)" />
182             <parameter key="SlipMode" value="1" comment="Slip mode for mDBC 1:DBC vel=0, 2:No-
                    slip (default=1)" />
183             <parameter key="NoPenetration" value="0" comment="No-Penetration active 0:Off, 1:On
                    (default=0)" />
184             <parameter key="StepAlgorithm" value="1" comment="Step Algorithm 1:Verlet, 2:
                    Symplectic (default=1)" />
185             <parameter key="VerletSteps" value="40" comment="Verlet only: Number of steps to
                    apply Euler timestepping (default=40)" />
186             <parameter key="Kernel" value="2" comment="Interaction Kernel 1:Cubic Spline, 2:
                    Wendland (default=2)" />
187             <parameter key="ViscoTreatment" value="1" comment="Viscosity formulation 1:
                    Artificial, 2:Laminar+SPS (default=1)" />
188             <parameter key="Visco" value="0.01" comment="Viscosity value" /> % Note alpha can
                    depend on the resolution. A value of 0.01 is recommended for near irrotational
                    flows.
189             <parameter key="ViscoBoundFactor" value="1.0" comment="Multiply viscosity value with
                     boundary (default=1)" />
190             <parameter key="DensityDT" value="2" comment="Density Diffusion Term 0:None, 1:
                    Molteni, 2:Fourtakas, 3:Fourtakas(full) (default=0)" />
191             <parameter key="DensityDTvalue" value="0.1" comment="DDT value (default=0.1)" />
192             <parameter key="Shifting" value="0" comment="Shifting mode 0:None, 1:Ignore bound, 2:
                    Ignore fixed, 3:Full (default=0)" />
193             <parameter key="ShiftCoef" value="-2.0" comment="Coefficient for shifting
                    computation (default=-2)" />
194             <parameter key="ShiftTFS" value="0.0" comment="Threshold to detect free surface.
                    Typically 1.5 for 2D and 2.75 for 3D (default=0)" />
195             <parameter key="ShiftAdvCoef" value="-0.01" comment="Coefficient for advanced
                    shifting computation (default=-0.01)" />
196             <parameter key="ShiftAdvALE" value="0.0" comment="ALE formulation for advanced
                    shifting  (default=0)" />
197             <parameter key="ShiftAdvNCPress" value="0.0" comment="Non conservative pressure
                    formulation for advanced shifting (default=0)" />
198             <parameter key="RigidAlgorithm" value="3" comment="Rigid Algorithm 1:SPH, 2:DEM, 3:
                    CHRONO (default=1)" />
199             <parameter key="FtPause" value="0.0" comment="Time to freeze the floatings at
                    simulation start (warmup) (default=0)" units_comment="seconds" />
200             <parameter key="CoefDtMin" value="0.05" comment="Coefficient to calculate minimum
                    time step dtmin=coefdtmin*h/speedsound (default=0.05)" />
201             <parameter key="#DtIni" value="0.0001" comment="Initial time step (default=h/
                    speedsound)" units_comment="seconds" />
202             <parameter key="#DtMin" value="1e-05" comment="Minimum time step (default=coefdtmin*
                    h/speedsound)" units_comment="seconds" />
203             <parameter key="DtAllParticles" value="0" comment="Velocity of particles used to
                    calculate DT. 1:All, 0:Only fluid/floating (default=0)" />
204             <parameter key="TimeMax" value="60.0" comment="Time of simulation" units_comment="
                    seconds" />
205             <parameter key="TimeOut" value="0.05" comment="Time out data" units_comment="seconds
                    " />
206             <parameter key ="MinFluidStop" value="0.01" comment="Minimum proportion of initial
                    fluid particles to continue the simulation 0:Never stops, 0.1:Stops when fluid
                    drops to 10%. (default=0)" />
207             <parameter key="RhopOutMin" value="700.0" comment="Minimum rhop valid (default=700)"
                     units_comment="kg/m^3" />
```

```
208             <parameter key="RhopOutMax" value="1300.0" comment="Maximum rhop valid (default
                    =1300)" units_comment="kg/m^3" />
209             <parameter key="XPeriodicIncY" value="0.0" comment="Increase of Y with periodic BC"
                    />
210             <parameter key="XPeriodicIncZ" value="0.0" comment="Increase of Z with periodic BC"
                    />
211             <parameter key="YPeriodicIncX" value="0.0" comment="Increase of X with periodic BC"
                    />
212             <parameter key="YPeriodicIncZ" value="0.0" comment="Increase of Z with periodic BC"
                    />
213             <simulationdomain comment="Defines domain of simulation (default=Uses minimum and
                    maximum position of the generated particles)" >
214                 <posmin x="default" y="default" z="default" comment="e.g.: x=0.5, y=default-1, z=
                        default-10%" />
215                 <posmax x="default" y="default" z="default+50.0%"/>
216             </simulationdomain>
217         </parameters>
218     </execution>
219 </case>
```

Listing B.1: `1_Standard_Configuration_Def.xml`

C

Overview of Results

C1. Fairlead tensions

In this Appendix an overview of the fairlead tensions for all cases are provided.

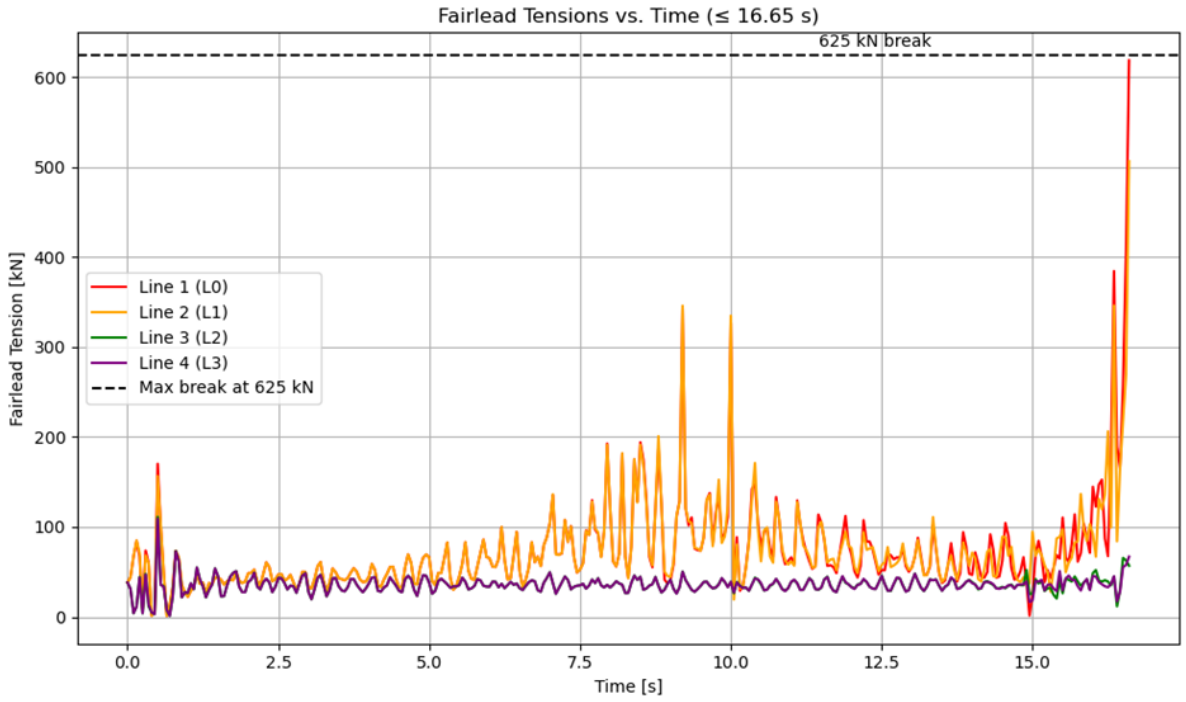

Figure C.1: Fairlead tensions for Case 1 (Original configuration)

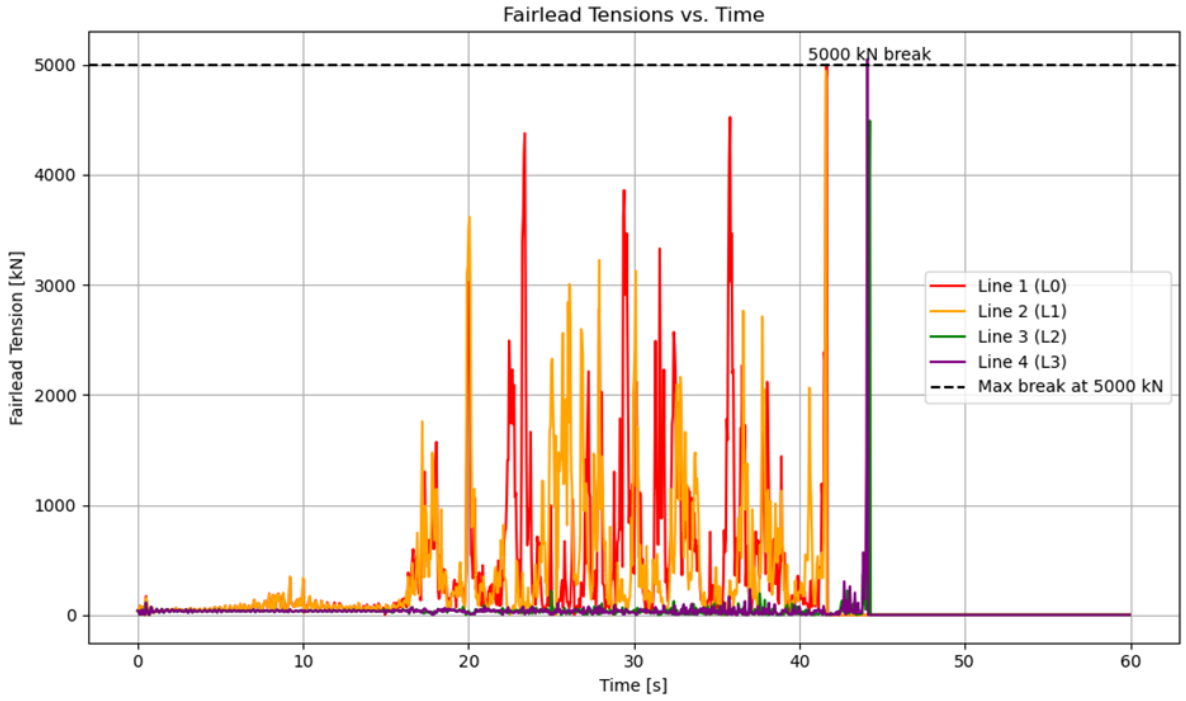

Figure C.2: Fairlead tensions for Case 1b (Original configuration with maximum tension increased to 5MN).

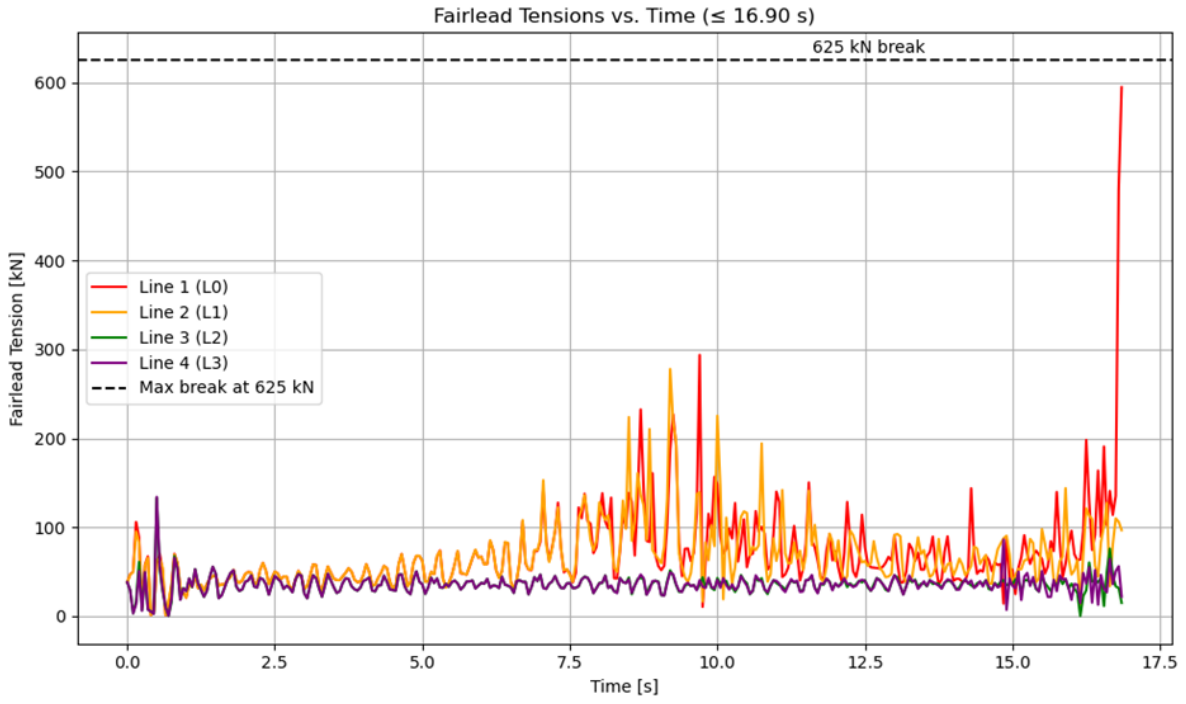

Figure C.3: Fairlead tensions for Case 2 (Configuration with adjusted angle for the ice ridge).

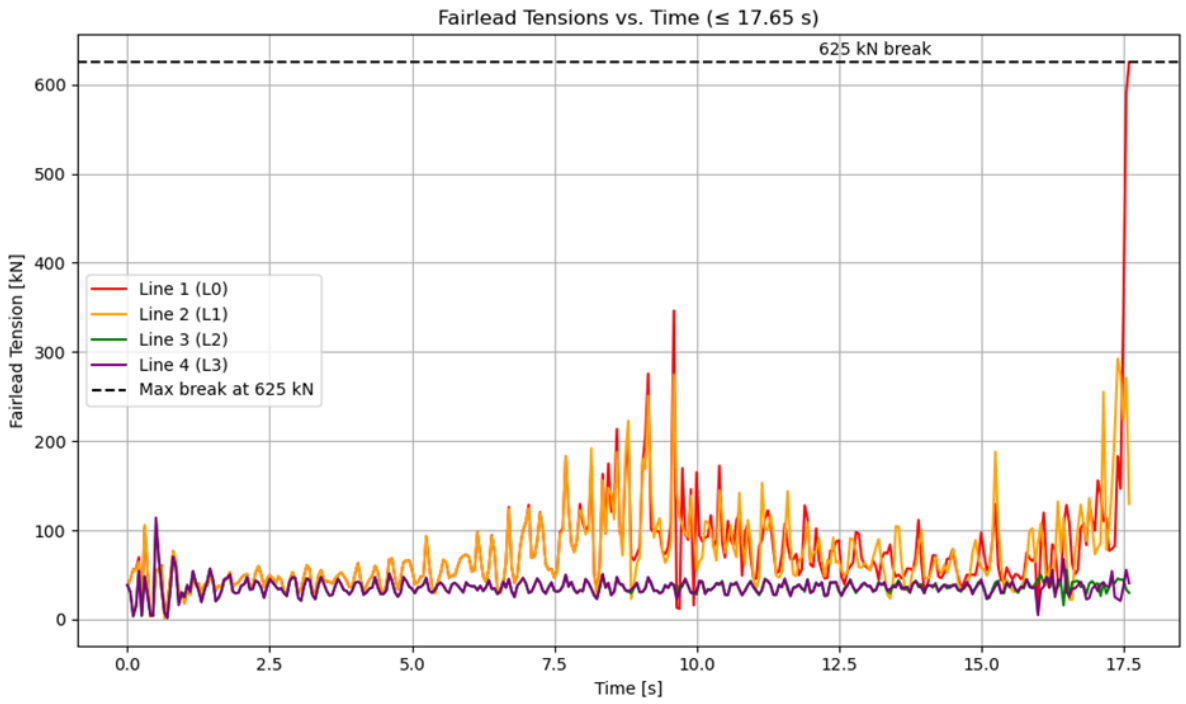

Figure C.4: Fairlead tensions for Case 3 (Configuration with an adjusted ice ridge size to 75% of original).

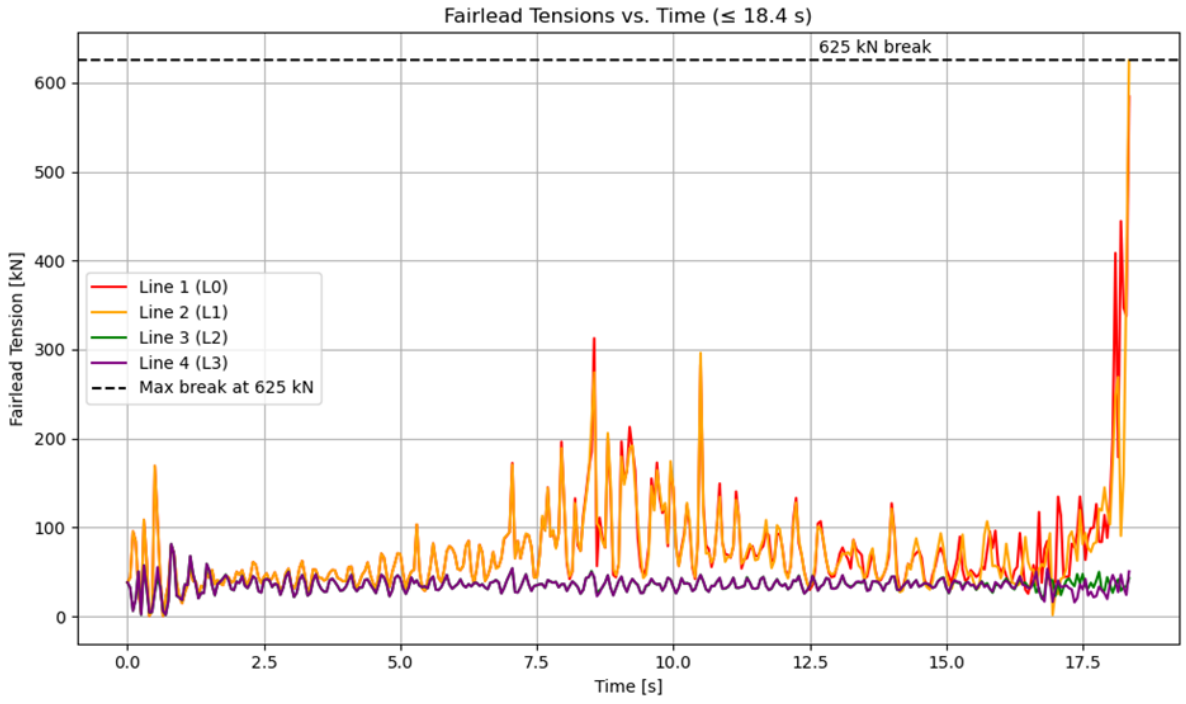

Figure C.5: Fairlead tensions for Case 3b (Configuration with an adjusted ice ridge size to 50% of original).

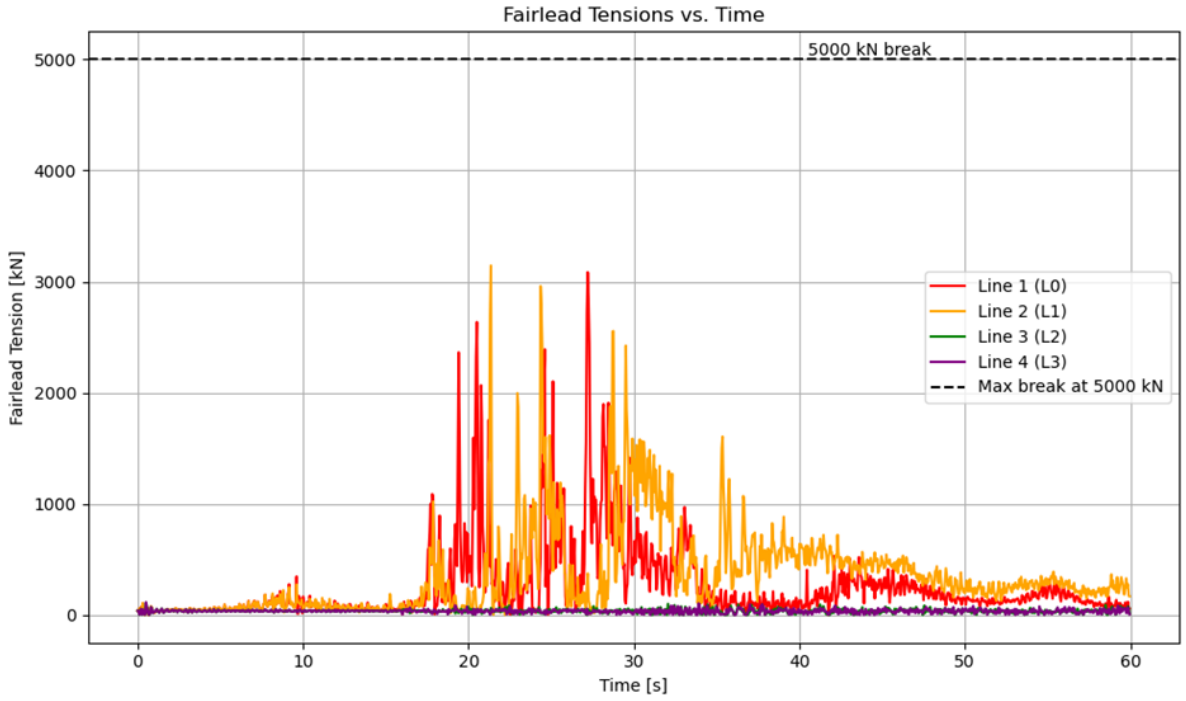

Figure C.6: Fairlead tensions for Case 3c (Configuration with an adjusted ice ridge size to 75% of original and increased maximum tension to 5MN).

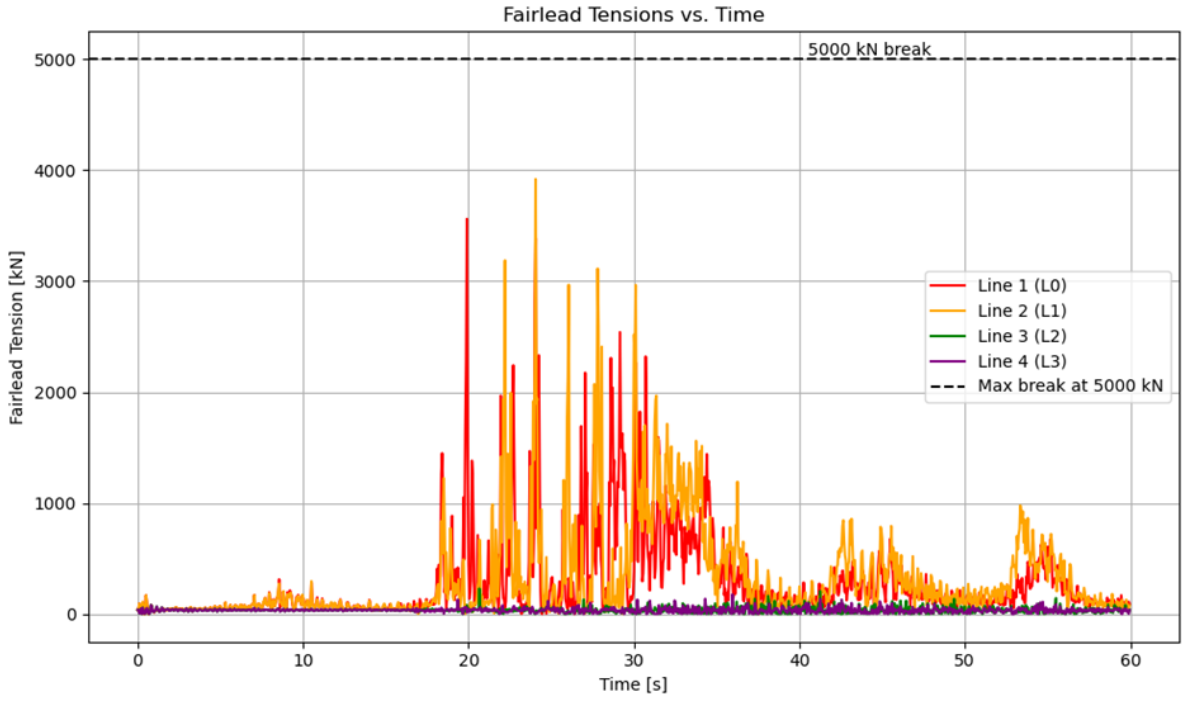

Figure C.7: Fairlead tensions for Case 3d (Configuration with an adjusted ice ridge size to 50% of original and increased maximum tension to 5MN).

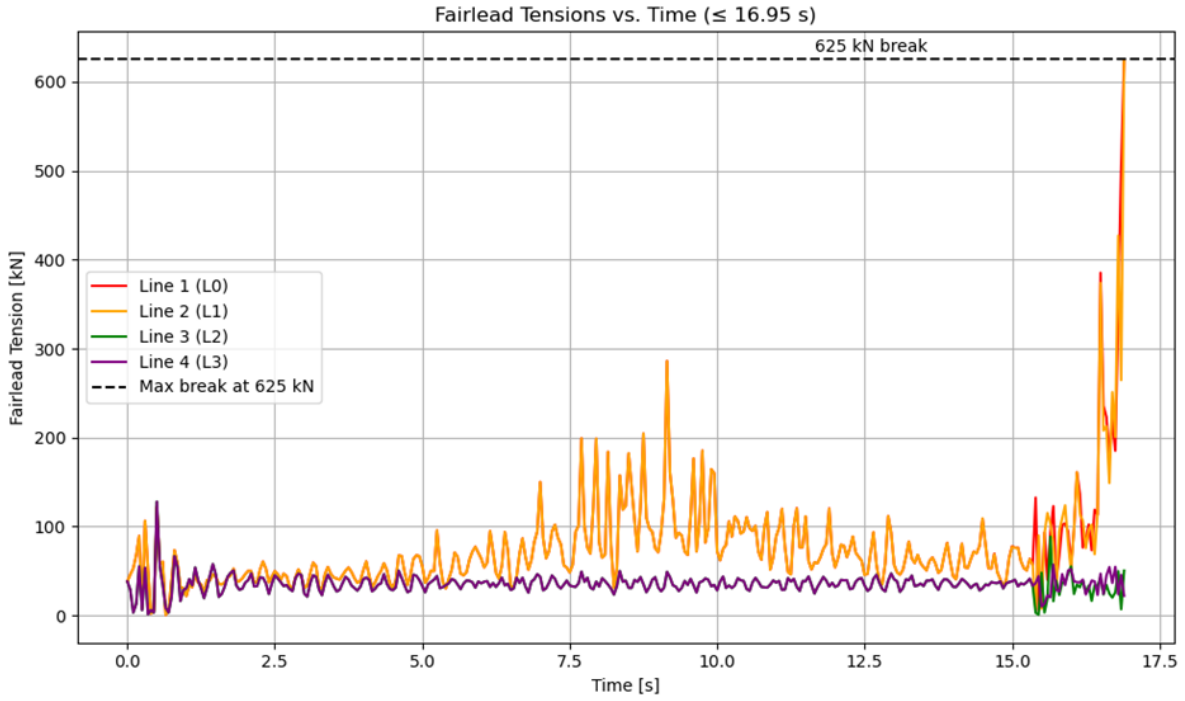

Figure C.8: Fairlead tensions for Case 4 (Configuration with smooth ice ridge).

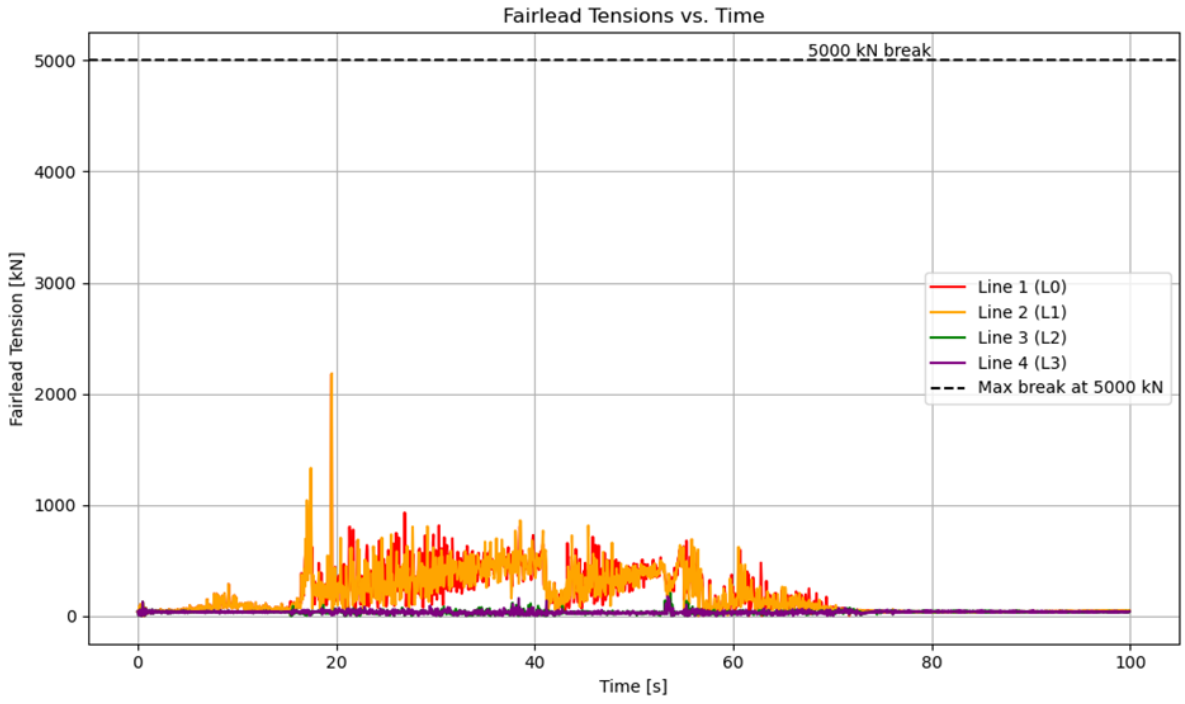

Figure C.9: Fairlead tensions for Case 4b (Configuration with smooth ice ridge and increased maximum tension to 5MN).

C2. Horizontal contact forces

In this Appendix an overview of the horizontal contact forces for all cases are provided. For the cases where the the mooring lines do not fail immediately or quickly after the initial contact, a medium filter and Butterworth filter is provided.

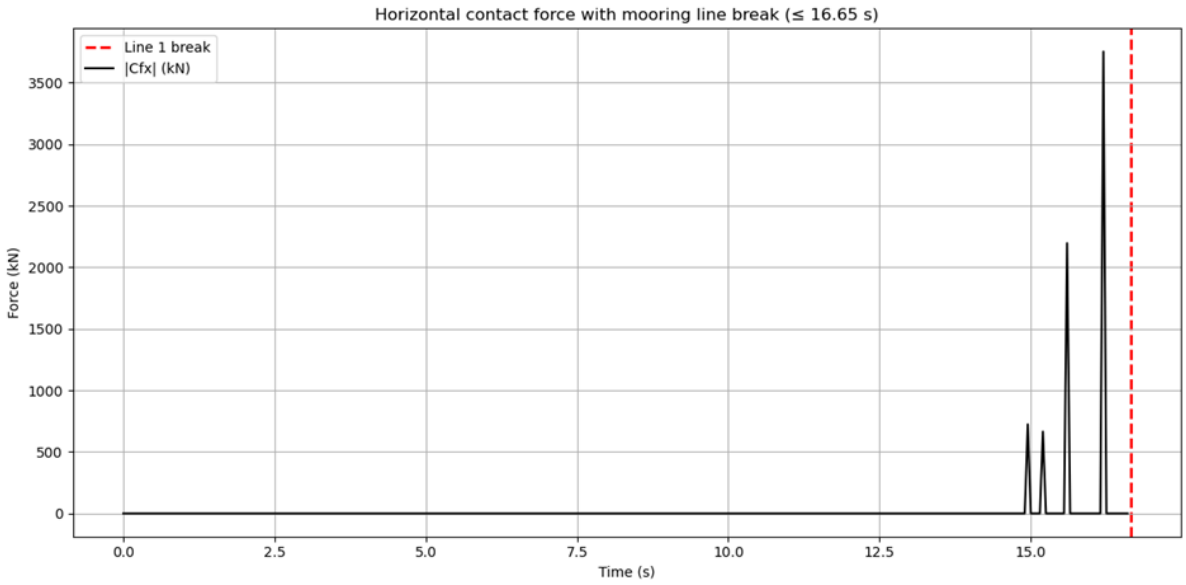

Figure C.10: Horizontal contact forces for Case 1 (Original configuration).

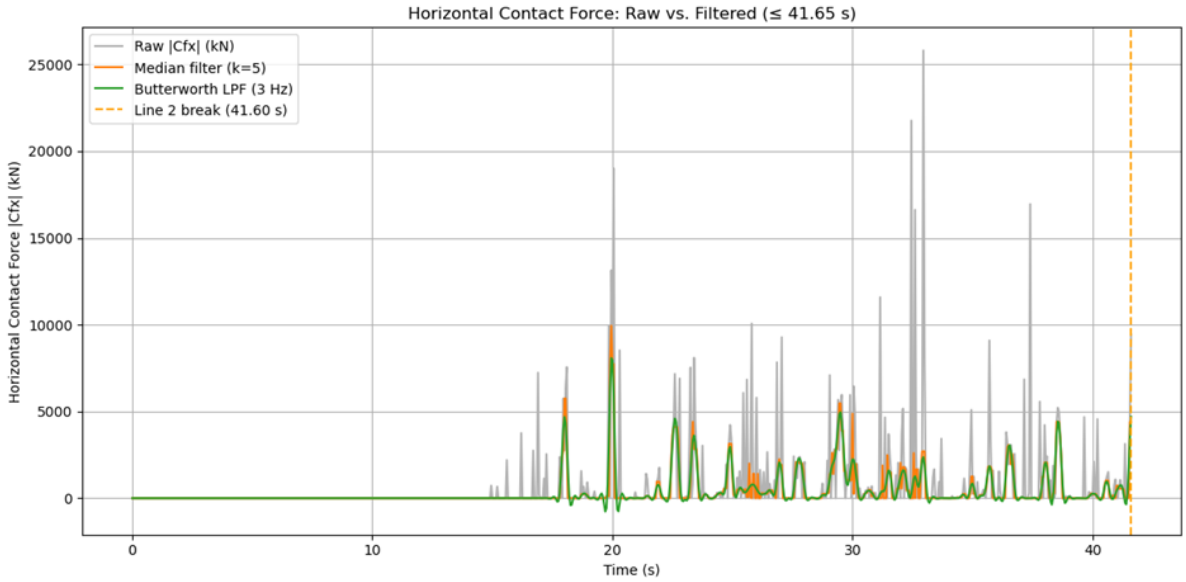

Figure C.11: Horizontal contact forces Case 1b (Original configuration with maximum tension increased to 5MN).

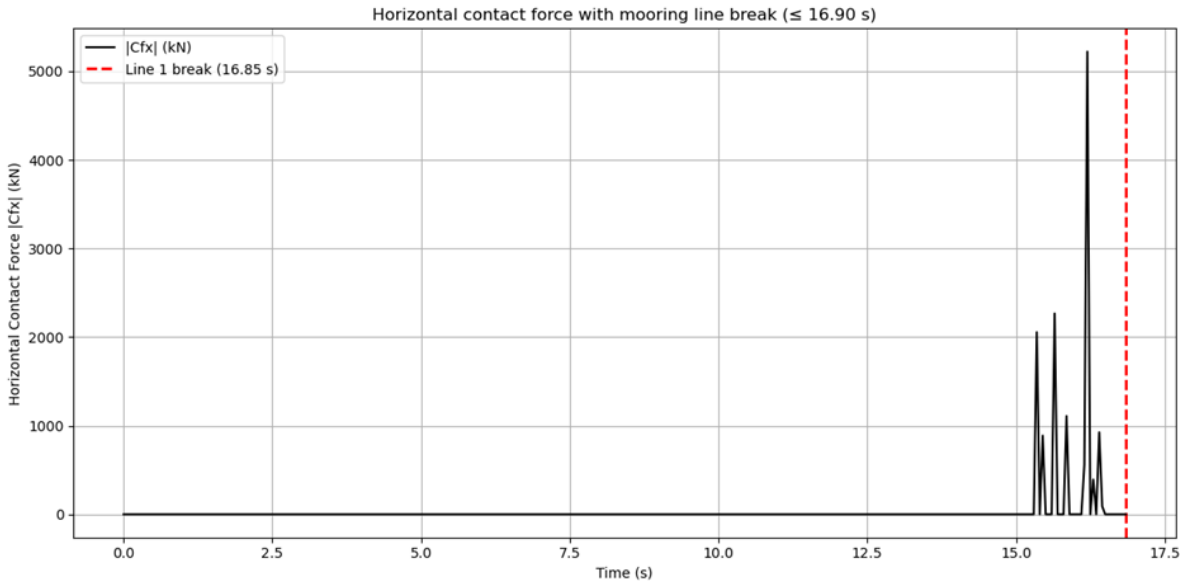

Figure C.12: Horizontal contact forces Case 2 (Configuration with adjusted angle for the ice ridge).

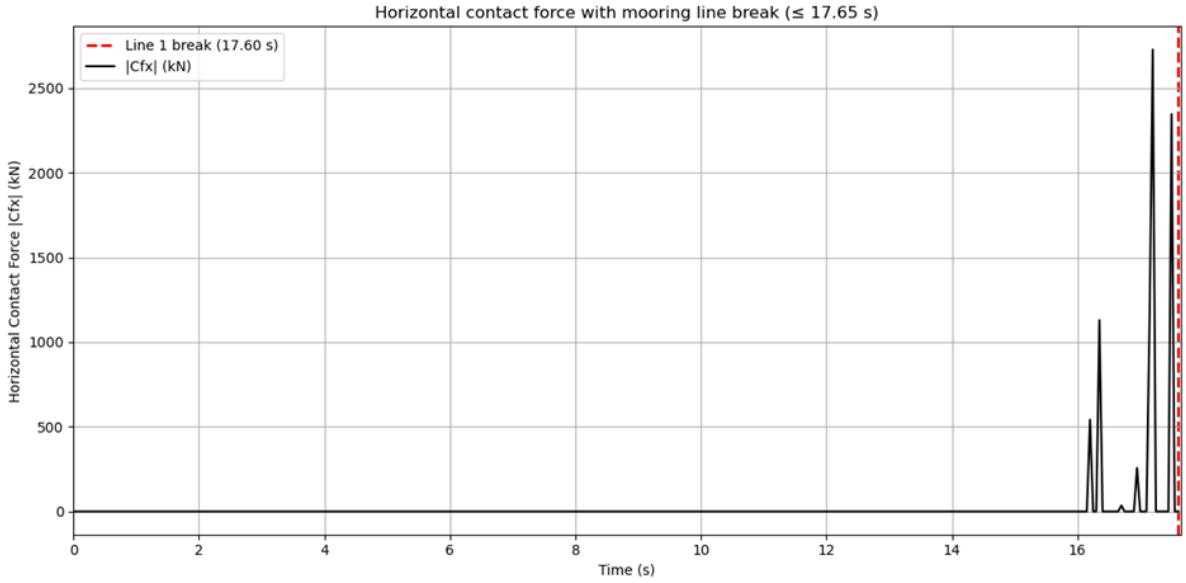

Figure C.13: Horizontal contact forces Case 3 (Configuration with an adjusted ice ridge size to 75% of the original).

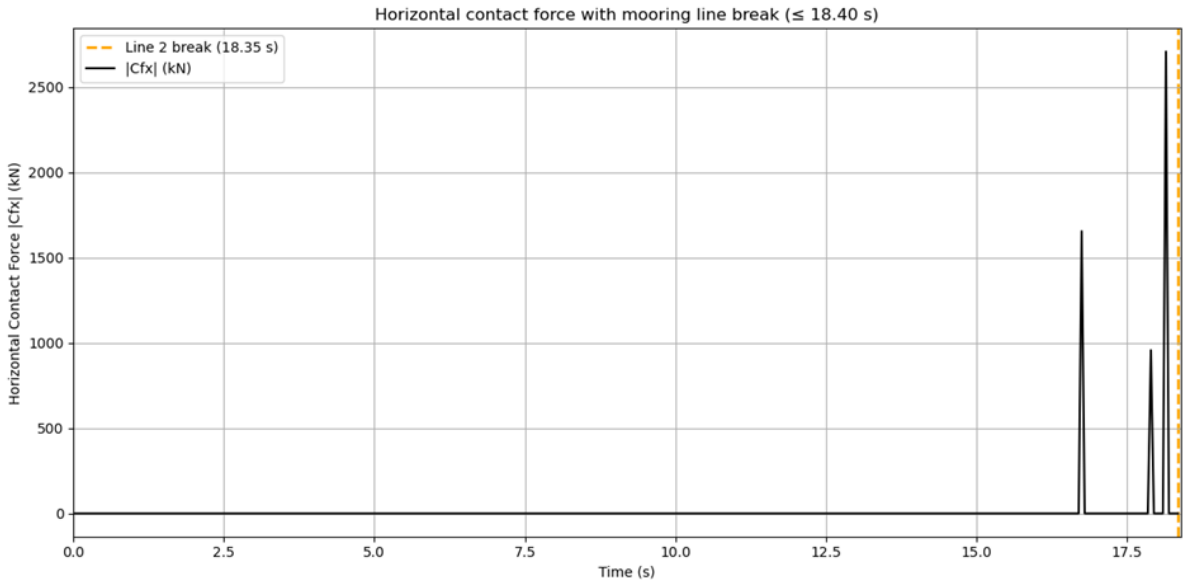

Figure C.14: Horizontal contact forces Case 3b (Configuration with an adjusted ice ridge size to 50% of the original).

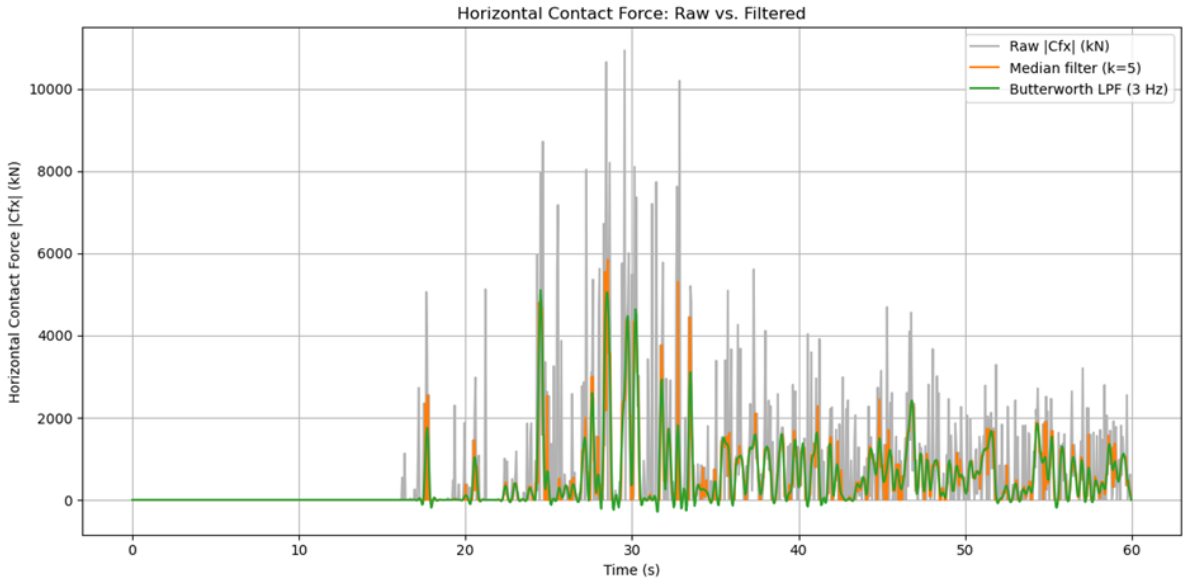

Figure C.15: Horizontal contact forces Case 3c (Configuration with an adjusted ice ridge size to 75% of original and increased maximum tension to 5MN).

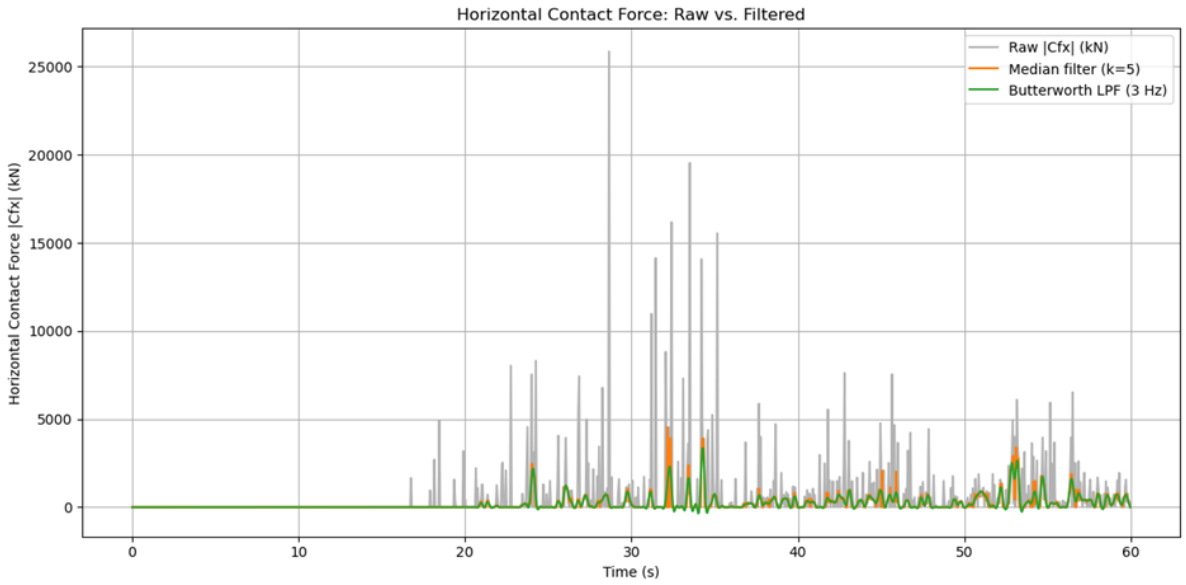

Figure C.16: Horizontal contact forces Case 3d (Configuration with an adjusted ice ridge size to 50% of original and increased maximum tension to 5MN).

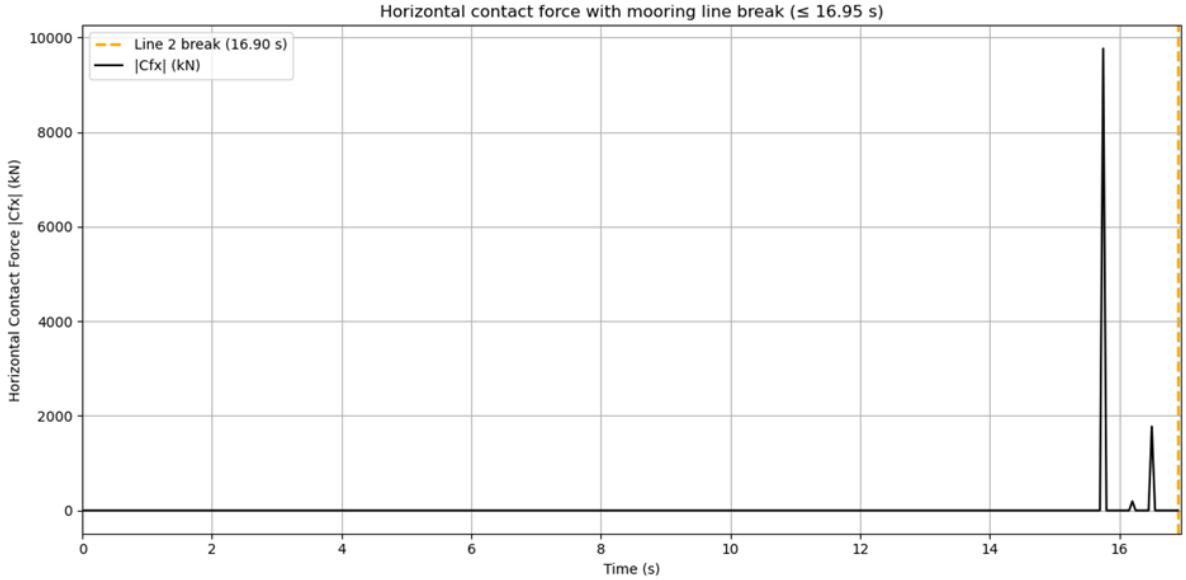

Figure C.17: Horizontal contact forces Case 4 (Configuration with smooth ice ridge).

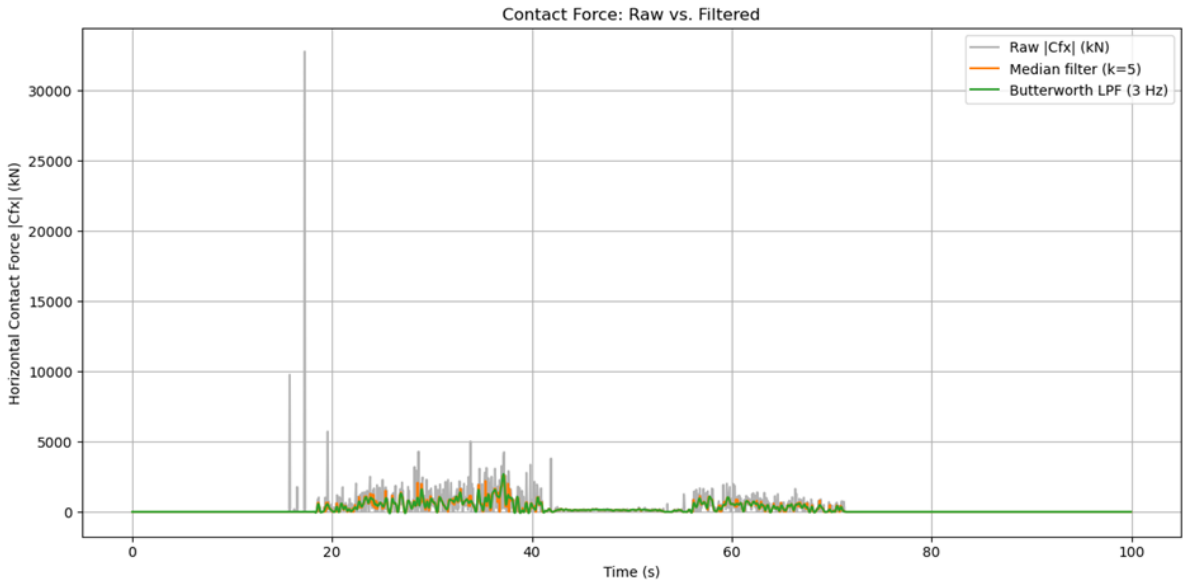

Figure C.18: Horizontal contact forces Case 4b (Configuration with smooth ice ridge and increased maximum tension to 5MN).

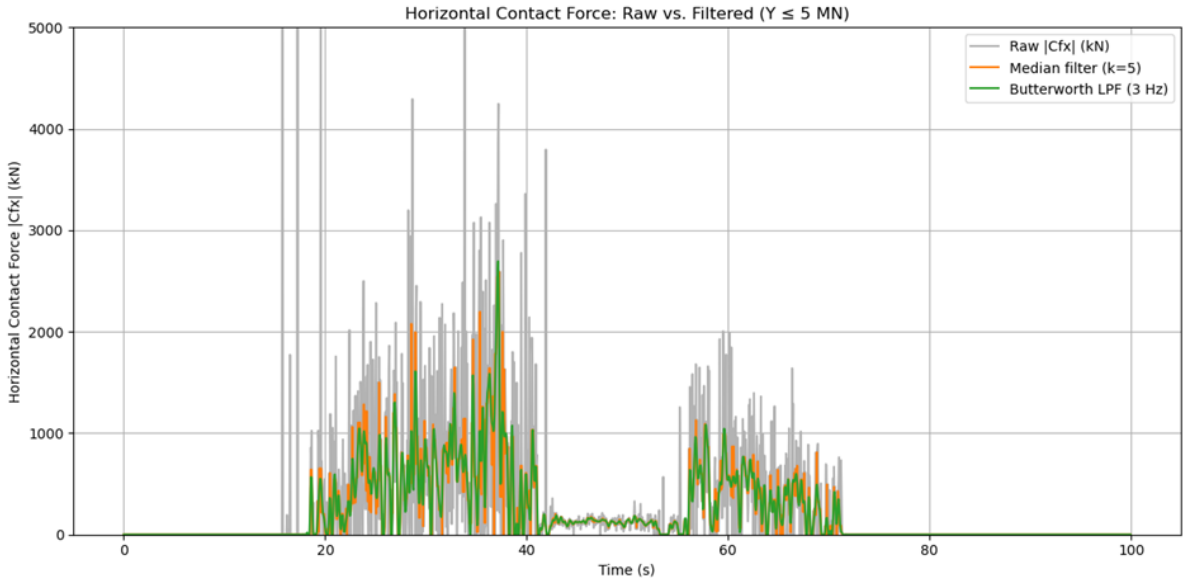

Figure C.19: Horizontal contact forces Case 4b (Configuration with smooth ice ridge and increased maximum tension to 5MN) capped at 5 MN for improved visibility.